REPORT DOCUMENTATION PAGE Dist A

Form Approved
OMB No. 0704-0188

1. AGENCY USE ONLY (Leave blank)	2. REPORT DATE	3. REPORT TYPE AND DATES COVERED
	NOV 94	final 30 Sep 92 - 30 Sep 94

4. TITLE AND SUBTITLE
Pressure Based High Order TVD Methodology for Dynamic Stall Control

5. FUNDING NUMBERS
F49620-92-C-0070
3005/5S

6. AUTHOR(S)
H Q Yang, Z J Wang, V J Harand, A J Przekwas

7. PERFORMING ORGANIZATION NAME(S) AND ADDRESS(ES)
CFD Research Corp
3325 Triana Blvd
Huntsville AL 35805

8. PERFORMING ORGANIZATION REPORT NUMBER
AFOSR-TR- 95 0020

9. SPONSORING/MONITORING AGENCY NAME(S) AND ADDRESS(ES)
AIR FORCE OFFICE OF SCIENTIFIC RESEARCH
DIRECTORATE OF AEROSPACE SCIENCES
BOLLING AFB, DC 20332-6448

10. SPONSORING/MONITORING AGENCY REPORT NUMBER
F49620-92-C-0070

11. SUPPLEMENTARY NOTES

12a. DISTRIBUTION/AVAILABILITY STATEMENT
APPROVED FOR PUBLIC RELEASE
DISTRIBUTION IS UNLIMITED

12b. DISTRIBUTION CODE
A

13. ABSTRACT (Maximum 200 words)

The objectives were to study various dynamic stall control concepts using a code developed under Phase I. The concepts studied were; vortex flaps, apex fence flaps, forebody strakes, spanwise blowing, leading edge blowing and suction, and forebody blowing and suction.

14. SUBJECT TERMS	15. NUMBER OF PAGES
Dynamic stall, CFD	16. PRICE CODE

17. SECURITY CLASSIFICATION OF REPORT	18. SECURITY CLASSIFICATION OF THIS PAGE	19. SECURITY CLASSIFICATION OF ABSTRACT	20. LIMITATION OF ABSTRACT
UNCLASSIFIED	UNCLASSIFIED	UNCLASSIFIED	

CFD Research Corporation

3325 Triana Blvd. • Huntsville, Alabama 35805 • Tel.: (205) 536-6576 • FAX: (205) 536-6590

CFDRC

PRESSURE-BASED HIGH-ORDER TVD METHODOLOGY FOR DYNAMIC STALL CONTROL

SBIR Phase II Final Technical Report

by

H.Q. Yang, Z.J. Wang, V.J. Harrand, and A.J. Przekwas

November 1994

CFDRC Report: 4171/4

prepared for
U.S. Air Force Office of Scientific Research
Bolling Air Force Base, DC 20332

Reporting Period: September 30, 1992 - September 30, 1994
Contract Number: F49620-92-C-0070
Project Managers: Major D. Fant and Dr. L. Sakell

PREFACE

This is the final report for the Small Business Innovative Research (SBIR) Phase II study performed for the U.S. Air Force Office of Scientific Research. The objective of the effort was to develop and validate an advanced pressure-based solution methodology for time-accurate solutions of Navier-Stokes equations for the simulation of unsteady separated flows, and to investigate flow separation control concepts. The duration for the Phase II study was two years. The achievements of the first year effort were presented in an Annual Report entitled, "Pressure-Based High-Order TVD Methodology for Dynamic Stall Control" SBIR Phase II Annual Report. That report described the following activities.

a. assessment of turbulence models;
b. validation of the developed code against 2D and 3D experimental measurements and data;
c. development of computational technique for 3D flow visualization; and
d. preliminary study on flow separation control concepts.

This Final Report summarizes the second year effort in the areas of flow control concepts for wing body and forebodies, especially in:

a. steady suction and blowing along the leading edge of a delta wing;
b. alternate suction and blowing on the delta wing;
c. vortex breakdown control on a delta wing using apex flap;
d. vortical flow control of delta wing configuration with a vectored trailing edge jet;
e. development of directional instability on F-16 forebody;
f. mechanical control of directional instability on F-16 forebody with chine and cutback LEX; and
h. jet blowing control of F-16 forebody.

All computations have been performed by adapting CFDRC's advanced general-purpose CFD code, CFD-ACE. For data analysis, flow visualization, and comparisons with experimental data, the 3D graphics code CFD-VIEW was used.

Both CFD-ACE and CFD-VIEW are commercially available from CFDRC.

The experimental data was obtained from Florida State University, Lehigh University, Wright Patterson Air Force Base, NASA Ames Research Center and United Technologies Research Center.

ACKNOWLEDGEMENTS

The authors wish to acknowledge and thank all those who have contributed to this project:

- Major Dan Fant, the AFOSR technical project monitor, for his constructive suggestions during this project;
- Mr. James Simon and Mr. Stanley Lash of WPAFB for providing experimental data on F-16 forebody, and helpful discussions on the flow physics involved;
- Professor Gad-el-Hak of the University of Notre Dame for helpful discussions on F-16 forebody vortical flow control;
- Professor C. Shih of Florida State University and Professor D. Rockwell of Lehigh University for providing experimental data;
- Dr. A.K. Singhal of CFDRC for his overall guidance;
- Dr. G. Mo of CFDRC for the assistance in the development of the 3D flow visualization tool;
- Mr. G. Hufford of CFDRC for his help in the use of ICEM-CFD; and
- Ms. J. Swann for preparing the typescript of this report.

TABLE OF CONTENTS

		Page
PREFACE		i
ACKNOWLEDGEMENTS		iii
1.	BACKGROUND, OBJECTIVES AND SUMMARY OF ACHIEVEMENTS	1
	1.1 Dynamic Stall	1
	1.2 Significance of Dynamic Stall and Its Control	1
	1.3 Study of Dynamic Stall	2
	1.4 Objectives of the Research Effort	2
	1.4.1 Further Refinement and Validation of the Developed Code	2
	1.4.2 Study of Dynamic Stall Control Schemes	3
	1.4.3 Computational Flow Visualization	5
	1.5 Work Plan	5
	1.6 Achievements of the Project	6
	1.7 Collaborative Efforts	6
	1.8 List of Publications	8
	1.9 Outline of this Report	9
2.	DELTA WING VORTICAL FLOW CONTROL	11
	2.1 Steady Blowing and Suction	12
	2.2 Alternating Blowing and Suction	22
	2.3 Flow Control Over Delta Wing Using Apex Flap	25
	2.4 Vectored Trailing Edge Jet	30
	2.5 Summary of Observations for Delta Wings	39

TABLE OF CONTENTS (Continued)

		Page
3.	F-16 FOREBODY CONTROL	41
	3.1 Computational Model	41
	3.2 Development of Directional Instability of Standard F-16 Forebody	42
	3.3 Use of Cut Back LEX	51
	3.4 Forebody Chines	56
	3.5 Use of Added Chine and Cutback LEX	60
	3.6 Jet Blowing	61
	3.7 Summary of Observations for F-16 Forebody Control	70
4.	POTENTIAL APPLICATIONS	72
	4.1 Examples of Successful Commercialization	72
	4.2 Commercialization of Codes	72
	4.3 Industrial Applications	74
	4.4 Aircraft Related Applications	74
	4.5 Potential Use by Federal Government	75
5.	REFERENCES	79

LIST OF ILLUSTRATIONS

Page

Figure 1.1. Potential Vortex Control Concepts for Phase II Study 4

Figure 2.1. Delta Wing with Rounded Leading Edge 13

Figure 2.2. Computational Grid for 75° Delta Wing with Rounded Leading Edge 14

Figure 2.3. Critical Points for Flow Over a 75° Delta Wing at $\alpha = 54°$, $Re = 1.7 \times 10^4$ 16

Figure 2.4. Comparison of Experimental and Computational Flow Visualization of Vortex Breakdown After Onset of Steady Suction at Time $tU/c = 0.0$ and Abrupt Cessation of Suction at $tU/c = 3.5$ 17

Figure 2.5. Flow Topology of a 75° Delta Wing at $\alpha = 54°$ Subject to Leading Edge Suction at Time $t = 0$ 18

Figure 2.6. Computational Flow Visualization of Vortex Breakdown after Onset of Steady Blowing at Time $tU/c = 0.0$ and Abrupt Cessation of Blowing at $tU/c = 3.5$ 20

Figure 2-7. Sectional Flow Topology for a Delta Wing Subject to Leading Edge Blowing and Suction 21

Figure 2-8. Computational Flow Visualization of Vortex Breakdown After Onset of Alternating Blowing-Suction at Time $tU/c = 0.0$ and Abrupt Cessation of Blowing at $tU/c = 3.9$. $Cm = 0.1$, $tU/c = 0.77$ 23

LIST OF ILLUSTRATIONS (Continued)

Page

Figure 2-9. Computational Flow Visualization of Vortex Breakdown After Onset of Steady (a) Suction (b) Blowing and (c) Alternating Blowing and Suction Along the Half Length of the Leading Edge at $tU/c = 0.0$ and Abrupt Cessation at $tU/c = 3.5$ 24

Figure 2.10. Configuration of Delta Wing with Apex Flap 26

Figure 2.11. Effect of Apex Flap on Vortex Breakdown Over a 75° Delta Wing at $\alpha = 40°$ 27

Figure 2.12. Distribution of Total Pressure Across the Plane of Vortex Core Over a 75° Delta Wing at $\alpha = 40°$ 28

Figure 2.13. Effect of Apex Flap with 15° Downward Deflection on the Vortex Breakdown Over a 70° Delta Wing at Several Angles of Attack 29

Figure 2.14. Effect of Deflection Angle of Apex Flap on Vortex Breakdown Over a 70° Delta Wing at $\alpha = 40°$ 31

Figure 2.15. Computational Model and Grid for Delta Wing Under Consideration 33

Figure 2.16. Vortical Flow Over a 70° Delta Wing at Angle of Attack of 40° 34

Figure 2.17. Control of Vortex Breakdown Using Thrust Vectoring. $Re = 10^5$, $\alpha = 50°$, Effect of Jet Velocity 36

Figure 2.18. Control of Vortex Breakdown Using Vectored Trailing Edge Jet. $Re = 10^5$, $\alpha = 40°$, Effect of the Direction of the Jet 37

LIST OF ILLUSTRATIONS (Continued)

Page

Figure 2.19. Velocity and Pressure Contours Across the Planes of Vortex Cores for a 70° Delta Wing Subject to Thrust Vectoring, Re = 10^5, $\alpha = 40°$ 38

Figure 3.1. Computational Grid Around an F-16 Forebody 43

Figure 3.2. Standard F-16 in Pitch from Experiments 44

Figure 3.3. Axis System and Positive Direction of Moments 45

Figure 3.4. Flow Over an F-16 Forebody at Different Angles of Attack 47

Figure 3.5. Vortical Flows Over a Standard F-16 Forebody at Angle of Attack of 40°, β Sideslip Angle 48

Figure 3.6. Cross Flow Topology Over Standard F-16 Forebody at $\alpha = 40°$ 49

Figure 3.7. Comparison of Body Axis Yawing Moment Coefficients between Present Computations for F-16 Forebody and Experiment of Simon et al for F-16 Full Body at $\alpha = 40°$ 50

Figure 3.8. C_n as a Function of α at $\beta = 4°$ 50

Figure 3.9. Configurations of Standard F-16 Forebody and F-16 Forebody with Cutback LEX 52

Figure 3.10. Comparison of Flow Fields Around an F-16 Forebody With and Without Cut Back LEX at $\alpha = 40°$ 53

LIST OF ILLUSTRATIONS (Continued)

Page

Figure 3.11. Effect of Cutback LEX on Pitching Moment for Experimental Measurement and Corrected Computational Values 54

Figure 3.12. Effect of Cutback LEX on Lift Coefficient for Experimental Measurement and Corrected Computational Values 54

Figure 3.13. Body Axis Yawing Moment Coefficient for F-16 Forebody with Cutback LEX, $\alpha = 40°$, $Re = 1.5 \times 10^5$ 55

Figure 3.14. Configurations of Standard F-16 Forebody and F-16 Forebody with Chine 57

Figure 3.15. Cross-Sectional Streamlines for an F-16 Forebody With and Without Chines; $\alpha = 40°$, $\beta = 0.0°$ 58

Figure 3.16. Effect of Added Chine on Lateral Directional Stability of an F-16 Forebody; $\alpha = 40°$, $\beta = 8°$ 59

Figure 3.17. Cross-Sectional Streamlines for an F-16 Forebody With and Without Chines; $\alpha = 40°$, $\beta = 8°$ 62

Figure 3.18. Yawing Moment Coefficients as a Function of Angle of Sideslip at $\alpha = 40°$ for Standard F-16 and F-16 with Chine 63

Figure 3.19. Configurations of Standard F-16 Forebody and F-16 Forebody with Chine and Cutback LEX 64

Figure 3.20. Vortical Flows over a F-16 Forebody with Chine and Cutback LEX at Different Angles of Attack 65

LIST OF ILLUSTRATIONS (Continued)

Page

Figure 3.21. Effect of Chine and Cutback LEX on Yawing Moment Coefficients at $\alpha = 40°$ 66

Figure 3.22. Forebody Blowing Slots 67

Figure 3.23. Vortical Flow Over F-16 Forebody with and without Jet Blowing 68

Figure 3.24. Cross-Section Streamlines for an F-16 Forebody with and without Jet Blowing; $\alpha = 45°$, $\beta = 0.0°$ 69

Figure 4.1 CFD-ACE Advertisement 76

Figure 4.2 CFD-VIEW Advertisement 77

Figure 4.3. Sample Stall Flows through Rotating Machines 78

1. BACKGROUND, OBJECTIVES AND SUMMARY OF ACHIEVEMENTS

1.1 Dynamic Stall

Dynamic stall is a complex physical event induced by a large amplitude motion of aerodynamic bodies. It is a phenomenon characterized by the shedding and passage over the upper surface of a lifting surface of vortex-like disturbances. Associated with this phenomenon is the generation of intense vorticity near the nose of the body, which occurs as the pitching of the lifting surface dynamically surpasses its stall angle of attack. This vorticity increases the circulation of the flow and thus the lift force acting on the body. As a result, large unsteady aerodynamic forces are generated from which the lift, drag, and moment coefficients greatly exceed their maximum static counterparts. Excellent reviews on the subject have been presented by McCroskey[1,2] and Carr.[3]

1.2 Significance of Dynamic Stall and Its Control

Dynamic stall is of importance in various aerodynamic applications including aircraft maneuverability, helicopter rotors, and wind turbines. For example, when the dynamic stall appears in the retreating blade of a helicopter rotor, it produces a loss of lift, thus an increase in power is required which in turn increases the pitching loads and vibratory stress. Therefore, significant efforts have been devoted to understand and eliminate the undesirable effects associated with dynamic stall on helicopter rotors. On the other hand, recent efforts are exploring the possibility of utilizing the unsteadiness of the flow field to enhance aircraft performance and to attain the sustained dynamic maneuvering in the post-stall flight regime.

The typical post-stall capability maneuver is characterized by a rapid pitch up to a very high angle of attack (up to 90 degrees) followed by a quick recovery to cruise configuration. To obtain efficient high lift, a controlled, separated, leading-edge vortex flow due to dynamic stall is used to produce vortex lift. When the vortex is located on the proper leading edge position, the vortical flow produces significant level of effective leading-edge thrust.

1.3 Study of Dynamic Stall

Dynamic stall research has proceeded along several avenues: analytical, experimental, and computational. Computational Fluid Dynamics (CFD) has in the recent past emerged as a very useful and powerful tool for studying some of the performance characteristics of unsteady separating flows on airfoil configurations. Computer simulation of unsteady flows has been found to be extremely useful in providing insight into the characteristics of the flow in regions inaccessible to flow probes. Indeed, the rapid development of CFD has transformed much of the conventional flow separation control from art to science.[4]

1.4 Objectives of the Research Effort

The overall objectives of the SBIR Phase II research were:

a. to further enhance and validate the pressure-based code developed in Phase I;
b. to use the validated code to study several dynamic stall control concepts; and
c. to develop and use advanced graphical techniques for visualization of complex 3-D flows and to compare numerical and experimental data.

The specific details of the objectives of Phase II are described in the following.

1.4.1 Further Refinement and Validation of the Developed Code

Refinement and enhancement of the present pressure-based methodology was accomplished in the following three aspects:

a. **Extension and Enhancement of Newton's Iteration Technique**
b. **Improved Turbulence Modeling**
c. **Validation Study**
   Systematic comparisons of 3D predicted drag, lift and moment coefficients were made with benchmark experimental measurements. The candidate validation cases include:

1. Compressibility and three-dimensional effects by Carr and Piziali of NASA Ames. These data have been undertaken at NASA Ames Research Center for 2D and 3D wings with NACA0015 and NACA0012 cross-sections;
2. Low Reynolds number 3D high alpha flow by Don Rockwell of Lehigh University;
3. Vortex dynamics on a pitching delta wing by Nelson *et al* of the University of Notre Dame; and
4. Compressibility effect on pitching airfoil by Peter Lorber of UTRC.

1.4.2 Study of Dynamic Stall Control Schemes

With an understanding of basic fluid physics, and the validated CFD code, the various controlling concepts will be investigated by computer simulations. In Phase II, some of the following control concepts were considered.

a. **Vortex flap concept**, Figure 1.1a.[5] The flaps function is to force the separation to take place on the flap and thereby produce a significant thrust component in the upward or downward direction.
b. **Apex fence flaps**, Figure 1.1b.[5] These devices are deployed at an angle to slender delta wing. They alter the vortical flow field and produce an intense suction at the apex which enhances the lift and gives a nose up pitching moment. At high angles of attack, they reduce apex lift and produce a desirable nose-down pitching momentum.
c. **Forebody strake**, Figure 1.1c[6]. These strakes are conformally stored in the forebody, and when deployed, force asymmetric vortex shedding from the forebody, generating a controlled yawing moment.
d. **Spanwise blowing**[6] Figure 1.1d. With realistic blowing rates, the jet momentum can stabilize the leading edge vortices and produce significant lift increments at high angles of attack.
e. **Leading-edge blowing and suction.**
f. **Forebody blowing and suction.**

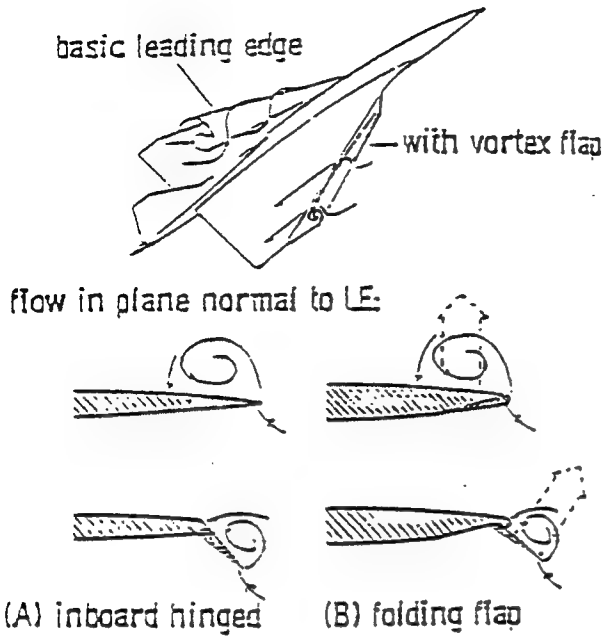

(a) vortex flap concept

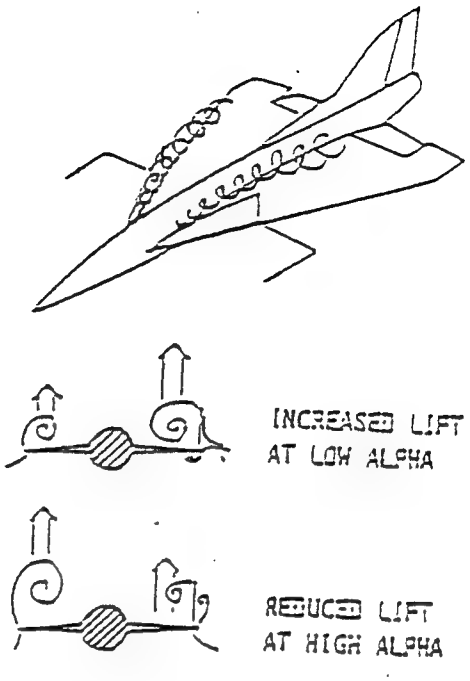

(b) apex fence concept

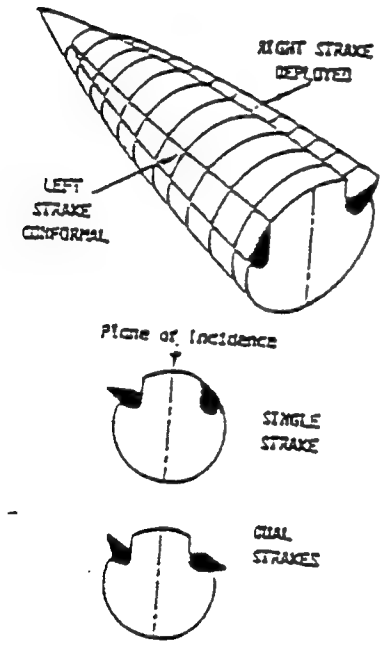

(c) deployable strake concept

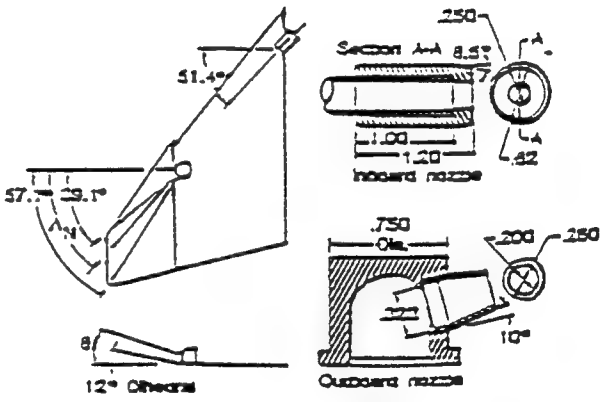

(d) spanwise blowing concept

Figure 1.1. Potential Vortex Control Concepts for Phase II Study

1.4.3 Computational Flow Visualization

Dynamic stall numerical simulations create large data sets which are difficult to analyze with existing graphic postprocessing tools. The following two types of graphic tools were proposed to be developed to process and validate the computational results:

a. Dynamic image generation with animation capabilities, capable of generating shadowgraphs, Schlierens, and interferometry images, smoke traces, *etc*. Automatic detection and display of critical point, lines and surfaces (separation lines, recirculation bubbles, *etc*) are also essential.

b. Graphical image examiner for alignment and comparison of computational versus experimental and computation versus computational flow images.

The objective of the Phase II study was to produce a validated 3-D CFD code, advanced graphics code, and to assess selected stall control concepts. All three of these are of significant value to the U.S. Air Force, Federal Aviation Administration and aircraft manufacturers. A validated code could provide a strong foundation for further research and development of various dynamic stall control schemes for advanced combat aircraft. The developed codes will also be adaptable to other industrial applications such as turbomachinery, compressors, fans and propellers.

1.5 Work Plan

To achieve the objectives stated above, the following work was planned:

a. assess turbulence models for several 2-D dynamic stall flows;
b. incorporate the most suitable high and low Reynolds number models into the 3-D computations;
c. compare computations to the experimental data of Carr and Piziali of NASA Ames Research Center;
d. validate computer code against selected experiments of Lorber, Rockwell, and Nelson;

e. assess two types of wing-body control concepts: (i) vortex flap or apex fence; and (ii) leading-edge blowing and suction;
f. assess two types of forebody control concepts: (i) deployable strake on forebody; and (ii) forebody blowing and suction; and
g. implement an automatic search for critical points to analyze the flowfield dynamics.

1.6 Achievements of the Project

All of the work objectives set forth at the onset of the project have been met. The major achievements of this project can be summarized as follows:

a. systematic assessment of turbulence models for steady and unsteady separated flows;
b. development of visualization software to display computational data as optical images (Shadowgraphs, Interferograms, Schlierens) and to locate and display critical points and lines;
c. quantitative validation of the developed code with a series of experimental data, measurements, and images for 2D airfoil and 3D wing bodies;
d. control study of vortex breakdown on a delta wing by leading-edge steady blowing and suction and alternating blowing and suction;
e. assessment of vortex breakdown using apex flap;
f. study of vortical flow control with a vectorized trailing edge jet;
g. physics of development of directional instability on F-16 forebody;
h. study of mechanical control of directional instability of F-16 forebody with chine and cutback LEX; and
i. investigation of jet blowing control of F-16 forebody.

1.7 Collaborative Efforts

During this project, close collaboration with government laboratories, NASA and universities has been established to validate the computer code and to investigate unsteady flow control concepts.

1. Cooperation with Dr. C. Shih of Florida State University has been established. His detailed flow velocity field from Particle Image Displacement Velocimetry (PIDV) has been used to validate unsteady incompressible flow over an airfoil pitching at a constant rate. Also, their results on vectorized trailing edge jet on delta wing configuration were used.

2. Dr. P.F. Lorber of United Technologies Research Center has been contacted. His experimental data of unsteady airloads and our computational results have been combined to study the compressibility and pitching rate effect on flow separation.

3. Cooperative effort has been established with Mr. Stanley Lash of Wright Patterson AFB, to study the role of nose probe and nose chine on lateral-directional stability and the interaction of the chine vortex system and LEX vortex system. Their experimental measurements were compared with our computations.

4. Dr. Don Rockwell of Lehigh University has been consulted. His PIDV measurement on unsteady flowfield over pitching delta wing was used as benchmark data to study flow topology and to compare detailed flowfields. The alternating blowing-suction at delta wing leading edge to control vortex breakdown was also investigated along with his data.

5. The experimental laboratory of Dr. Carr of NASA Ames Research Center was visited. Their interferograms on pitching NACA 0012 airfoils has been used to compare the "numerical" interferograms which we have produced using our own visualization software. This study gives detailed flowfield and separating flow characteristics unavailable from airload data.

6. Prof. M. Gad-el-Hak of the University of Notre Dame, was consulted on different control techniques for F-16 forebody.

1.8 List of Publications

During this two year effort, the following work related to the present project has been prepared, presented, or published.

1. Yang, H.Q., "Static and Dynamic Stalls on a Forward Swept Wing," Bulletin of American Physical Society, vol. 37, no. 8, pp. 174, 1992.
2. Yang, H.Q. and Przekwas, A.J., "Dynamic Stall on a Three-Dimensional Rectangular Wing," AIAA 31st Aerospace Sciences Meeting, AIAA Paper 93-0637, Reno, NV, 1993.
3. Yang, H.Q., and Przekwas, A.J., "Pressure-Based TVD Methodology for Dynamic Stall Simulation," AIAA 31st Aerospace Sciences Meeting, AIAA Paper 93-0680, Reno, NV, 1993.
4. Yang, H.Q., and Przekwas, A.J., "An Efficient Newton Method for Pressure-Based Methods," Proceeding of 11th AIAA Computational Fluid Dynamics Conference, pp. 1047-1048, Orlando, FL, July 1993.
5. Yang, H.Q., and Przekwas, A.J., "Three-Dimensional Unsteady Separating Flows Around an Oscillatory Forward Swept Wing," AIAA 24th Fluid Dynamics Conference, AIAA Paper 93-2976, July 1993.
6. Yang, H.Q., Habchi, S.D., and Przekwas, A.J., "A General Strong Conservation Formulation of Navier-Stokes Equations in Non-Orthogonal Curvilinear Coordinates," AIAA Journal, vol. 32, pp. 936-941, 1994.
7. Yang, H.Q. and Antonison, M., "Study of Unsteady Flow Field Over a Forward-Looking Endoatmospheric Hit-to-Kill Interceptor," Journal of Spacecraft and Rockets, 1994 (to appear).
8. Yang, H.Q., "Control of Vortex Breakdown on a Delta Wing by Leading Edge Blowing and Suction," AIAA 32nd Aerospace Sciences Meeting, AIAA Paper 94-0622, Reno, NV, 1994.
9. Yang, H.Q., "Numerical Simulation of Dynamic Stall at High Reynolds Numbers," AIAA 32nd Aerospace Sciences Meeting, AIAA Paper 94-0287, Reno, NV, 1994.
10. Yang, H.Q., "Comparison of Numerical and Experimental Optical Images of Compressible Dynamic Stall," AIAA 12th Applied Aerodynamics, AIAA Paper 94-1947, Colorado Springs, CO, 1994.
11. Yang, H.Q., Wang, Z.J., and Przekwas, A.J., "Study of Vortex Breakdown on F-

16 Forebody with Chine and Cut Back LEX," AIAA 12th Applied Aerodynamics Conference, AIAA Paper 94-1805, Colorado Springs, CO, 1994.

12. Wang, Z.J., and Yang, H.Q., "A Unified Conservative Zonal Interface Treatment for Arbitrarily Patched and Overlapped Meshes," AIAA Paper 94-0320, 1994.
13. Wang, Z.J., Yang, H.Q. and Przekwas, A.J., "Numerical Simulation of Acoustic Waves in a Combustor Using Total-Variation-Diminishing Schemes," AIAA Journal, vol. 32, no. 4, pp. 875-878, 1994.
14. Wang, Z.J., Mitchell, C.R., Yang, H.Q. and Przekwas, A.J., "An Enriched Hybrid Grid Approach for Unsteady Multi-Body Flow Computation," 12th AIAA Applied Aerodynamics Conference, AIAA Paper 94-1916, 1994.
15. Wang, Z.J., and Yang, H.Q. "Unsteady Flow Simulation Using a Zonal Multi-Grid Approach with Moving Boundaries," AIAA 32nd Aerospace Sciences Meeting, AIAA Paper 94-0057, 1994.
16. Yang, H.Q., Wang, Z.J., and Przekwas, A.J., "Mechanical Control of Vortices on F-16 Forebody," AIAA 33rd Aerospace Sciences Meeting, AIAA Paper 95-0044, Reno, NV, 1995.
17. Yang, H.Q., Ho, S.Y. and Przekwas, A.J., "A Numerical Study of a Two-Dimensional Foil Subject to High Reduced Frequency Gust Loading," submitted to AIAA 26th Fluid Dynamics Conference, San Diego, CA, 1995.
18. Yang, H.Q., Wang, Z.J., and Przekwas, A.J., "Control of Vortices on F-16 Forebody Using Jet Blowing," submitted to AIAA 13th Applied Aerodynamics Conference, San Diego, CA, 1995.
19. Yang, H.Q., "Control of Vortex Breakdown on a Delta Wing Using Vectorized Trailing Edge Jet," submitted to AIAA 13th Applied Aerodynamics Conference, San Diego, CA 1995.

1.9 Outline of this Report

In the following sections, the results of the second year effort are presented in the areas of:

a. **Delta wing vortical flow control:**
   - steady blowing or suction
   - alternating blowing and suction

- leading edge flap
- trailing edge vectorized jet

b. **F-16 forebody flow control:**
- development of directional instability
- mechanical control using chine and cutback LEX
- pneumatic control at nose tip
- unsteady effect due to constant rate pitching

c. **Potential applications:**
- example of successful commercialization
- commercialization of codes
- industrial applications
- aircraft related applications
- potential use by Federal Government

2. DELTA WING VORTICAL FLOW CONTROL

Modern aircraft rely on the development of strong, stable vortices over the upper surface of the wing to enhance their lifting capability. At high angle-of-attack, however, the vortices become unstable and break down, thus causing a significant loss of lift. Detailed insight and proper control of vortex breakdown is of importance to extend the flight envelope of current aircraft. A series of works have been documented in the literature on the study and control of leading edge vortices[1-37]. It is generally realized that the control of leading-edge vortices can be accomplished by altering the vortex trajectory using active techniques such as blowing and suction. As the leading-edge is the vortices emanating region, blowing and suction at the leading-edge is expected to be very effective. Shi *et al* [34] conducted a sensitivity study of the blowing jet position on the vortex breakdown point in water tunnel test. Reward blowing and tangential blowing to the core were shown to delay breakdown. While spanwise blowing was shown to be specially effective at moderate angles and lower Reynolds numbers. A comprehensive investigation on the effect of using a jet of air to control vortex breakdown position was carried out by Visser *et al* [36] to optimize the blowing position. Their results showed that the location of air jet was critical in achieving the maximum lift increment for a given momentum coefficient, and the nozzle position was at an optimum location when lying at the leading edge and aligned with it.

Numerical investigation of leading-edge blowing was performed by Findlay *et al* [37]. Several blowing arrangements including variable slot size and location as well as different blowing directions and rates were addressed. More recently, Gu *et al* [33] investigated experimentally the control of vortical flow past a half delta wing at high angle of attack. The application of steady blowing, steady suction or alternating suction-blowing in the tangential direction along the leading edge of the wing is shown to substantially retard the onset of the vortex breakdown and stall. The most effective period of the alternating suction-blowing is found to be of the order of one convective time scale of the flow past the wing.

The objective of the present research is to numerically study the control of vortex breakdown on a delta wing. The application of the control includes steady blowing, steady suction, and alternative blowing-suction. The special interest is on the

response of vortex breakdown point to the application of control. The change of flow field will be studied by flow topology. Comparison with experiments of Gu, Robinson, and Rockwell [33] will also be made.

2.1 Steady Blowing and Suction

The transient response of the vortex core to the application of blowing and suction is studied. The model under consideration is the same as that of Gu *et al* [33]., and is shown in Figure 2.1. The delta wing has a rounded leading-edge and a sweep angle λ of 75°. The wing is subject to an angle-of-attack of α=54°. The computational grid as shown in Figure 2.2 is of the O-H type, and is obtained by simple algebraic interpolation. The mesh has 80 grid points in circumferential direction, 40 in the normal direction and 50 in the streamwise direction. Due to symmetry property of the flow, only half of the field is modeled. The far field boundary is located two chord lengths away from the wing surface in the normal direction and one and half chord lengths away in the upstream and downstream directions. The effect of far field boundary is found insignificant with further far boundary. At the inlet, the free stream properties are specified, and symmetry conditions are applied along the mid-plane of the wing. On the wing surface, no slip condition is imposed. The Reynolds number corresponding to the chord length is 1.7×10^4, and the flow is taken as laminar. Since the experiment was carried out in a water tunnel, the flow is assumed to be incompressible in the computation. It should be emphasized that the current pressure-based method can handle both incompressible and compressible flows with equal efficiency. It is for comparison purposes that incompressible flow is assumed.

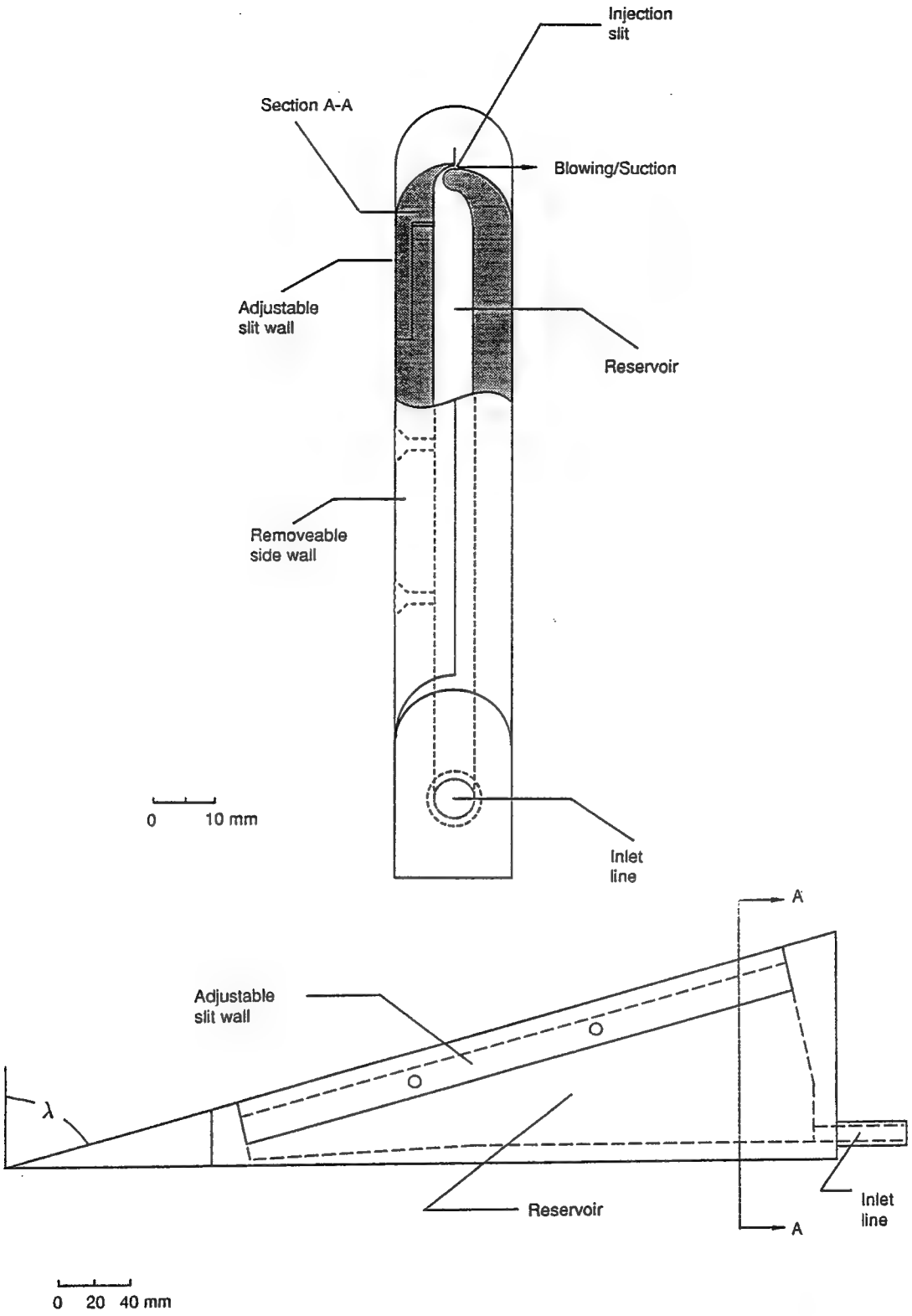

Figure 2.1. Delta Wing with Rounded Leading Edge. The steady or alternating blowing-suction is in the direction tangential to leading edge of wing.

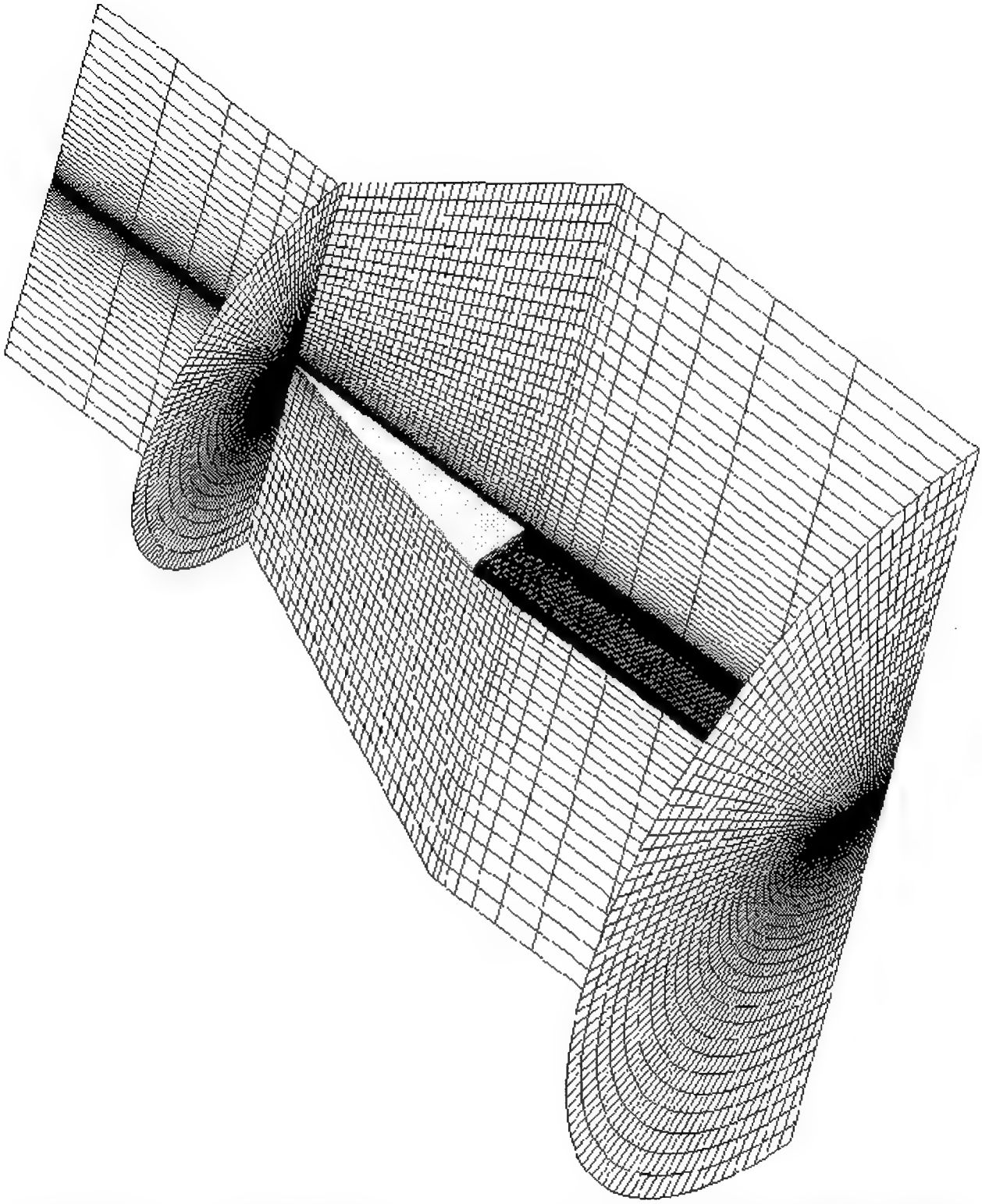

Figure 2.2 Computational Grid for a 75° Delta Wing With Rounded Leading Edge

Steady Suction

The effectiveness of blowing and suction on the vortex breakdown is studied at α = 54°. The suction coefficient is C_μ = -0.10. First the flow field at α = 54° without blowing and suction is computed, and is demonstrated in Figure 2.3. The flow topology analysis gives two critical points related to the leading edge vortex. One is a repelling spiral saddle and the particle trace approaching the point is the vortex core. This point is the vortex burst point. Another critical point is an attracting spiral saddle located at the trailing edge of the delta wing. The sectional vorticity field indicates that (not shown here) before the vortex breakdown point, the vorticity field is strong and coherent near the leading edge. Downstream of the point, the vorticity is quite dissipated.

The flow characteristics under the condition of suction is then considered. The time step size is chosen such that $\Delta t\, U/c = 0.005$. Further decrease in time step size is found to produce negligible differences in the flow field. The suction starts abruptly at $tU/c = 0$ and is discontinued at $tU/c = 3.5$. The dynamic response of the vortical field is shown in Figure 2.4. The vortex burst point moves downstream with time, and there seems to be an overshoot at tU/c=1.7. Once the suction stops at tU/c=3.5, the vortex breakdown point relaxes to its equilibrium position. The corresponding experimental dye visualization of Reference 33 is also given in Figure 2.4 for comparison. It is clear that the present computation agrees favorably with the experiment.

Figure 2.5 shows the flow topology during the initial time after the application of suction. As with Figure 23, at $tU/c = 0.0$, there are one repelling spiral saddle (denoted by S^+) and one attracting spiral saddle (denoted by S^-). By $tU/c = 0.8$, two additional saddles appear, one attracting and one repelling. It is also noted that S_1^+ and S_2^- approach each other. Referring to Figure 2.4 at $tU/C = 0.8$, it can be seen that the vortex breakdown is of bubble type, and the bubble size is represented by the distance between S_1^+ and S_3^- in Figure 2.5. By time $tU/c = 1.7$, two more saddles are generated between S_3^- and S_4^+. It also appears that another bubble is formed next to the preceding bubble, and its size is measured by S_3^- to S_5^+. This type of bubble has

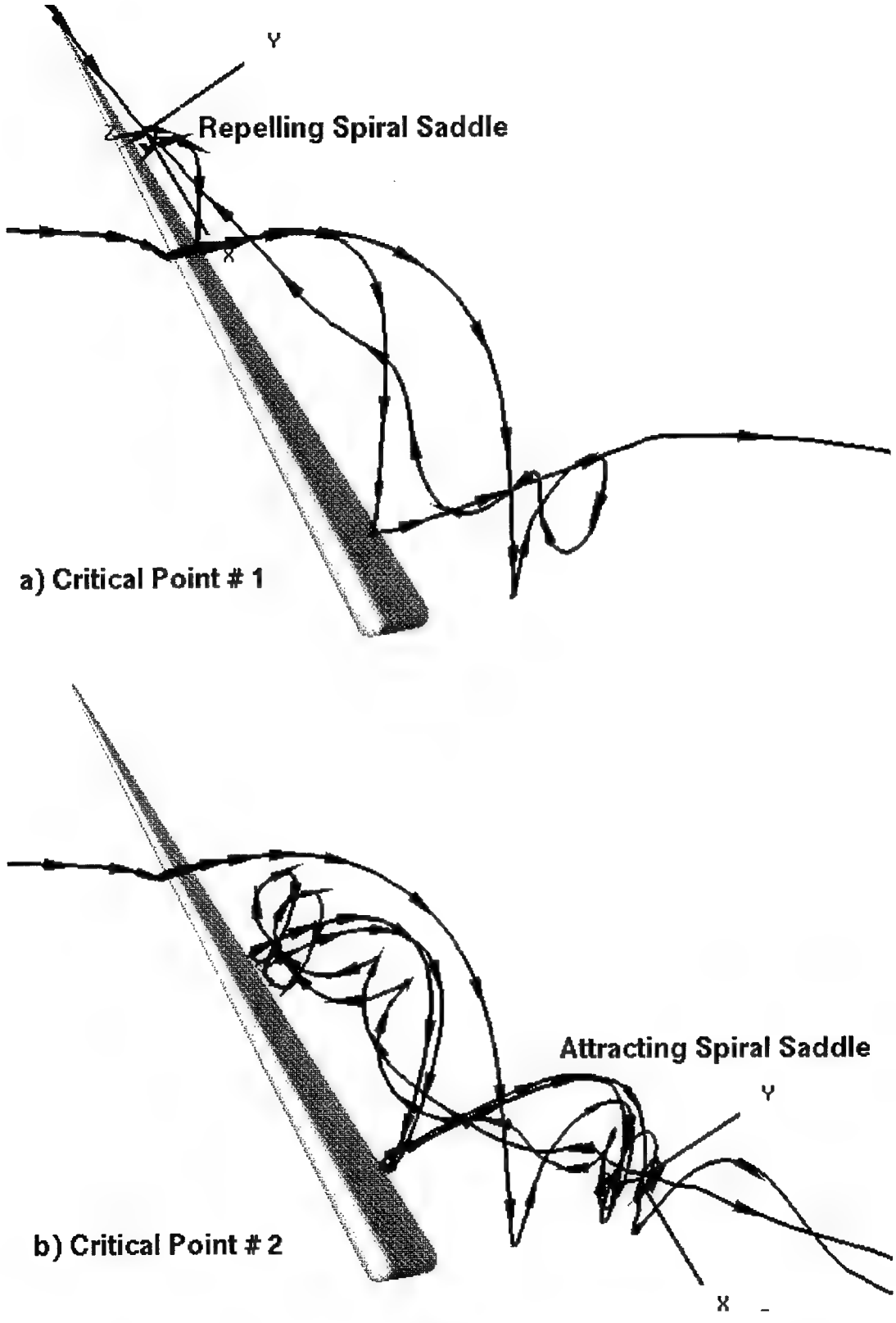

Figure 2.3 Critical Points for Flow Over a 75° Delta Wing at α=54°, Re=1.7x10^4

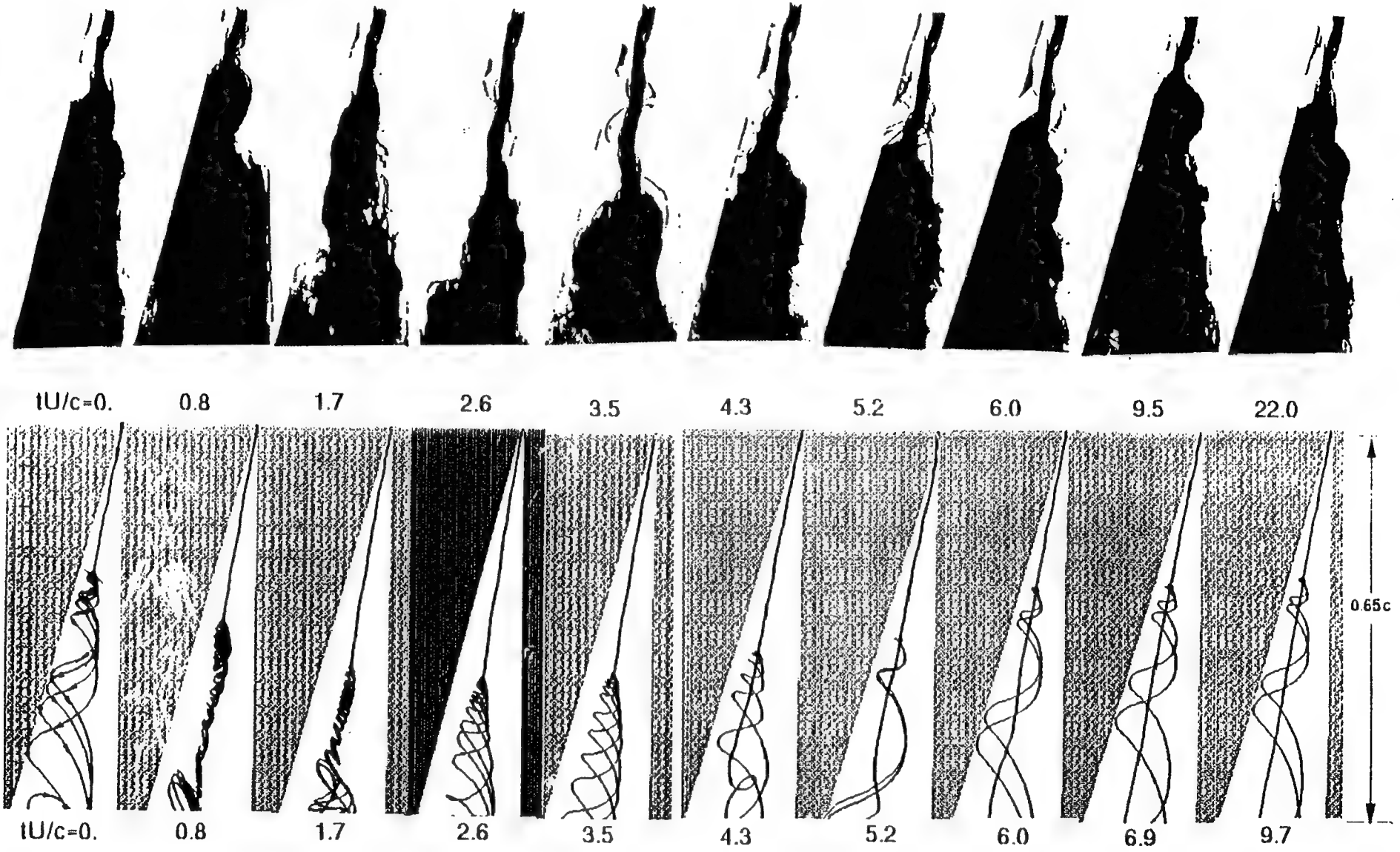

Figure 2.4. Comparison of Experimental and Computational Flow Visualization of Vortex Breakdown After Onset of Steady Suction at Time tU/c = 0.0 and Abrupt Cessation of Suction at tU/c = 3.5

4171/4

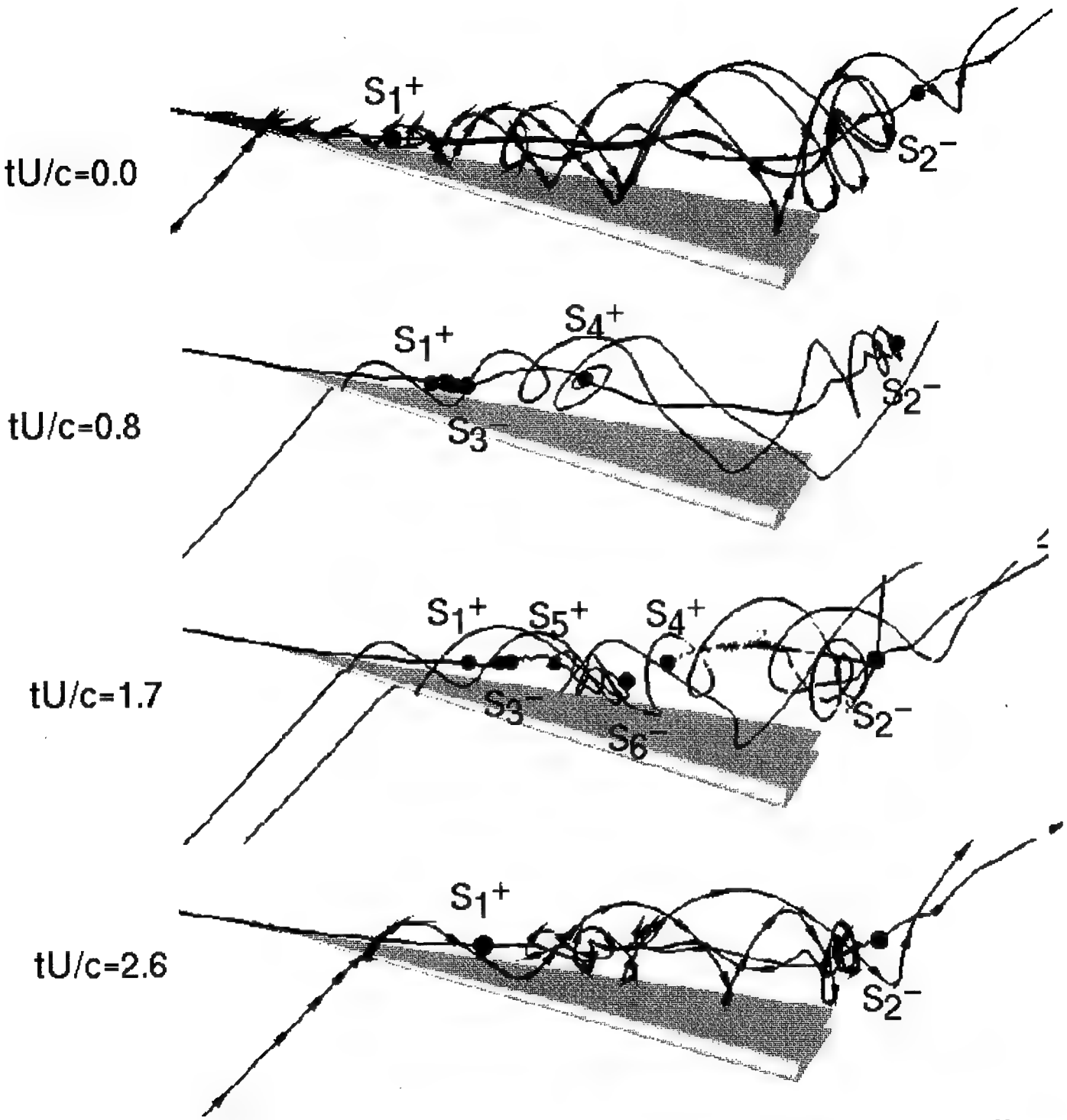

S^+ : Repelling Spiral Saddle; S^- : Attracting Spiral Saddle

Figure 2.5 Flow Topology of a 75° Delta Wing at α=54° Subject to Leading-Edge Suction at Time t=0.

also been found in Visbal's computation for pitching delta wing.[32] By time tU/c = 2.6, the two bubbles combine together, critical points S_3 to S_6 collapse and disappear, and the breakdown becomes spiral type again.

Steady Blowing

Instead of suction as in the previous case, the computations with steady blowing were made. The flow conditions are the same *i.e.*, $\alpha = 54°$, and the blowing coefficient is now $C_\mu = 0.10$. The transient characteristics of the vortex breakdown are shown in Figure 2.6. With the onset of blowing, the vortex burst point responds quickly and with a significant overshoot. At the same time, the vortex core moves away from the leading edge and produces a "buckling" shape. After the initial transient, the vortex core starts to stabilize as evident at tU/c = 0.8, and is recovering to its equilibrium position under steady blowing (see Figure 2.6 for tU/c = 1.7, 2.6 and 3.5). It is interesting to note that the abrupt cessation of blowing at tU/c = 3.5 produces another overshoot of downstream movement of the vortex breakdown point. It is also noticed that the vortex core moves toward the leading edge. The vortex breakup pattern at cessation of blowing (tU/c = 4.3) is found to follow the same route as the onset of suction (see Figure 2.4 at tU/c = 1.7): bubble type breakdown is formed for a short period of time and is switched rapidly to the spiral type.

Figure 2.7 illustrates the crossflow topology of the vortical flow without blowing and suction, and with blowing (tU/c = 3.5) and with suction (tU/c = 3.5) at the same location of 0.3c from the apex. The flow topology is characterized by an unstable focus and a limit cycle. The streamline pattern exhibits an outward spiral motion near the vortex core and is approaching the limit cycle. On the other hand, the separating streamline from the leading edge spirals inward toward the limit cycle. The limit cycle, according to Visbal and Gordnier[38] is called stable limit cycle. For characterization of crossflow topology of vortical flow, the reader is referred to an excellent article by Visbal and Gordnier.[38]

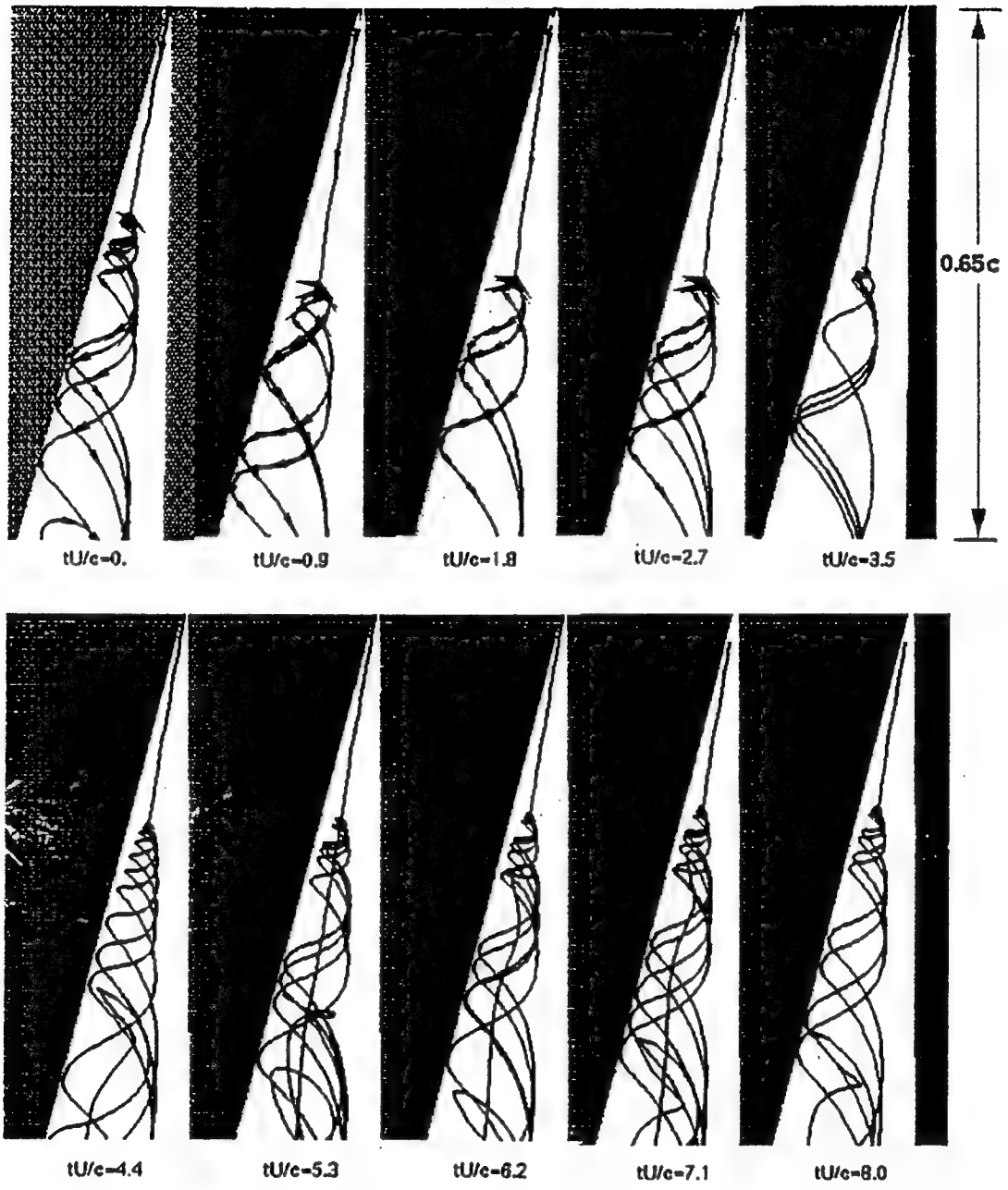

Figure 2.6. Computational Flow Visualization of Vortex Breakdown after Onset of Steady Blowing at Time tU/c = 0.0 and Abrupt Cessation of Blowing at tU/c = 3.5

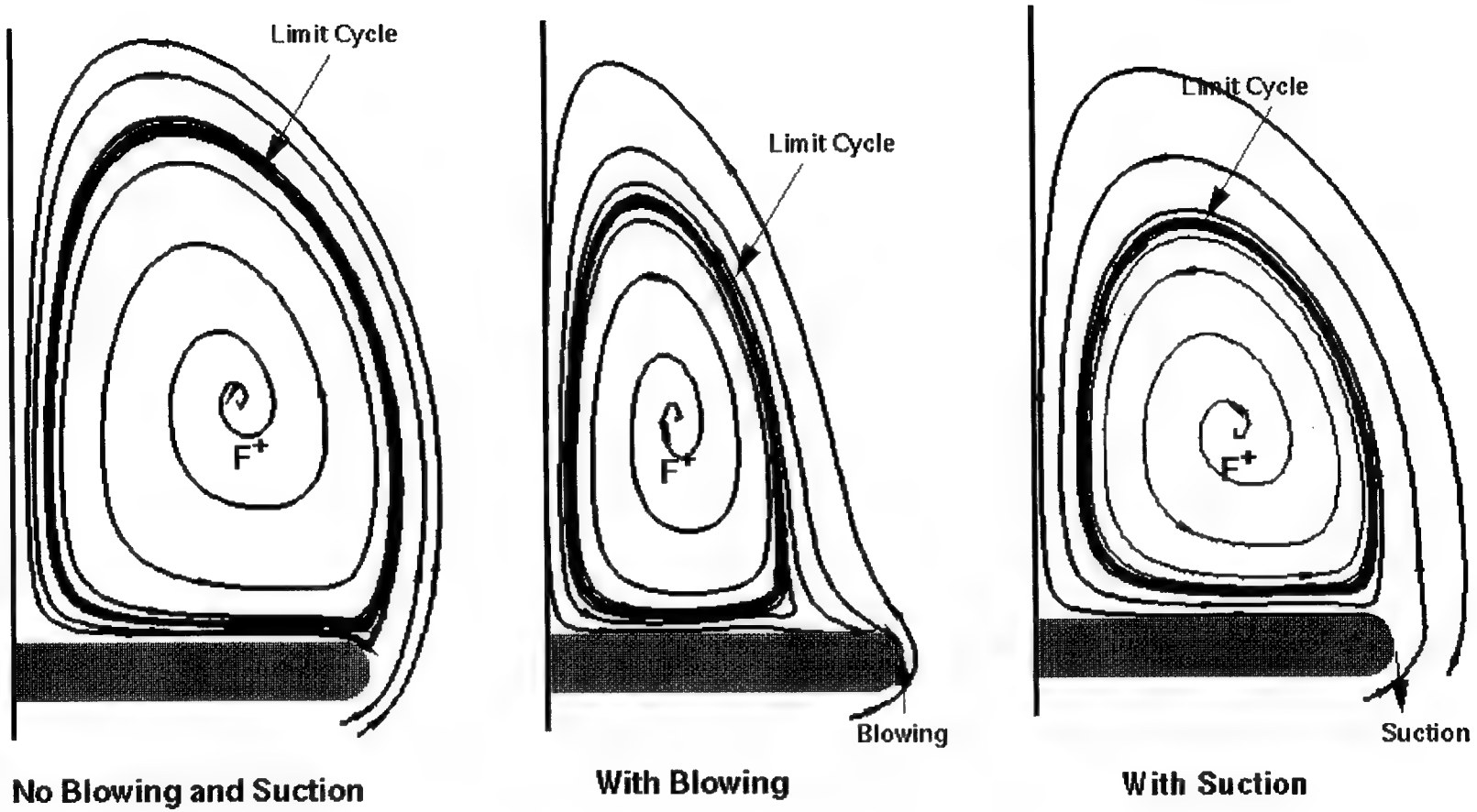

Figure 2.7 Sectional Flow Toplogy for a Delta Wing Subject to Leading Edge Blowing and Suction

As seen from Figure 2.7, blowing at the leading edge in the tangential direction pushes the vortex core inboard and reduces the size of the limit cycle. It is also noted that the flow from the blowing slot feeds into the limit cycle and hence increases the rotational context of the vortical flow. As a result, the vortex core is stabilized and the vortex breakdown point moves downstream. As for the suction, the limit cycle is also reduced, and the suction increases the velocity of feeding stream and changes the rotation content of the vortex.

2.2 Alternating Blowing and Suction

The above calculations for the transient response of vortex breakdown to the instantaneous application of blowing or suction shows that there is a significant overshoot in the movement of the vortex burst point. This overshoot can be efficiently utilized through alternating blowing and suction.[39] As seen from Figure 2.8, the response time of vortex motion to the abrupt application or cessation of blowing or suction is about $tU/c \sim 1.0$. Indeed, the experimental study of Gu *et al*[33] concluded that the optimum period of the alternating blowing and suction corresponds approximately to one convective time scale for optimum displacement of the onset of vortex breakdown. With this in mind, an alternating blowing-suction period of $tU/c = 0.77$ shown in Figure 2.8a is applied at the delta wing leading edge. The corresponding vortex breakdown pattern is given in Figure 2.8b. As expected, the overshoot property of the vortex breakdown is fully utilized (see $tU/c = 1.7$ and 2.5) and the vortex breakdown point has been moved down toward the trailing edge for a significant distance for the whole time.

Effect of Blowing-Suction Location

For the results reported above, the blowing and suction slot extended along the entire leading edge. Figure 2.9 represents the same type of computations: steady blowing, steady suction, and alternating blowing-suction. The blowing and suction is only applied along the half chord length from the apex. The general characteristics of the vortex breakdown movement is about the same as those in Figures 2.4, 2.6, and 2.8, the distance of movement, however, is shorter.

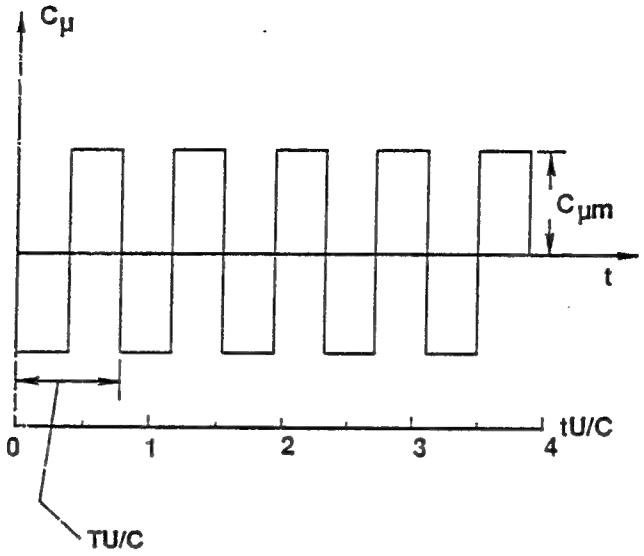

(a) schedule of alternate blowing-suction

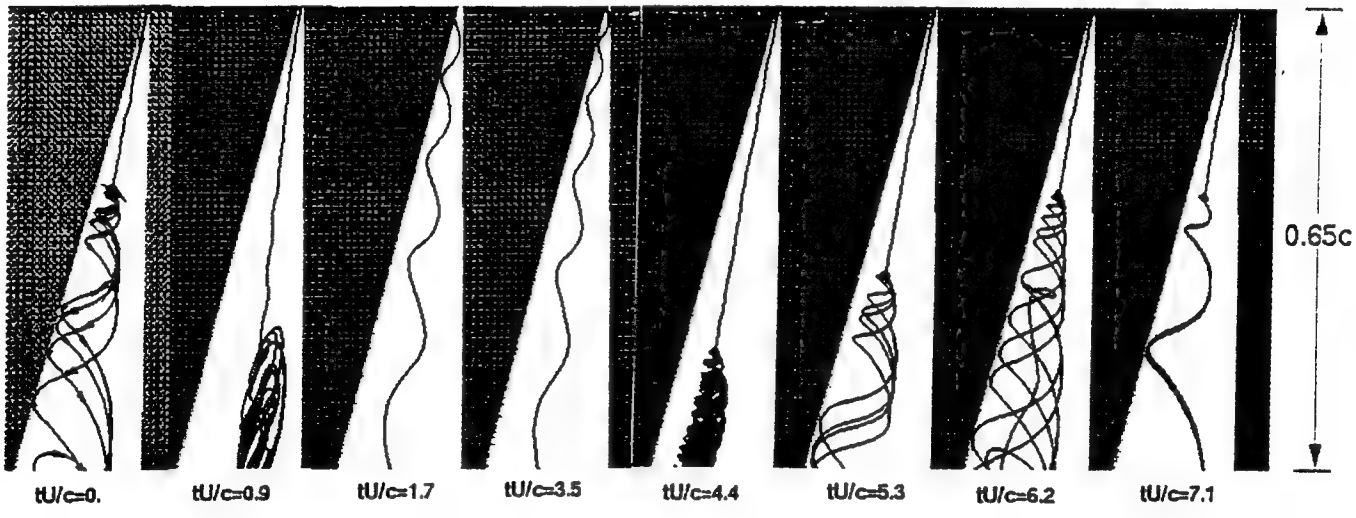

(b) response of vortex breakdown to the alternating blowing-suction

Figure 2-8. Computational Flow Visualization of Vortex Breakdown After Onset of Alternating Blowing-Suction at Time $tU/c = 0.0$ and Abrupt Cessation of Blowing at $tU/c = 3.9$. $C_m = 0.1$, $tU/c = 0.77$

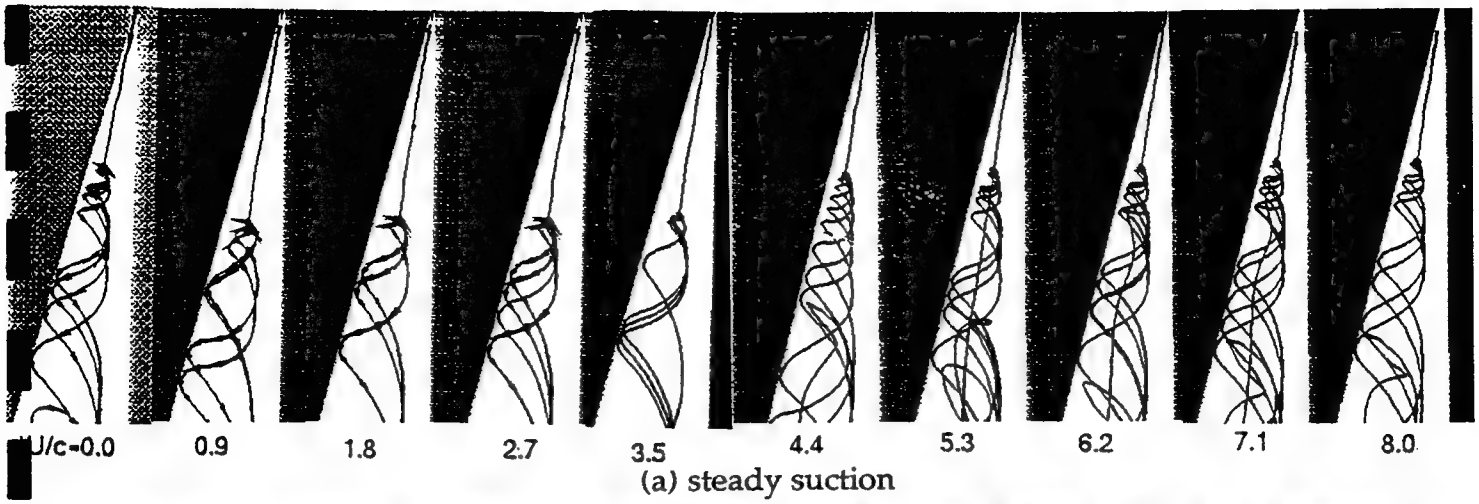

(a) steady suction

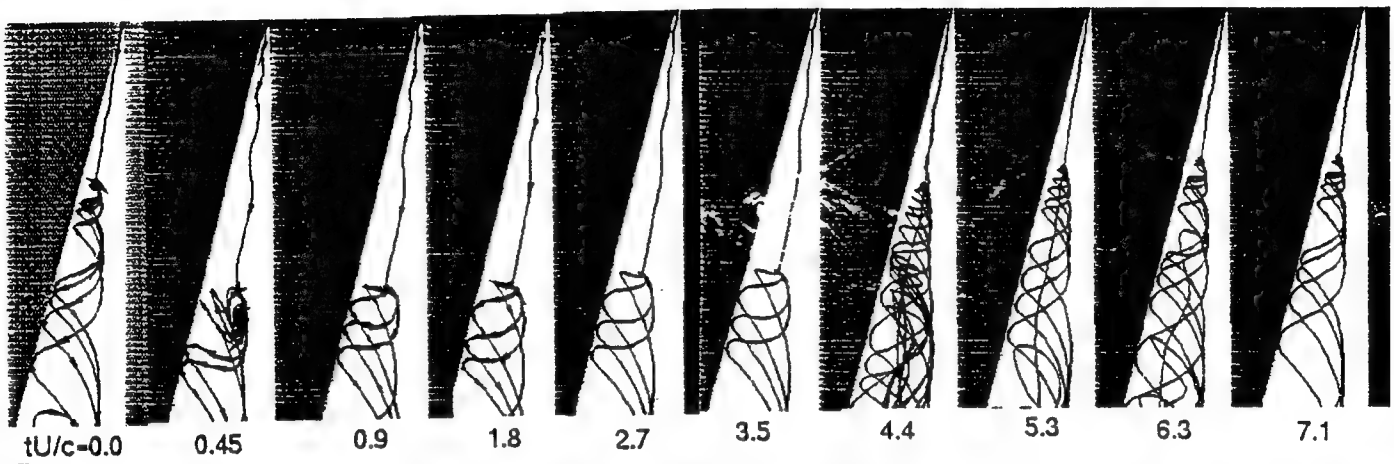

(b) steady blowing

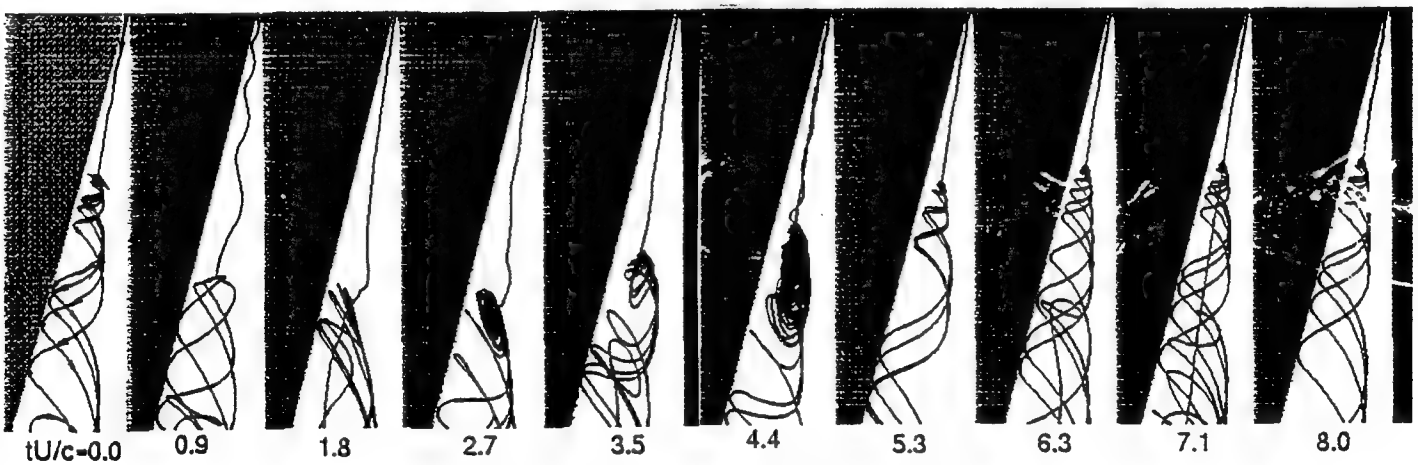

(c) alternating blowing and suction

Figure 2-9. Computational Flow Visualization of Vortex Breakdown After Onset of Steady (a) Suction (b) Blowing and (c) Alternating Blowing and Suction Along the Half Length of the Leading Edge at $tU/c = 0.0$ and Abrupt Cessation at $tU/c = 3.5$

2.3 Flow Control Over Delta Wing Using Apex Flap

In addition to blowing and suction, the control surface can be used to control vortex breakdown and to influence forces and moments over delta wings. Rao and Cumbell[40] discussed several vortical flow devices including leading edge vortex flap which can operate either on the lower or upper surfaces of a delta wing. Klute et al[41] studied experimentally the possibilities of delaying vortex breakdown to higher angles of attack by employing a control surface, such as apex flap. They employed flow visualization, surface pressure measurements, and Laser-Doppler velocimetry to map out pressure, velocity and vorticity fields. It was found that a dropping apex flap can delay vortex breakdown by angles of 8° beyond the steady flow breakdown angle, and the most effective device was the apex flap.

In this study, we simulated the effect of the apex flap on the vortex breakdown using a 70° delta wing. The Reynolds number is 1.5×10^6. The computational model is shown in Figure 2.10. The deploying angle is defined as positive when the front portion of the delta wing model is dropping. Figure 2.11 shows the vortex breakdown features at $\alpha = 45°$ with two steady flapping angles, one is up at 15°, and the other is down at 15°. The vortical flow of a standard delta wing is also given. It is seen that when the apex of the delta wing is flapped upward, it promotes vortex breakdown, thus the burst point moves to the apex. Actually, for the apex, the equivalent angles of attack is increased for this case. When the apex is flapped downward, the vortex breakdown point shifts to the trailing edge of the delta wing.

Figure 2.12 depicts the distribution of total pressure across the plane of the vortex core. The vortex breakdown point is seen to correspond to the local minimum total pressure. Also, there is a recovery of total pressure following the breakdown point.

Figure 2.13 shows the effect of angles of attack on the efficiency of vortex breakdown delay due to apex flap. Here the apex flap is on the 15° downward deflection. Comparison is made with the standard delta wing configuration without apex flap. It appears that for $\alpha > 35°$, the breakdown is delayed for about 5°~8° by using apex flap. This is in fair agreement with the experiment of Klute et al[41] which showed 8° delay.

Top View

Side View

(a) Delta Wing Configuration

Top View

Side View

(b) Delta Wing with Apex Flap

Figure 2.10 Configuration of Delta Wing with Apex Flap

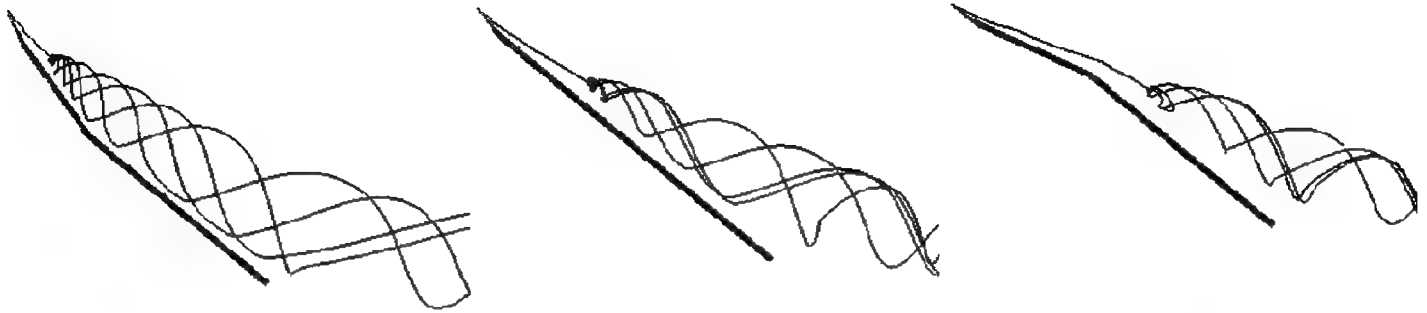

Side View

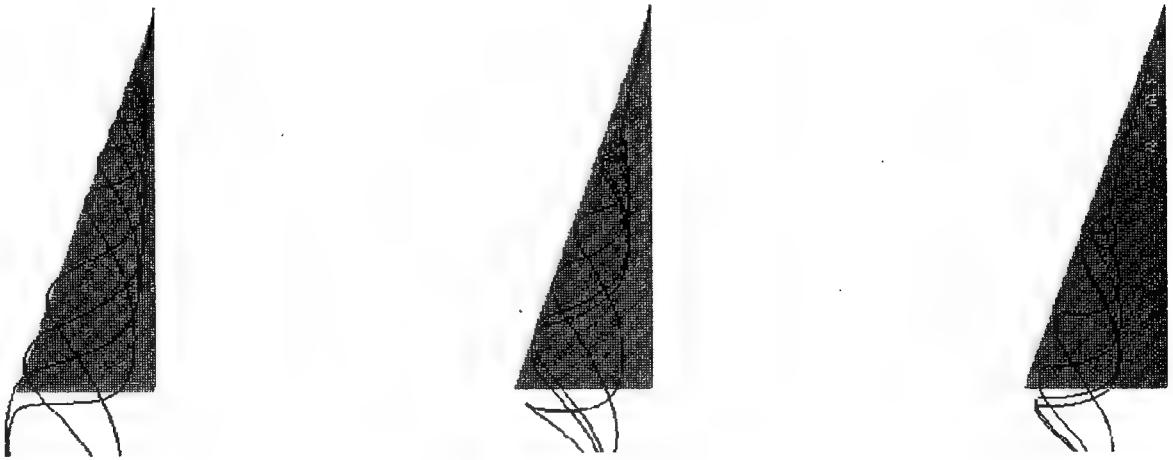

Top View

Flap Up 15° | No Flap | Flap Down 15°

Figure 2.11 Effect of Apex Flap on Vortex Breakdown Over a 70° Delta Wing at α=40°, Re=1.5x10^6

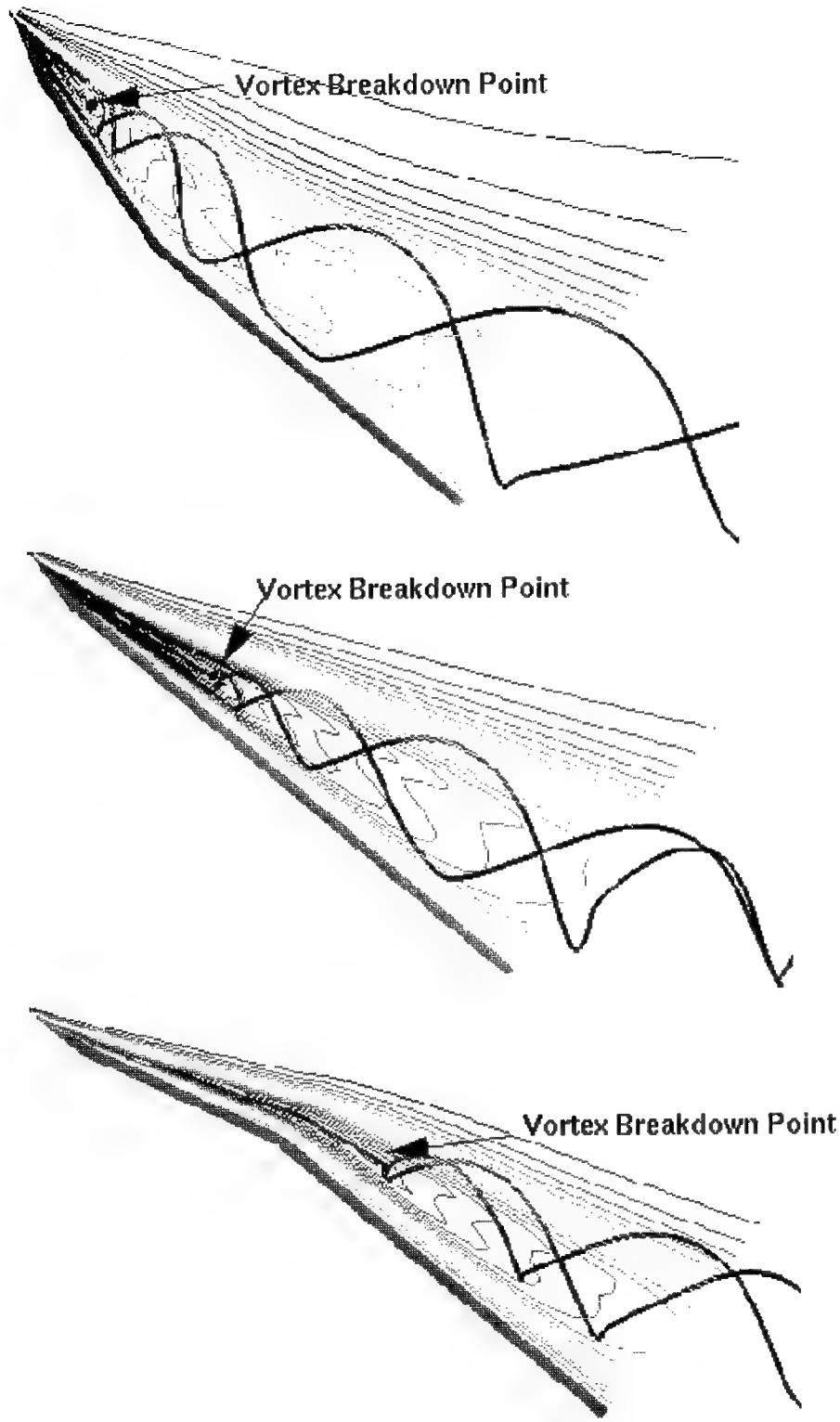

Figure 2.12 Distribution of Total Pressure Across the Plane of Vortex Core Over a 70^{o} Delta Wing at $\alpha=40^{o}$

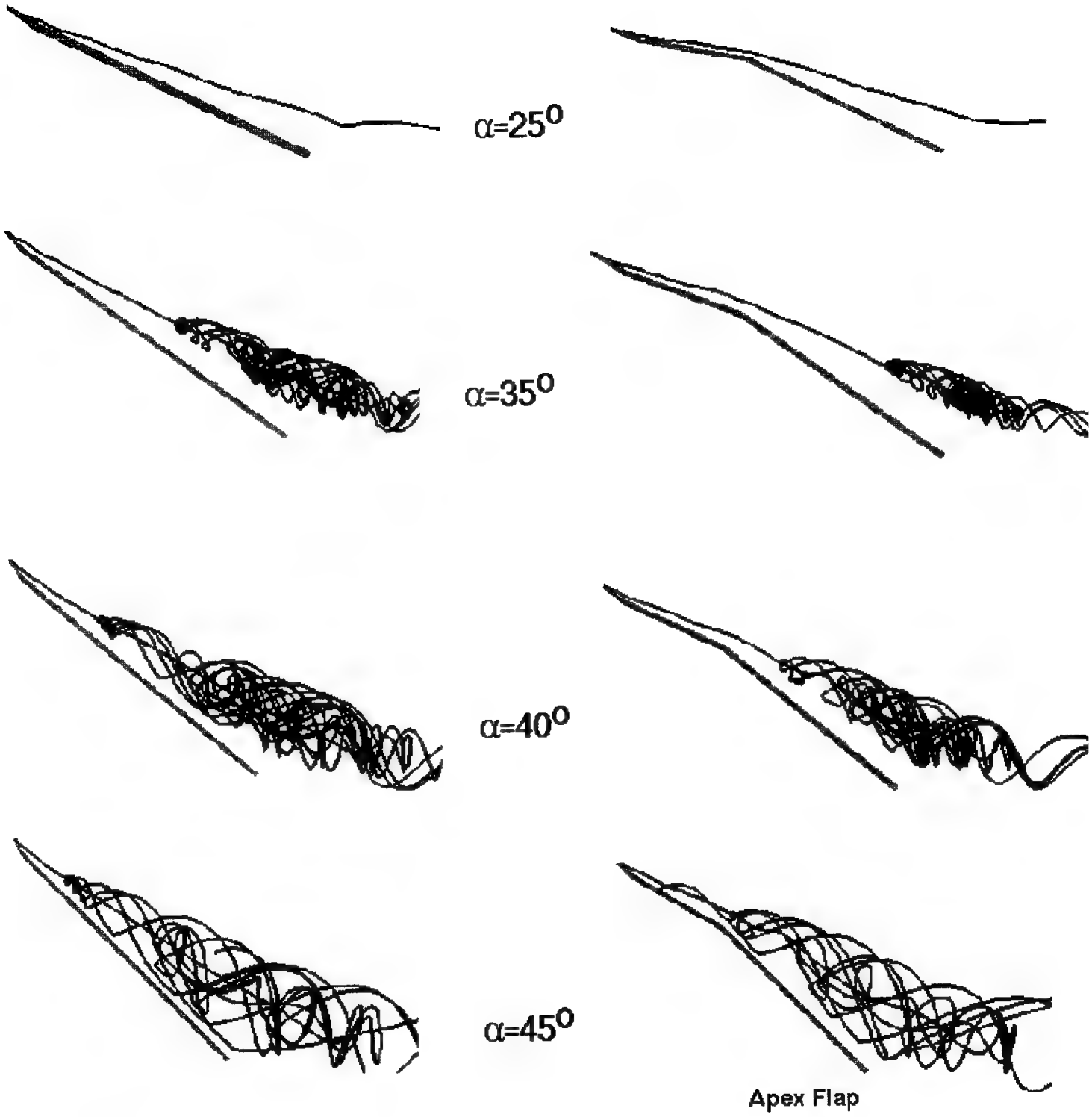

Figure 2.13 Effect of Apex Flap With 15° Downward Deflection on the Vortex Breakdown Over a 70° Delta Wing at Several Angles of Attack

Figure 2.14 shows the variation of vortical flow field with the angle of apex flap reflection. Apparently, upward deflection promotes breakdown and downward deflection suppresses the breakdown. Also, the delay of vortex breakdown reaches the maximum at about $\beta = 15°$, as shown in the experiment[41].

2.4 Vectored Trailing Edge Jet

Aircraft maneuverability and controllability were typically determined by aerodynamic control surfaces. The performance of these control surfaces were limited by the stall barrier at high angles of attack, and at extremely high pitch, yaw, and rolls, where well-established aerodynamic concepts and flight control means fail. Consequently, various means of control techniques, such as boundary-layer blowing/suction, geometrical modifications, *etc.* have been attempted previously to extend the flight envelop. The application of thrust vectoring techniques, while relatively common in rocket and missile propulsion, is in its infancy with air-breathing propulsion. Current design trends indicate that future fighter aircraft will rely heavily on two- and three-dimensional thrust vectoring engines to boost their maneuverability. There are only very few studies on thrust vectoring control of delta wing vertices. Helin and Watry[42] used a 60° delta wing model in water tunnel to study the effect of trailing edge jet exhaust on the burst location. Their results showed that at moderate angles of attack, it is possible to delay the burst location up to 18% of the chord by increasing the flow velocity from the exhaust ports. In addition, at high angles of attack, the trailing edge jets stabilized the asymmetric separated vertices by reattaching the flow and moving the burst location aft on the wing. Shih *et al.*[43] studied the motion-induced aerodynamic effects during rapid angular motions (pitch) in the presence of thrust vectoring. They showed that the favorable pressure gradient produced by the 30 degree downward positioning trailing edge jet delays the vortex burst for all angles of attack tested.

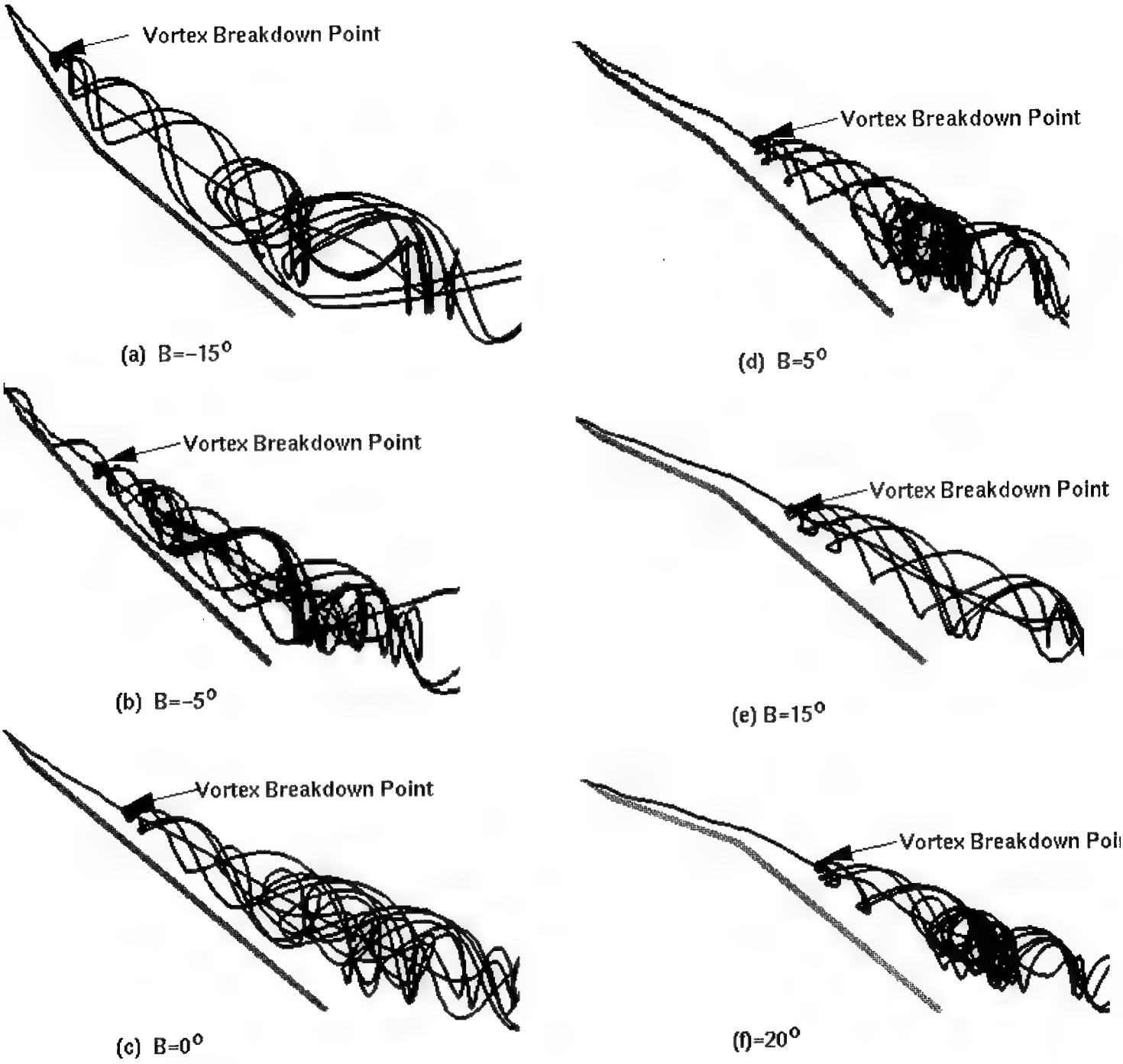

Figure 2.14 Effect of Deflection Angle of Apex Flap on Vortex Breakdown Over a 70° Delta Wing at α=40°

The overview of the whole delta wing (rather than half delta wing) configuration and computational grid are given in Figure 2.15. The wing has a chord length of 0.762 m and a 25° under-surface beveling along the leading and trailed edges. The sweep angle λ of the wing is $\lambda = 70°$. The corresponding computational grid is of the O-H type, and is obtained by simple algebraic interpolation. The mesh has 160 grid points in circumferential direction, 40 in the normal direction and 50 in the streamwise direction. The far field boundary is located two chord lengths away form the wing surface in the normal direction and one and half chord lengths away in the upstream and downstream directions. As before, the Reynolds number is 1.5×10^6.

Figure 2.16 shows the vortical flow field over the above 70° delta wing at $\alpha = 40°$. The vortex breakdown points are determined by the topological analysis package developed in this project. These vortex breakdown points are associated with the stagnation point (critical point) of the flow field. By releasing particles from the critical point, one can find the vortex core, and envelope of the bursting region. One may notice that the flow is not quite symmetric even though the conditions are symmetric. Indeed, experiments have been reported on the asymmetry of flows at high angles-of-attack. The cross flow topologies are also shown in Figure 2.16. At the station A-A, near the apex of the delta wing, the topology of the flow is characterized by two attracting focuses, where particle flows into the critical point. This represents the local axial acceleration of vortex. At station B-B, the critical point leaves repelling focus, and there are two limiting cycles in the cross-section. The particles from both leading edge and repelling focus are attracted to the limiting cycle. Visbal and Gordiner[38] named the cycle as "stable limiting cycle".

At downstream station C-C, (before the vortex breakdown point) the limit cycle breaks up, such that the fluid particles spiral outward from the vortex core, and the particles released at the leading edge become a separation line between the outside ir-rotational flow and outward spiral vortical flow.

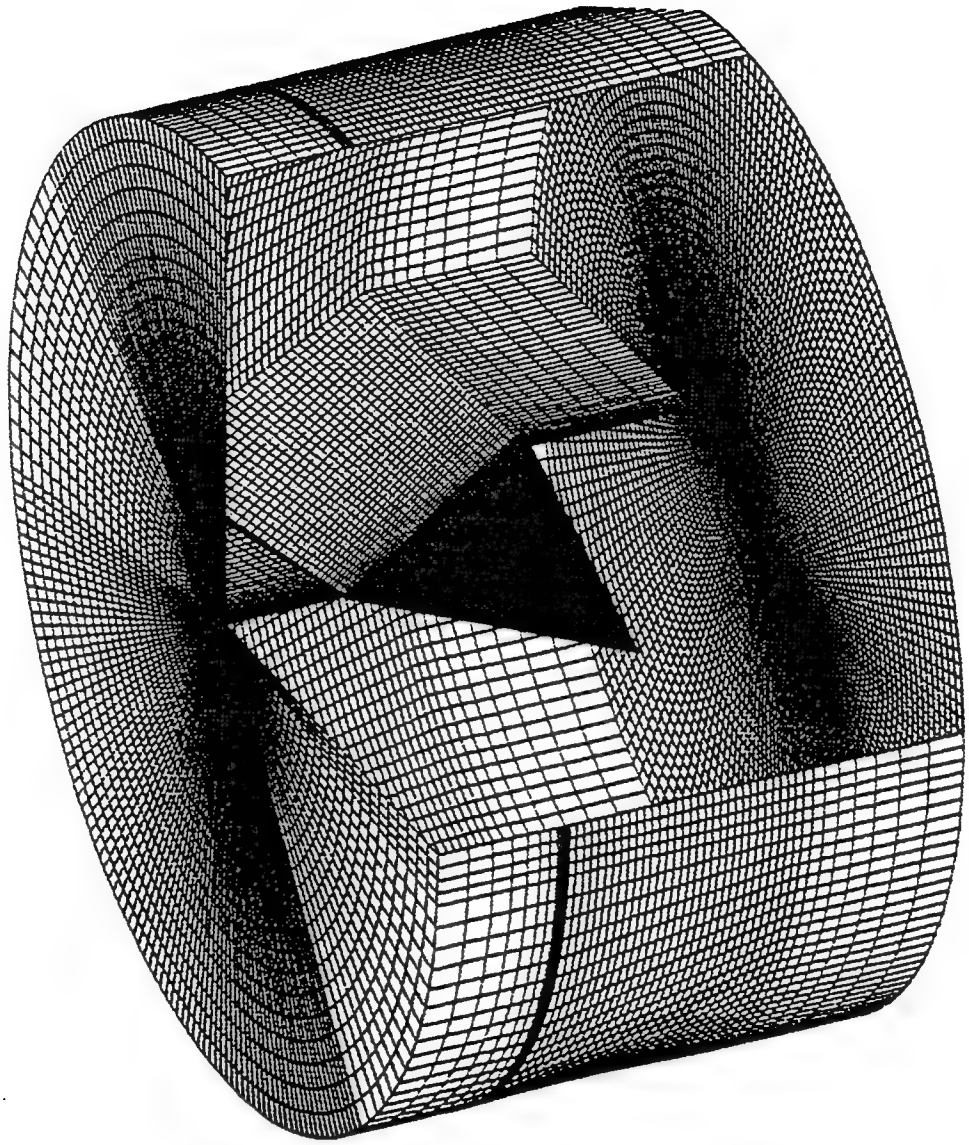

Figure 2.15. Computational Model and Grid for Delta Wing Under Consideration

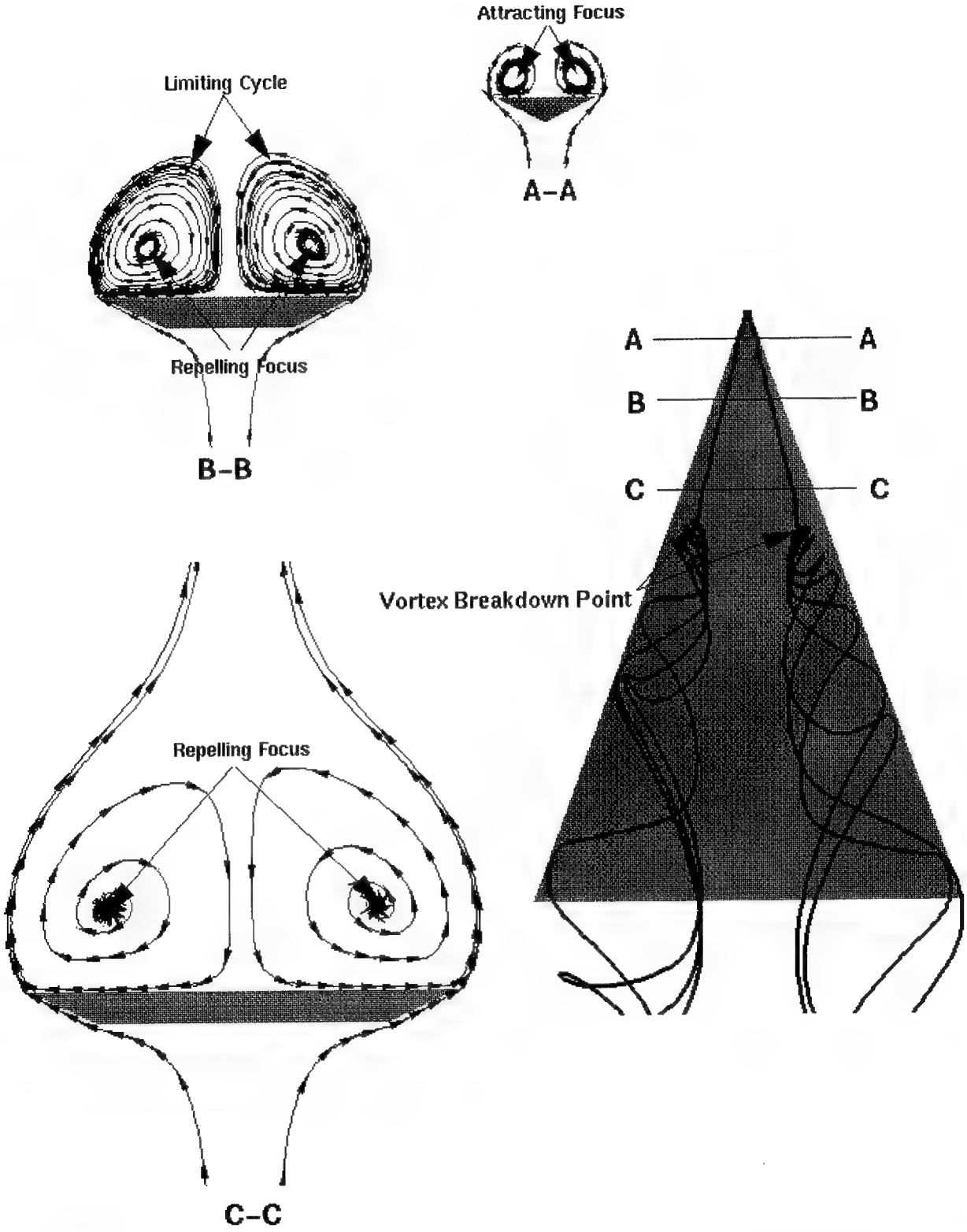

Figure 2.16 Vortical Flow Over a 70° Delta Wing at α=40°, Re=1.5x10^6

Thrust Vectoring at α= 50°

Figure 2.17 shows the response of vortex breakdown to the thrust vectoring. Here the jet is applied across the whole plane of the trailing edge. Without the trailing edge jet (see Figure 2.17a), the vortex breaks down at the apex of the wing. It is also noted that the flow is asymmetric. When the jet velocity is at the same magnitude as the free stream V_o, the breakdown point only moves slightly downstream. Even at $V_{jet} = 3V_o$, the movement is still not significant. However, the symmetrical property of the flow field has been improved. Dramatic delay of vortex breakdown has been observed for $V_{jet} = 8V_o$ (see Figure 2.17d). Also observed is much improvement of symmetry properties.

These sets of computations showed that trailing edge jet can delay vortex breakdown and improve the symmetry of the flow field and hence enhance the directional stability.

Thrust Vectoring at α = 40°

At α = 40°, we study the effect of the direction of the jet. The results are shown in Figure 2.18. Here the jet is applied only at half of the delta wing trailing edge. It is interesting to note that while the breakdown point at the jet moves downstream, the other side's point moves upstream. There is a mutual interaction of the two vortices. This interaction improves the efficiency of the jet at directional stability control.

Figure 2.19 shows the freestream velocity component and pressure coefficient contours across the vortex core areas. As for the velocity, the inertial effect of the trailing edge jet drives the negative velocity zone downstream, and hence the vortex breakdown point. Also, the jet produces a high pressure gradient along the vortex core.

Figure 2.18 implies that upward vectoring can further delay the vortex breakdown.

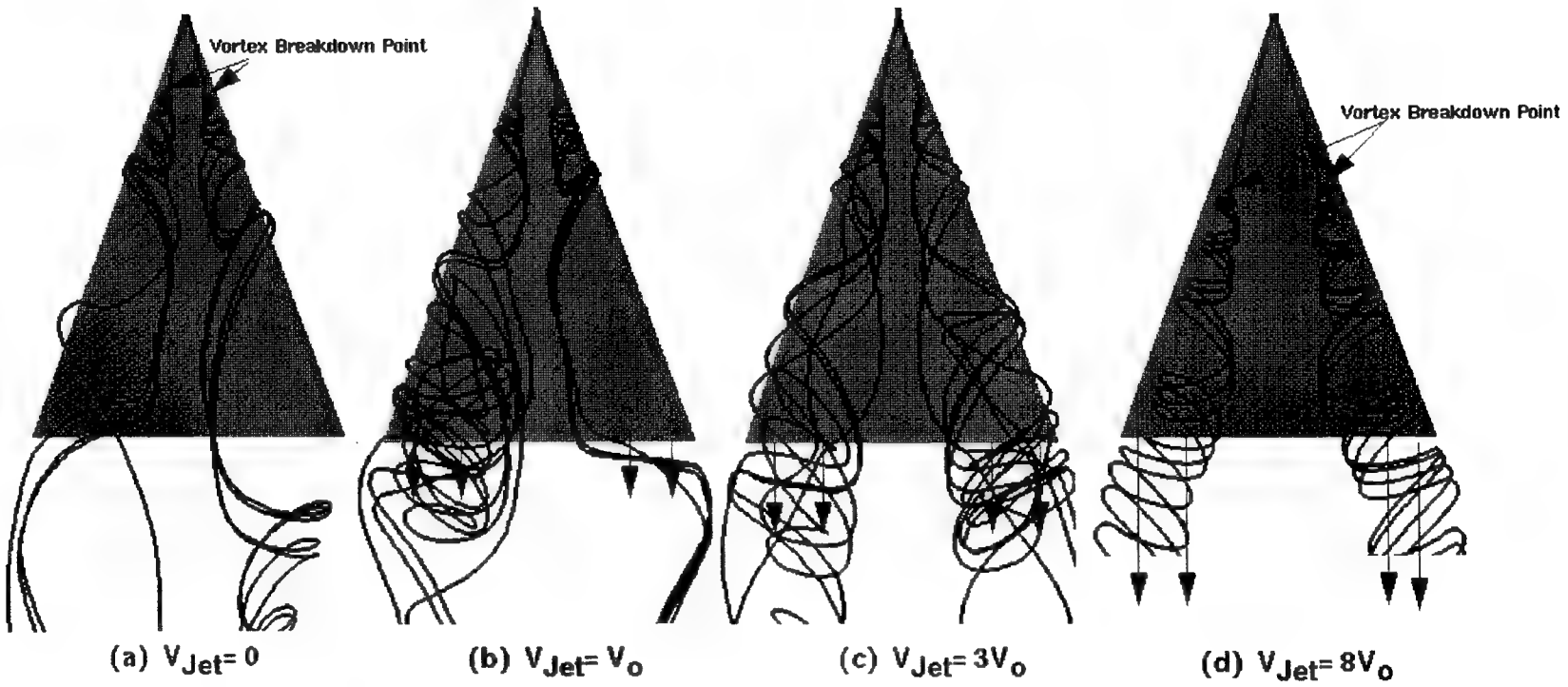

Figure 2.17 Control of Vortex Breakdown Using Vectored Trailing Edge Jet. $Re=1.5x10^6$, $\alpha=50^o$. Effect of Jet Velocity

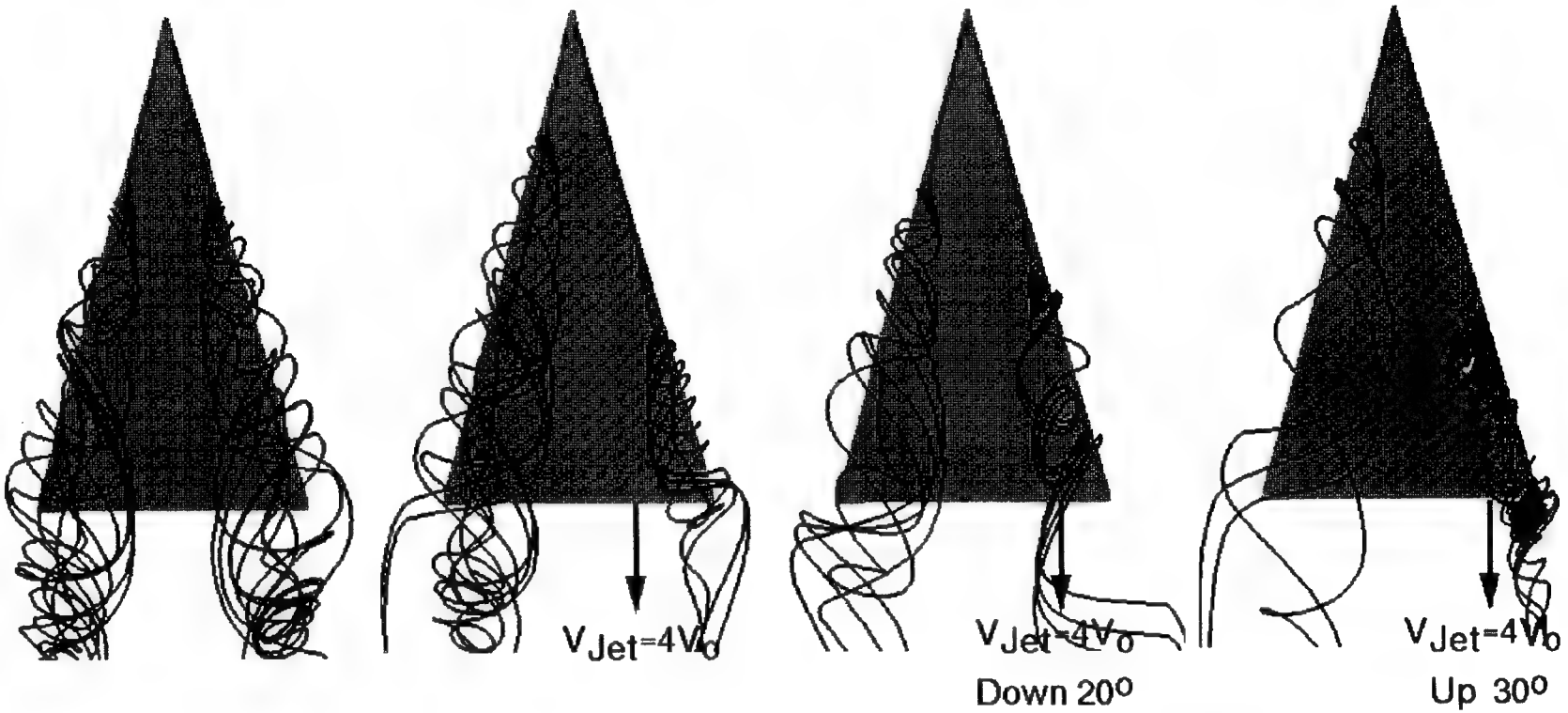

Figure 2.18 Control of Vortex Breakdown Using Vectored Trailing Edge Jet. $Re=1.5x10^6$, $\alpha=40^o$. Effect of the Direction of the Jet

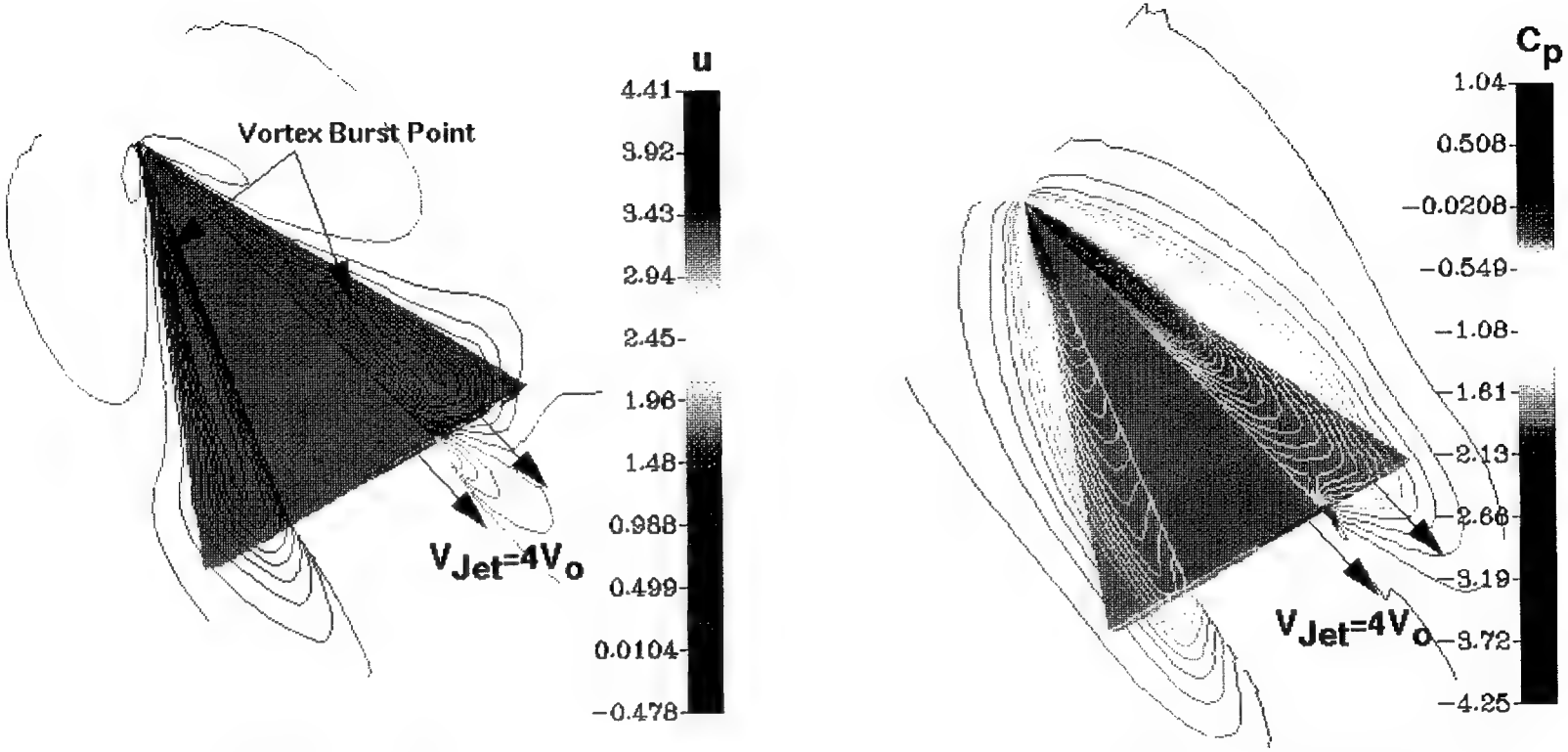

(a) Velocity Contours

(b) Pressure Coefficient Contours

Figure 2.19 Velocity and Pressure Contours Across the Planes of Vortex Core for a 70° Delta Wing Subject to Vectored Trailing Edge Jet. $Re=1.5x10^6$, $\alpha=40^o$

2.5 Summary of Observations for Delta Wings

This section reported the investigation of vortical flow management over a delta wing. The control technique includes: steady blowing and steady suction along the leading edge, alternating blowing and suction along the leading edge, use of vortex flap, and used of vectored trailing edge jet. A three-dimensional flow topology analysis was applied to study the response of vortex burst point and vortex core location to the application of control means. The major conclusions can be summarized as follows.

1. The present computational results show that the vortex breakdown responds quickly to the abrupt onset of suction and blowing along the leading edge with an overshoot. This overshoot is especially pronounced for the onset of blowing. The response (or lag) time of vortex burst point movement is typically one convective time $tU/c \sim 1.0$. An alternating blowing and suction of the order of one convective time scale is shown to be very effective in retarding vortex breakdown.

2. The present computations show that vortex breakdown over a stationary delta wing is of mainly spiral type. Bubble type breakdown is observed only at the onset of suction or at the abrupt cessation of blowing at the leading edge for a short period of time. It switches rapidly to the spiral type again.

3. The possibility of delaying vortex breakdown to higher angles of attack was studied numerically using apex flap. Computational flow visualization shows that when the apex flap is deflected downward, the vortex breakdown point will move toward the trailing edge. While when the apex flap is deflected upward, the vortex breakdown point will move toward the apex. For a 70° delta wing, the delay of vortex breakdown is in the range of 5°-8°, which matches well with experiments. Also, the most efficient downward deflection angle is 15°.

4. The use of trailing edge entrainment to control delta wing vortices was also investigated. The jet is from the whole cross-section of the delta

wing. The velocity of the jet can vary from 0 to 8 times the free stream velocity. Its direction can be upward or downward with respect to the delta wing trailing edge. Our results show that application of leading edge jet can significantly change the vortical flow over the delta wing. When applied symmetrically the jet can pull the vortex breakdown point toward the trailing edge. At high jet velocities, the asymmetry inherent in the vortical flow at high angles of attack can be suppressed. When applied asymmetrically, the trailing edge jet can generate yaw and roll moments, and can be used for directional and lateral controls.

3. F-16 FOREBODY CONTROL

The flight envelopes of current aircraft have been limited in part by controllability at high angles of attack. An example of this is sudden departures in roll and yaw and pitch-up or deep stall. One of the special phenomena contributing to the forebody instability is that the long forebodies, typical of modern high-performance aircraft, shed vortices assuming asymmetric positions at high angles of attack and hence cause unacceptably large lateral and directional loads. The potential of using forebody vortex manipulation to ensure directional control at high angles of attack has been an active research topic in the last several years.[45-58] A number of manipulation techniques have been explored including movable forebody strakes, forward, aft and tangential blowing/suction from circular nozzle or slot on the forebody, rotable nose tip devices, different forms of small perturbation and chined forebody.

This section reports a study of the vortical flow control of F-16 forebody. The standard F-16 configuration develops a directional instability at angle of attack above 30°. As a result, the F-16 is currently limited to angles of attack below the maximum lift to avoid the problem area, and hence the maneuver performance potential has not been fully utilized. The objective of the present research is to investigate various concepts to increase lateral and directional stability to levels greater than 30° angle of attack for the F-16, and to shed light on the role of breakdown and interaction of vortex system on the forebody directional stability.

3.1 Computational Model

The overview of the F-16 forebody configuration and computational grid are given in Figure 3.1. The grids are of the O-H type and are generated by the software package, ICEM-CFD. The configuration is modeled from the nose boom longitudinally back to $x/c = 2.0$, where the rear of the canopy is located. Here, $c = 11.32$ ft for the full scale model. As a result, any effect or interaction of the forebody flow field on the wing was not included. To eliminate downstream boundary condition effect, an extension of the model is made by repeating the cross-sectional geometry from the last $x/c = 2.0$ to $x/c = 3.0$. The current computation used 112 grid points in circumferential direction, 30 in the normal direction and 94 in the

streamwise direction. The 94 streamwise grids contain 10 stations extending upstream from the nose and 10 stations extending downstream from the station x/c = 2.0. The grids in both extensions are stretched to provide resolution near the configuration. The grids are also clustered near the surface to adequately resolve the boundary layer. Since k-ε model with wall functions is used, the y^+ is typically about 15, which is optimal for the use of wall function. The fluid is assumed to be compressible with M=0.02 as used in the experiments of Reference 59. The Reynolds number based on 10% full scale model as in Reference 59 is 1.5×10^5 . The far field boundary is located two chord lengths away from the body. At the inlet, the free stream properties are specified, at far boundary the extrapolation condition is used. On the body surface, no slip condition is imposed.

3.2 Development of Directional Instability of Standard F-16 Forebody

Standard F-16 forebody configuration develops directional instability at angles of attack above 30°. Figure 3.2 shows the yawing moment coefficient with respect to sideslip angle β at several angles of attack. Figure 3.3 shows the definition of coordinates and moments. Here, the axis system used for forces and moments is the wind axis system. The x-coordinate runs positive down the forebody, the y-coordinate runs positive out the right wing, and the z-coordinate runs positive up. A positive pitching moment is nose up, a positive yawing moment is nose to the right, and a positive rolling moment is right wing down. The sideslip angle is positive when measured to the left and it has the same magnitude as the yaw angle but the opposite sign.

As seen in Figure 3.2, for a positive sideslip angle β, C_n, the yawing moment, is positive for $\alpha < 30°$. This represents a directional stability. When $\alpha > 30°$, at positive β, the C_n is negative and the F-16 suffers directional instability.

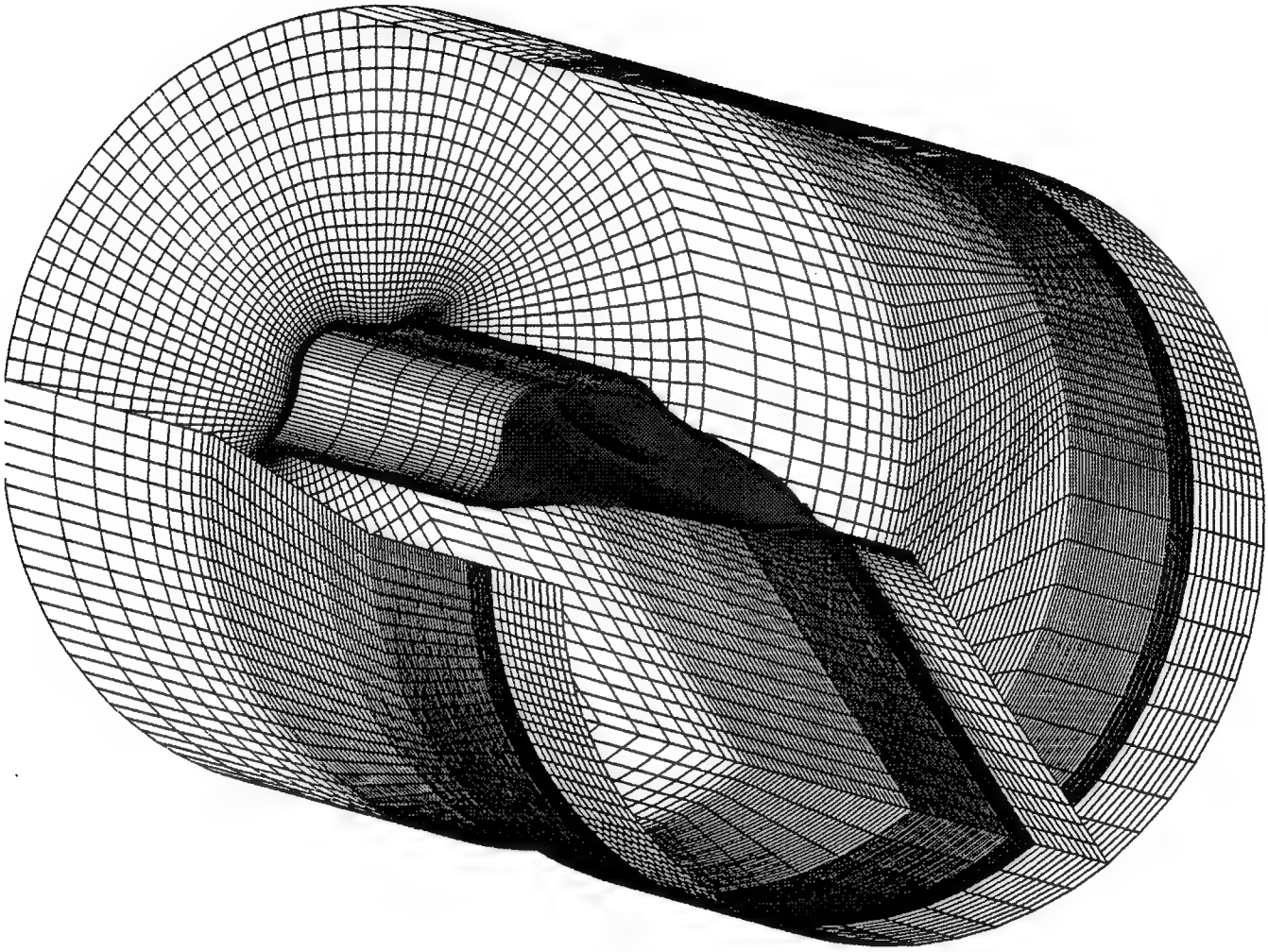

Figure 3.1. Computational Grid Around an F-16 Forebody

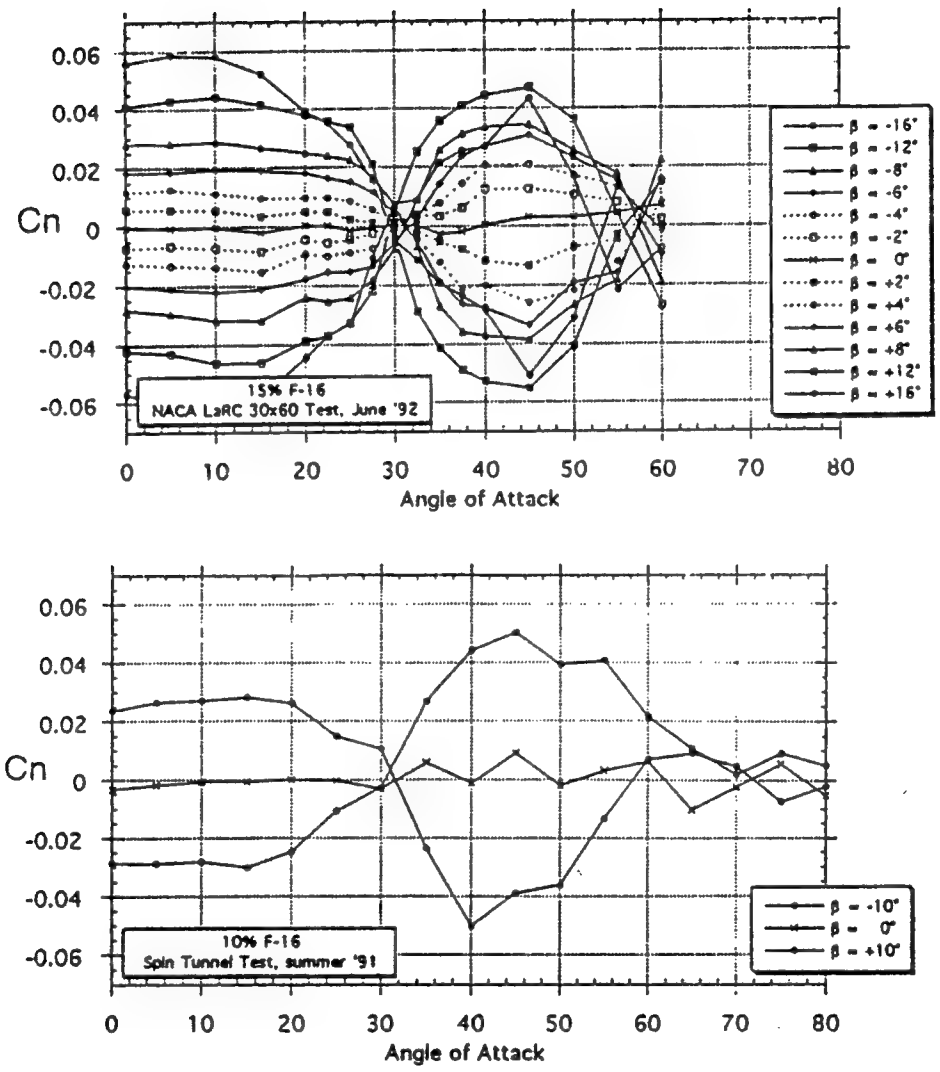

Figure 3.2. Standard F-16 in Pitch from Experiments

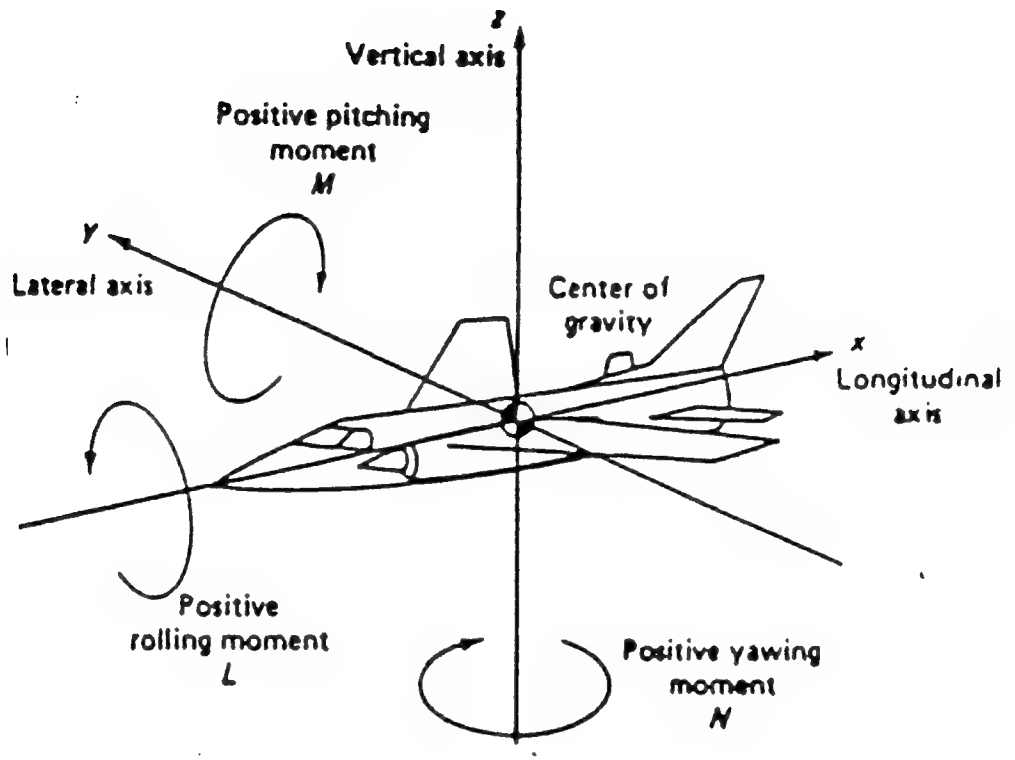

Figure 3.3. Axis System and Positive Direction of Moments

Figure 3.4 shows the flow field around the baseline F-16 forebody at angles of attack of 30° and 50°. The vortex system above the Leading Edge Extension (LEX) is represented by the vortex core, vortex breakdown point, and particle traces from the vortex breakdown point. At $\alpha = 30°$, the vortex breakdown point is located at the rear end of the canopy. It is seen that the breakdown is of spiral type. The aircraft surface is rendered by pressure coefficient. As seen, associated with LEX vortices is local high suction pressure, which dissipates rapidly downstream from the vortex breakdown point. The forebody vortices are represented by particle traces released from the nose. The front view of the 3D flow field illustrates that the forebody vortices propagate over the canopy region, and then interact with the LEX flow field. It seems that the swirl due to LEX vortex sucks the forebody vortices into the wake

of the vortex breakdown zone. At $\alpha = 50°$, the vortex breakdown point moves to the tip of the LEX and forebody vortex lifts further away from the body of the model. Although interaction pattern of the vortex system seems to be the same as $\alpha = 30°$, the location where the interaction starts moves forward.

As shown in Figure 3.4, LEX vortices and forebody vortices are the main features of flow over the F-16 forebody. It is expected that directional stability of the F-16 forebody has much to do with the vortices. The vortical flows corresponding to Figure 3.4 at angles of attack of 40° and angles of sideslip of 4° and 10° are shown in Figure 3.5. Asymmetry of the flow field is apparent due to the sideslip. What is more significant is the LEX vortices. For positive sideslip, the vortex breakdown point on the upwind (windward) side of LEX moves to the apex of the LEX, while the vortex breakdown point on the downwind side (lee side) moves toward the trailing edge. Consequently, there is a larger suction pressure zone on the top of LEX at the downward side than that of the upwind side. The result is a net side force from the right to the left, and a negative yawing moment. This negative yawing moment causes the aircraft further to the left and the aircraft is in the directional unstable situation. At even higher angles of sideslip ($\beta = 10°$), the upwind side vortex breakdown point moves even more to the apex, and the above directional instability persists.

The role of forebody vortices can be appreciated from Figure 3.6 which shows the sectional topology of the forebody. The cross flow due to sideslip is from the right to the left. Sideslip causes the forebody vortices to shift to the left. Also, downwind side vortex lifts off the surface. Near the nose, the shifting of vortices to the left produces a net force to the left, and promotes the directional instability. Further downstream, for example at B-B, the lifting of the left vortex reduces the suction pressure associated with it, and hence there is a tendency of net force to the right. The combination effect of LEX vortices and forebody vortices is that there is an initial decrease in C_n with β, and then a recovery at high β. This is true as shown in Figure 3.7. The experimental measurement of Simon et al[59] is also shown in Figure 3.7 for the F-16 full body. Comparison is very favorable, especially the trend of C_n with β. It also indicates that forebody has significant impact on the directional

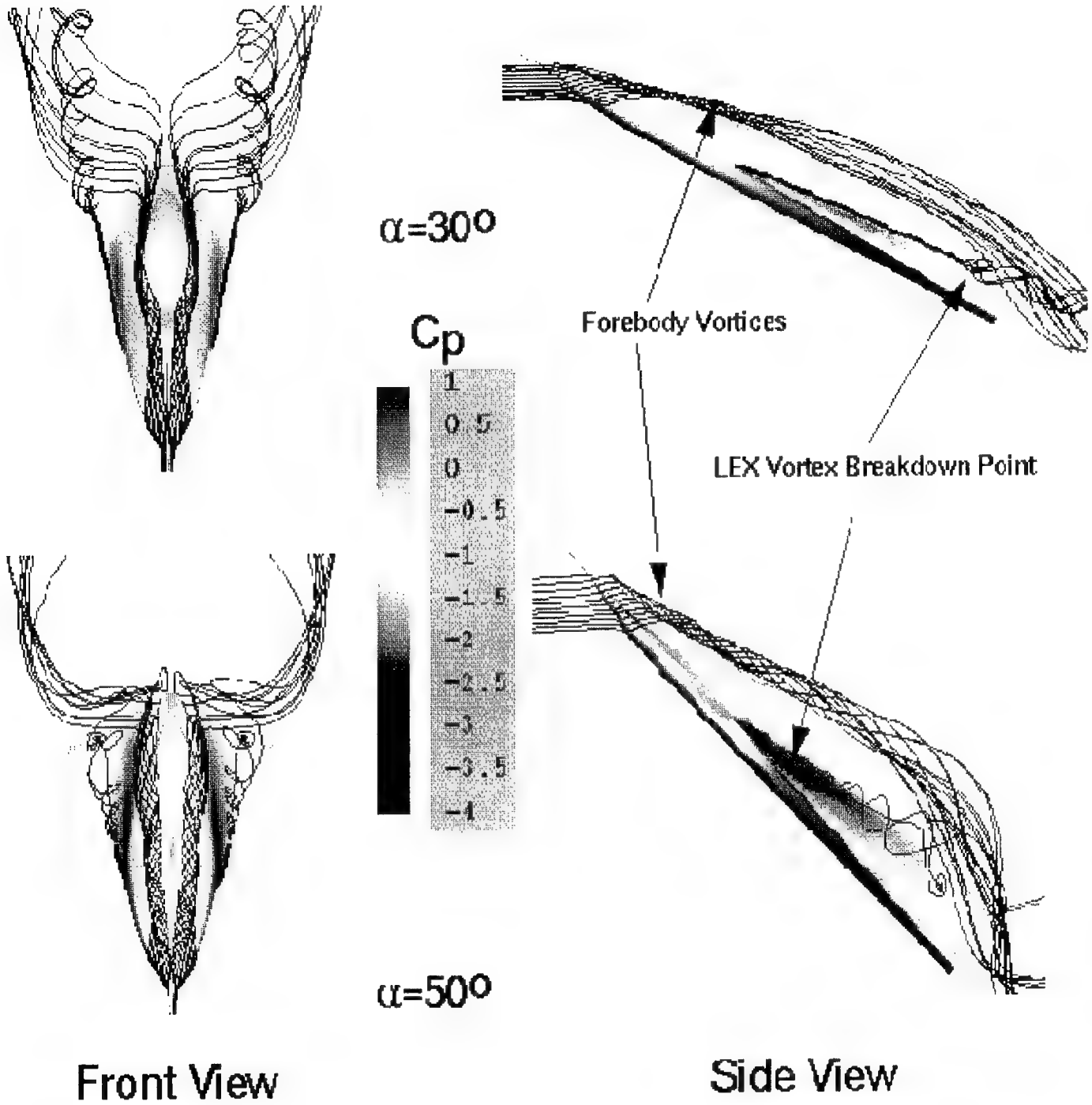

Figure 3.4 Flow Over a Standard F-16 Forebody at Different Angles of Attack; $\alpha=30^{\circ}$ and $\alpha=50^{\circ}$. $Re=1.5 \times 10^5$

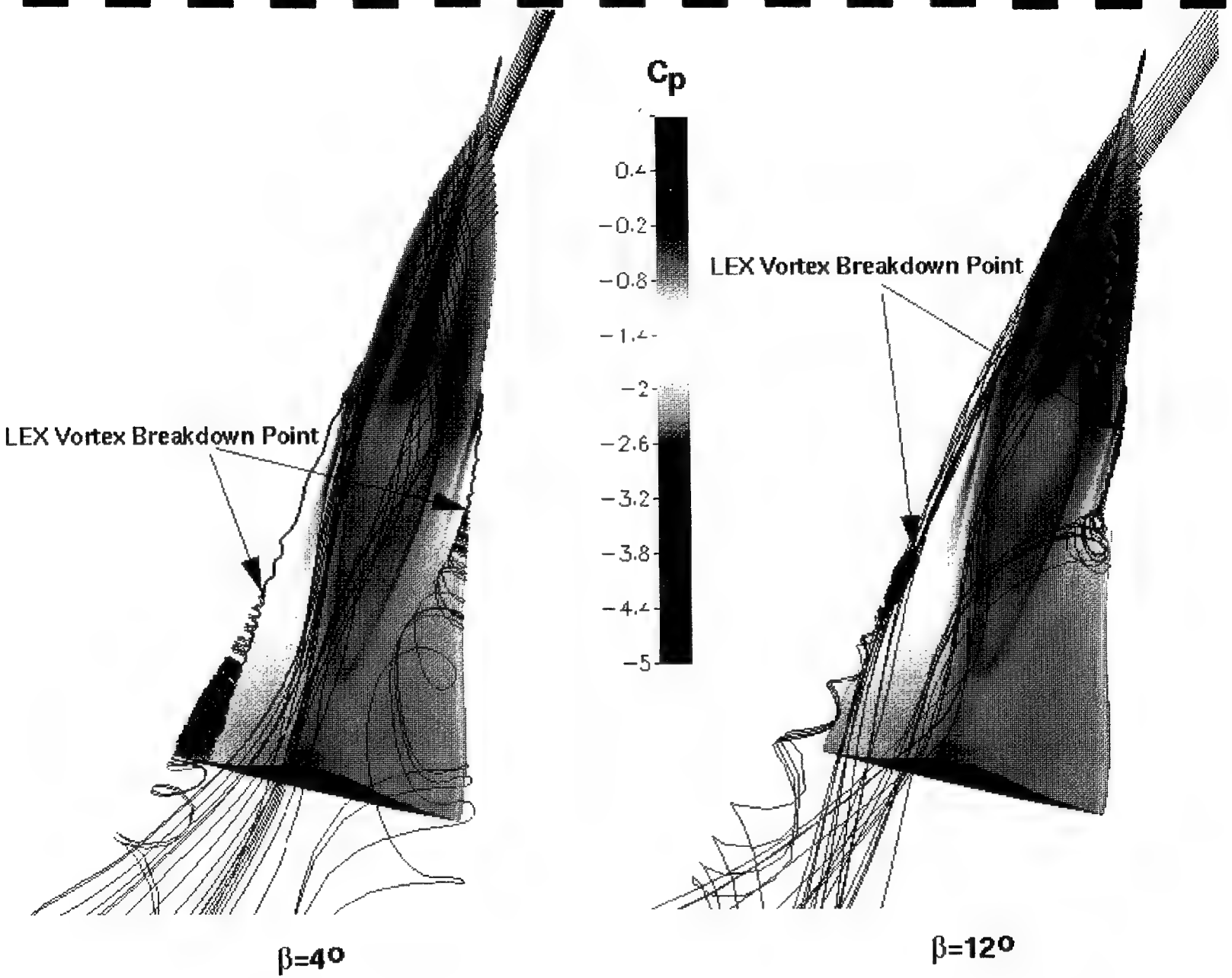

Figure 3.5 Vortical Flows Over a Standard F–16 Forebody at Angle of Attack of 40° , β: Sideslip Angle

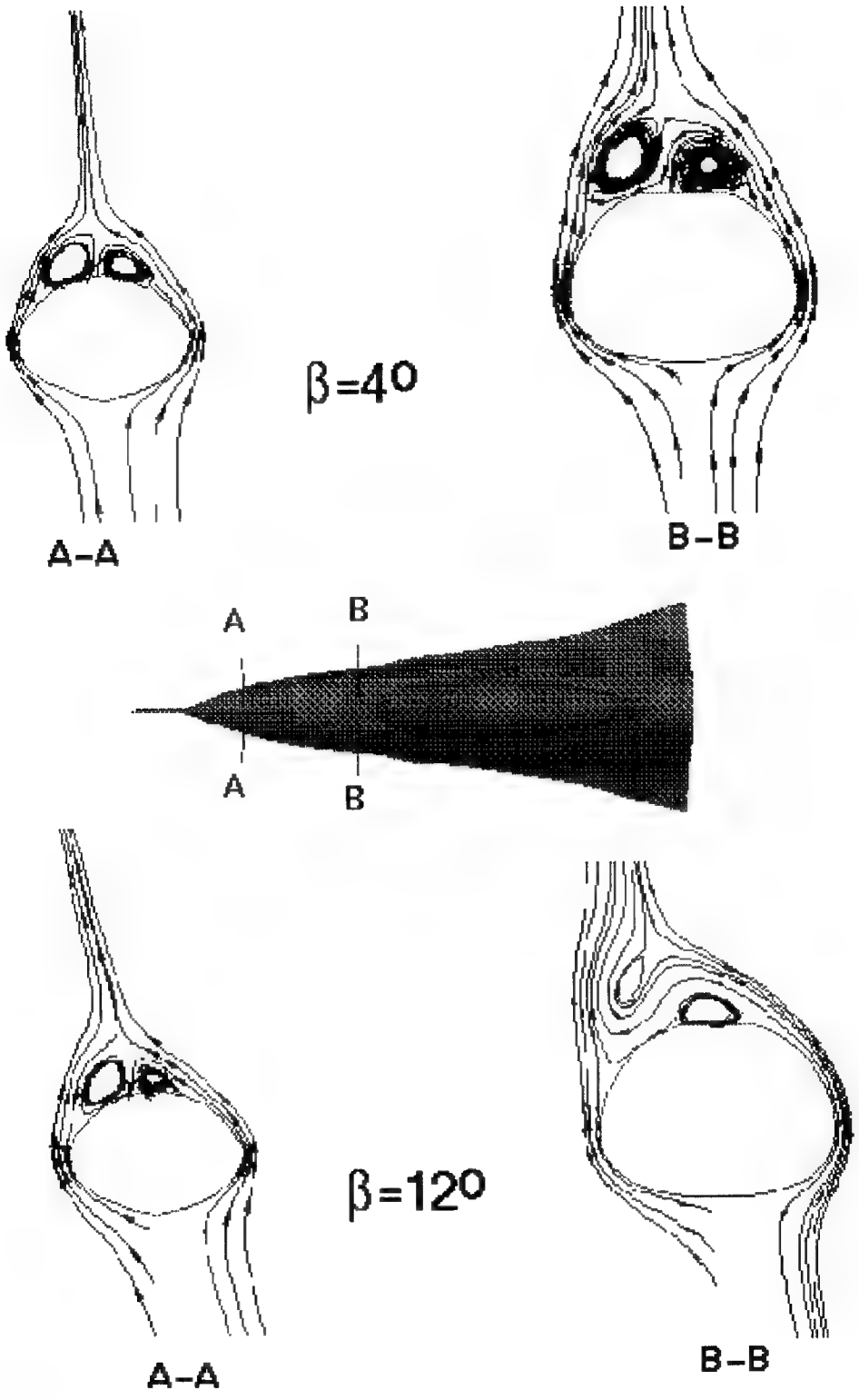

Figure 3.6 Cross Flow Topology Over Standard F-16 Forebody at α=40°.

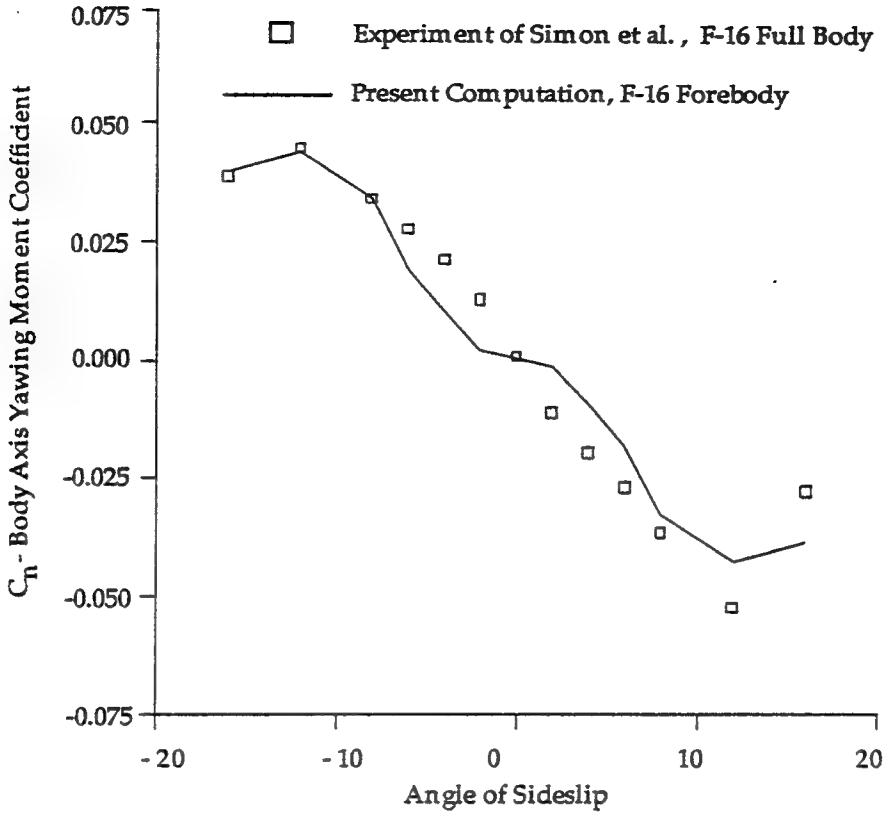

Figure 3.7. Comparison of Body Axis Yawing Moment Coefficients between Present Computations for F-16 Forebody and Experiment of Simon et al for F-16 Full Body at $\alpha = 40°$

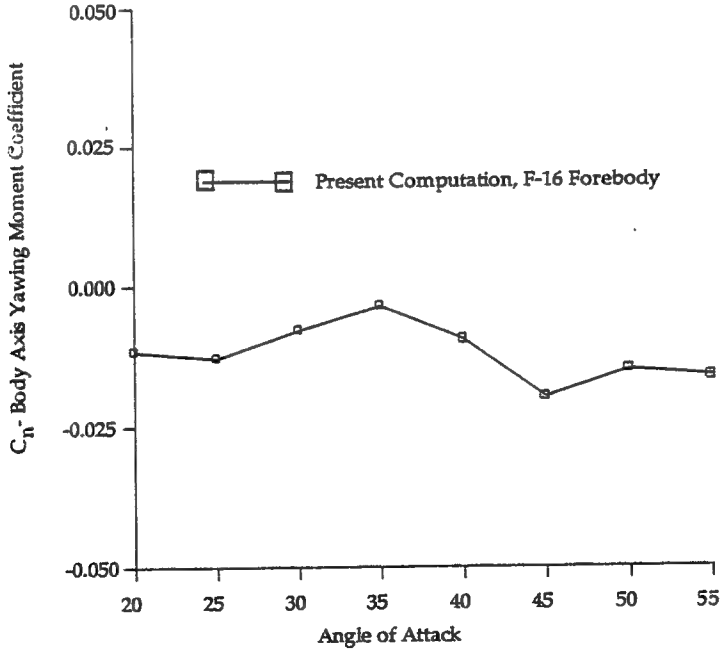

Figure 3.8. C_n as a Function of α at $\beta = 4°$

stability. The negative slope of C_n with respect to β indicates directional instability. Figure 3.8 shows C_n at different angles of attack with $\beta = 4°$.

3.3 Use of Cut Back LEX

In the experiments of Simon *et al*[59], the Leading Edge Extension (LEX) was cut approximately 48 inches full scale as shown in Figure 3.9. This modification was expected to provide a nose-down pitching moment increment at high angles of attack. Figure 3.10 shows the effect of cut back LEX on the flow field at $\alpha = 40°$. First, the vortex breakdown point for the baseline F-16 is located at the central region of the canopy longitudinally. In comparison to Figure 3.5 this further shows the effect of angles of attack on the vortex breakdown location. With cut back LEX, the LEX vortex system almost fully breaks down, leaving lower suction pressure on the upper surface. The forebody vortices are about the same, indicating little effect of cut back LEX on lateral-directional stability.

The effect of cutback LEX on the pitching moment is shown in Figure 3.11. There, the experimental data for baseline F-16 and with cutback LEX are also given. The computational results reflect the difference in the pitching moments due to cutback LEX. The computed results in Figure 3.11 are calculated as:

$$C_m(\text{Figure 3.11}) = C_m(\text{cutback LEX computation}) - C_m(\text{standard F-16 computation}) + C_m(\text{standard F-16 experiment})$$

It is clear that there is drop and equivalent nose down pitching moment due to the cutback LEX. This shows the role of LEX vortex breakdown in the force balance. Similar results for lift coefficients are shown in Figure 3.12. There is only a slight drop in the lift coefficient when the LEX is cut.

The directional stability at $\alpha = 40°$ is shown in Figure 3.13. Again, fairly good comparison with the experiment is obtained. The characteristics of C_n with β is about the same as the baseline F-16.

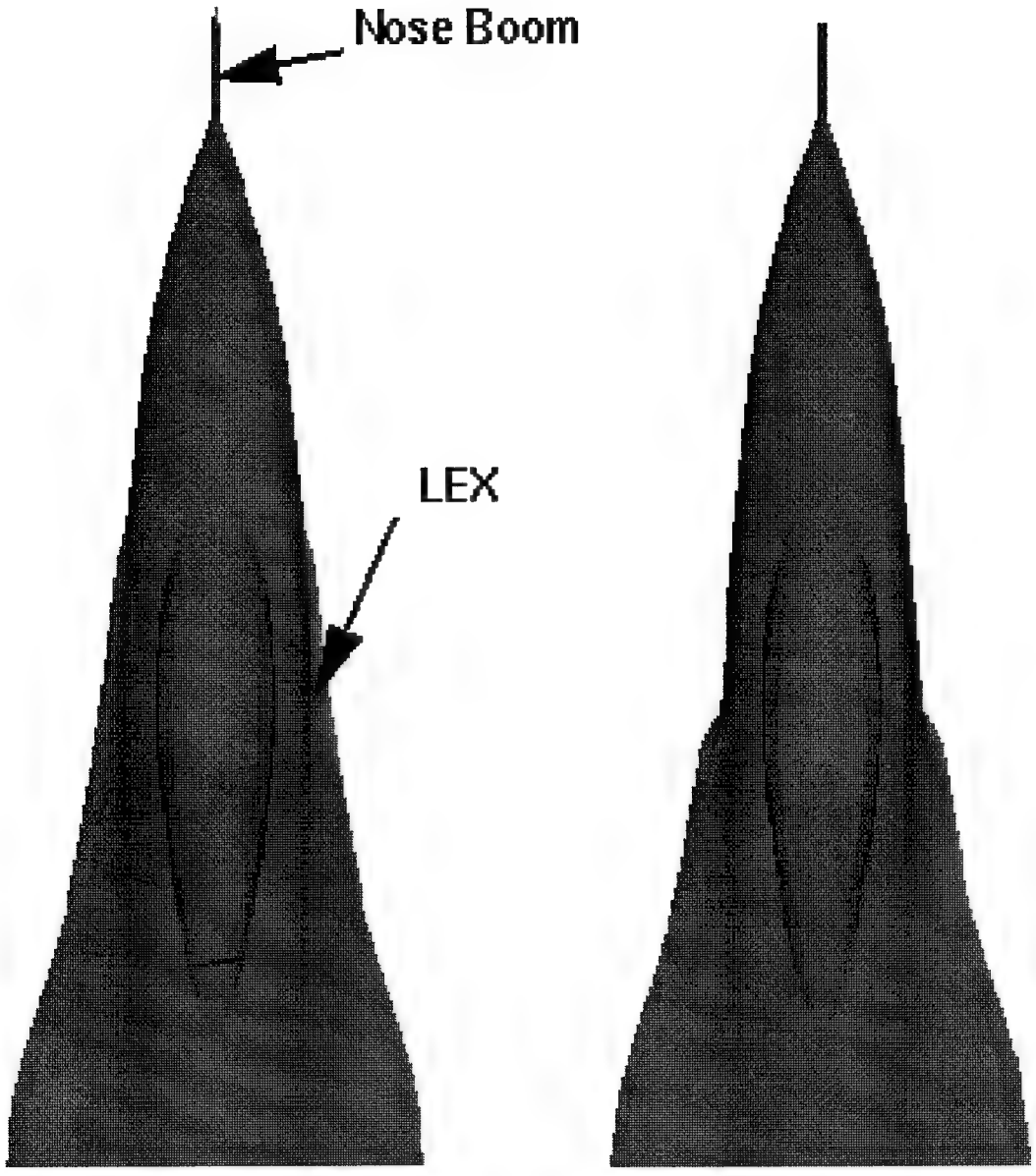

Figure 3.9 Configurations of Standard F-16 Forebody and F-16 Forebody with Cutback LEX.

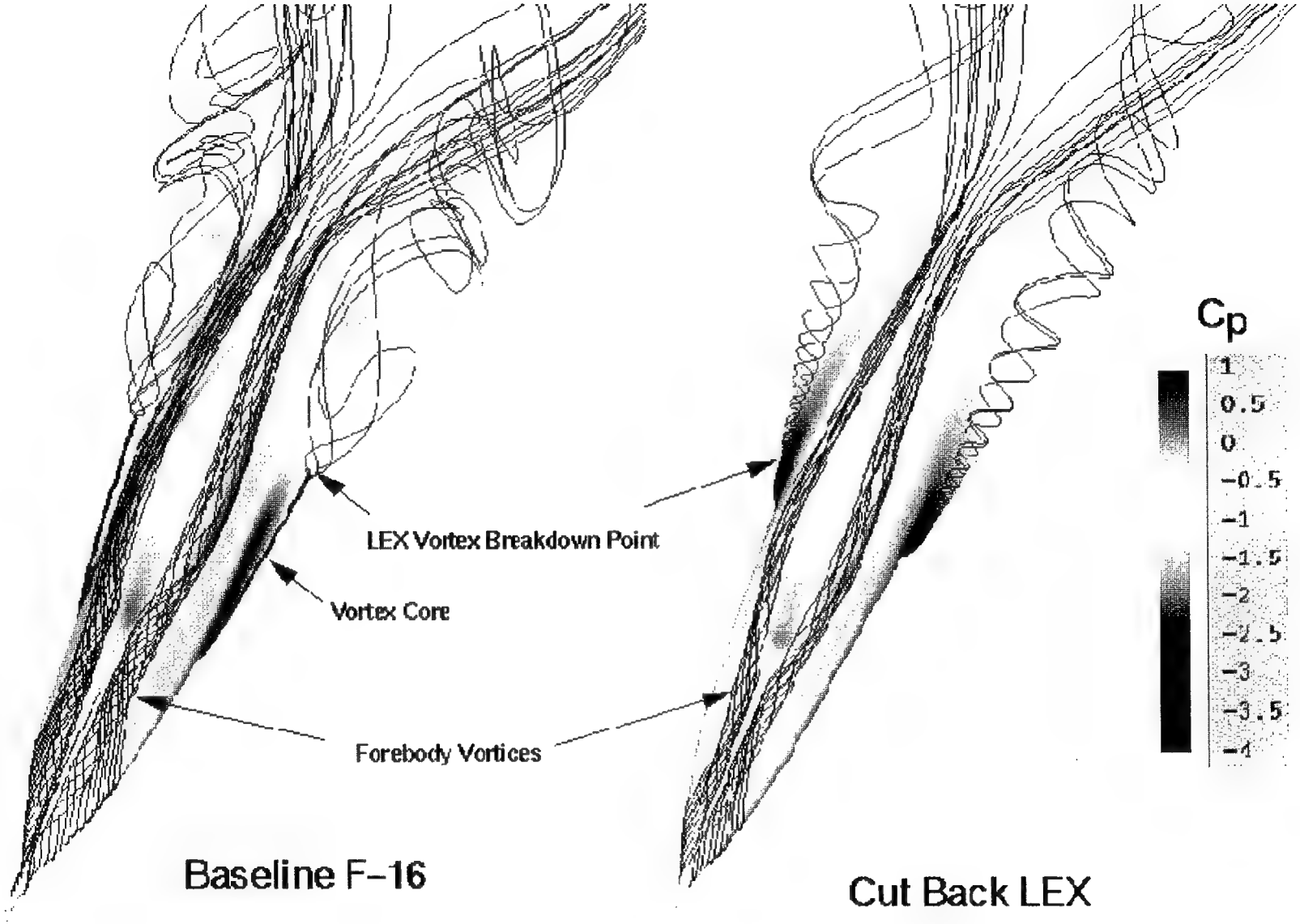

Figure 3.10 **Comparison of Flow Fields Around an F-16 Forebody With and Without Cut Back LEX; $\alpha=40^{o}$ and $\beta=0^{o}$**

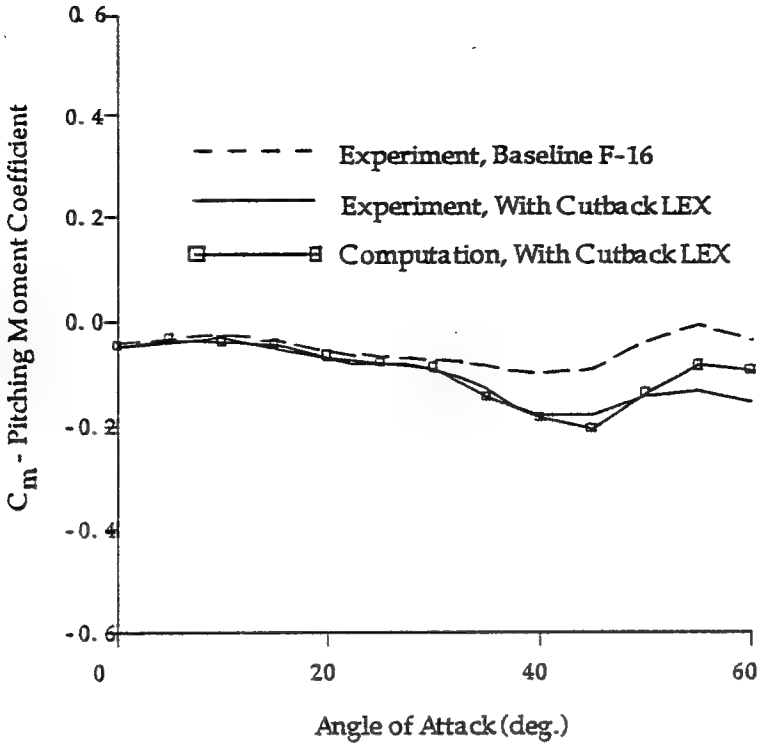

Figure 3.11. Effect of Cutback LEX on Pitching Moment for Experimental Measurement and Corrected Computational Values

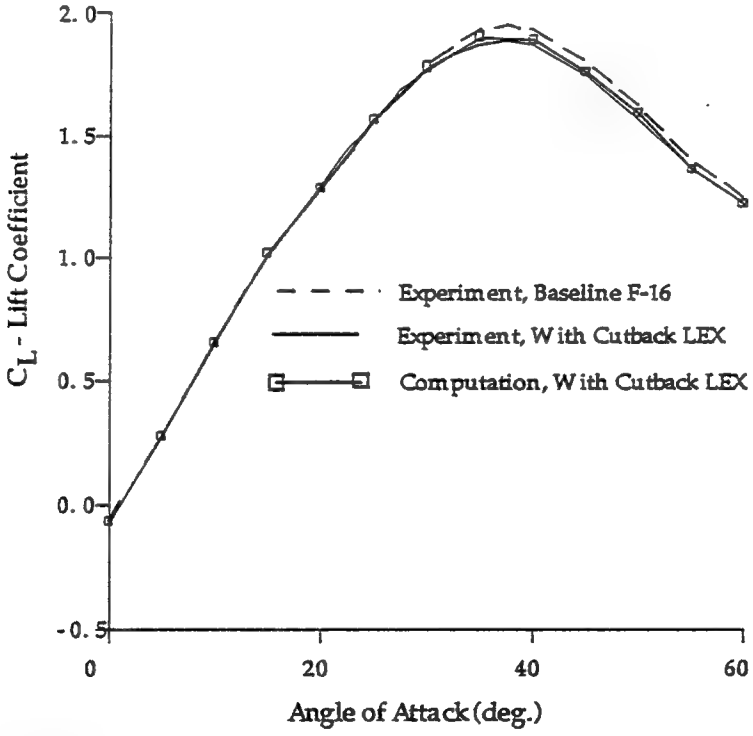

Figure 3.12. Effect of Cutback LEX on Lift Coefficient for Experimental Measurement and Corrected Computational Values

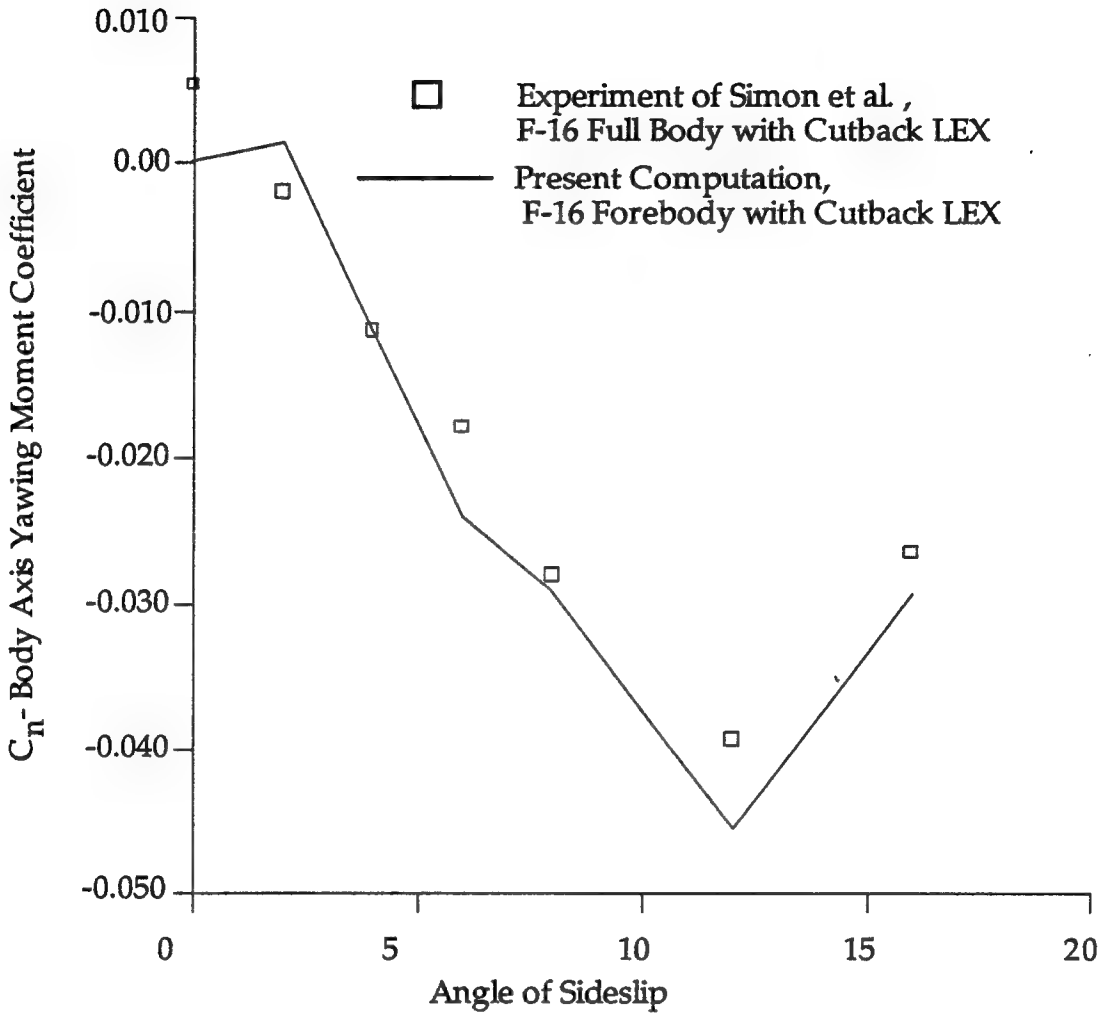

Figure 3.13. Body Axis Yawing Moment Coefficient for F-16 Forebody with Cutback LEX, $\alpha = 40°$, $Re = 1.5 \times 10^5$

3.4 Forebody Chines

The purpose of using forebody chines is to improve the static lateral-directional characteristics at high angles of attack by forcing symmetric separation of forebody vortices. The chine in the experiment of Reference 59, shown in Figure 3.14, is used in this study. Figure 3.15 shows the sectional streamlines for the baseline F-16 forebody and for the one with added chines under condition of $\alpha = 40°$. At a station of $x/c = 0.133$, the vortex pair is clearly seen for both configurations. The topological analysis indicates that the vortex is of attracting focus, meaning local stretching or stabilization of the vortex core. The separation point for the forebody with chine starts from the chine tip, whereas for baseline F-16, it is free to move in response to the local pressure and boundary layer conditions. At the stations of $x/c = 0.379$ and $x/c = 0.605$, the forebody vortices exist in a limiting cycle form. By $x/c = 0.878$, the canopy produces another pair of vortices and LEX vortex emerges. It is also noted that the particles flow into the forebody vortices, indicating the stabilization effect of the canopy.

The LEX vortex is represented by an attracting focus. At $x/c = 1.252$, the vortices due to the canopy disappear, and both forebody and LEX vortices experience compression. In general, the primary forebody vortex pair from chined forebody comes closer and stands at a higher distance from the body surface.

To study the effect of chined forebody on lateral directional stability, computations were made at $\alpha = 40°$ and sideslip angle $\beta = 8°$. The results are shown in Figure 3.16. With baseline F-16, the sideslip induces a finite cross flow component (from the left side with front viewing), and causes the lateral shifting of both LEX and forebody vortices. It is also readily evident that sideslip promotes the LEX vortex bursting on the upwind side of the forebody and correspondingly suppresses the bursting of downwind LEX vortex. The interaction pattern of forebody and LEX vortices are different from that under zero sideslip: the two forebody vortices are sucked into the downwind side LEX vortex. When chines are added near the F-16 nose, the lateral movement of LEX vortex is about the same as the one without chine, but the bursting location shifts further to the LEX apex for the upwind side and to the rear end of the forebody for the downwind side. The forebody vortices behave quite

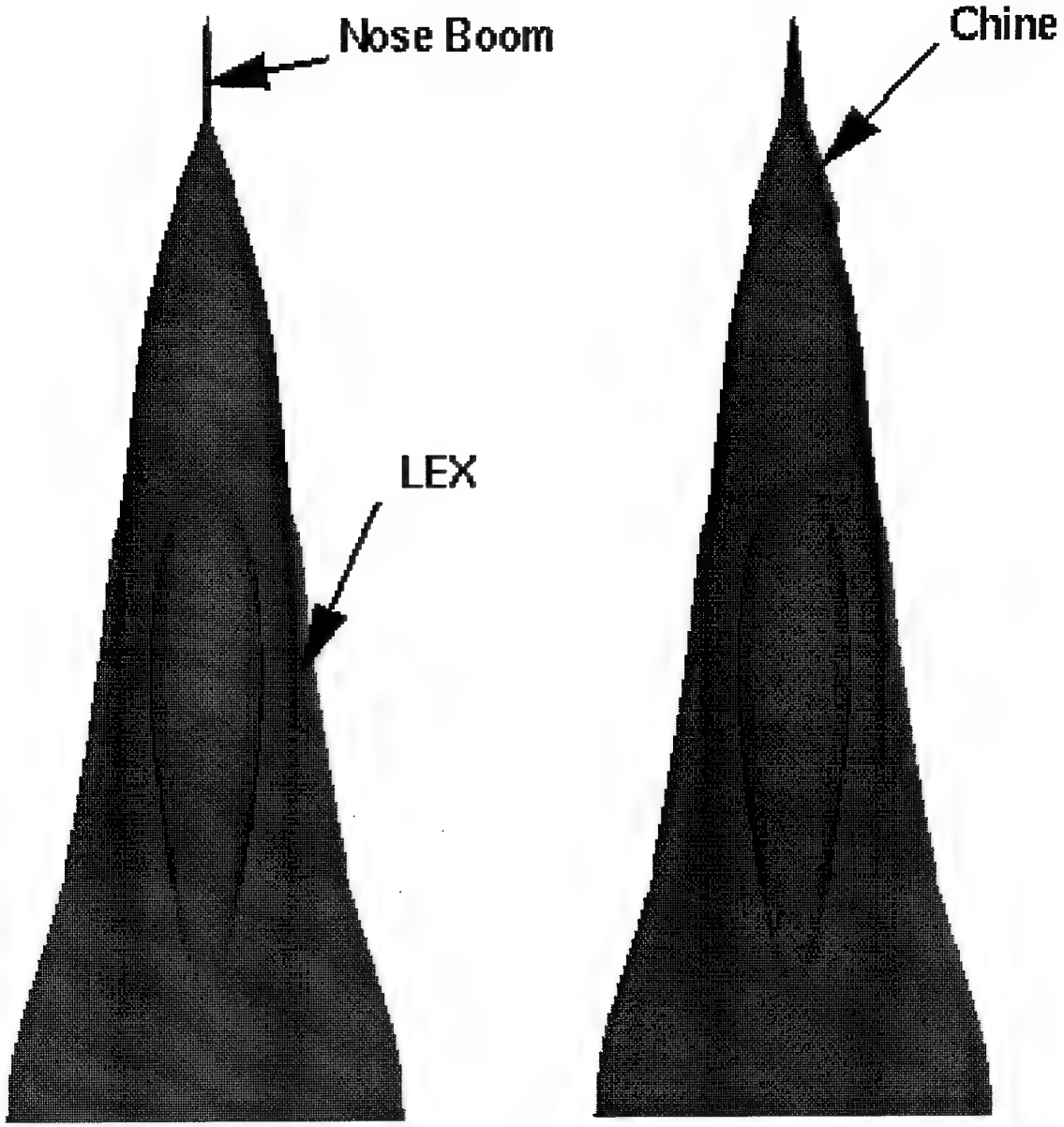

Figure 3.14 Configurations of Standard F-16 Forebody and F-16 Forebody with Chine.

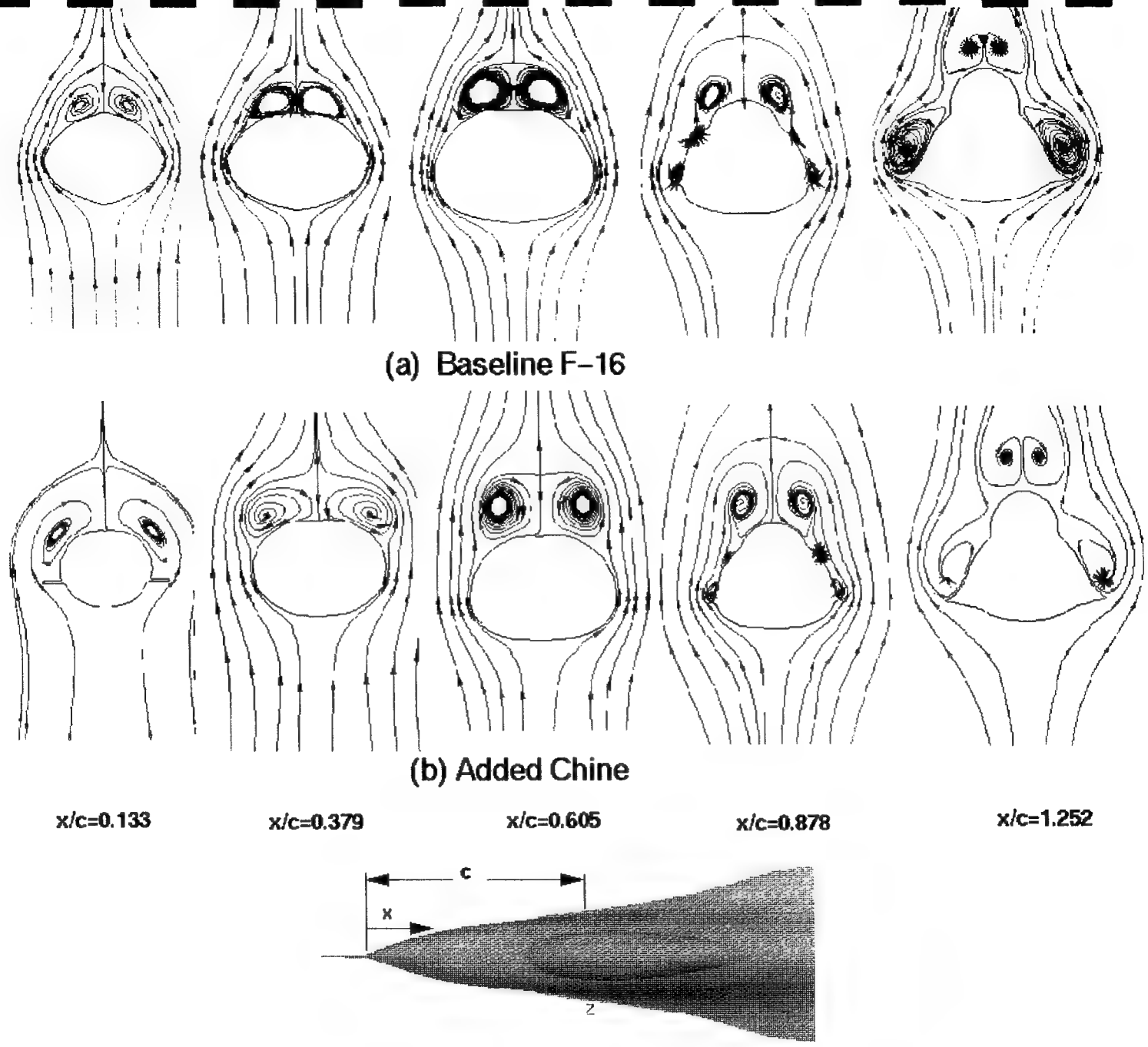

Figure 3.15 Cross–Sectional Stremlines for an F–16 Forebody With and Without Chines; α=40^{o} and β=0^{o}

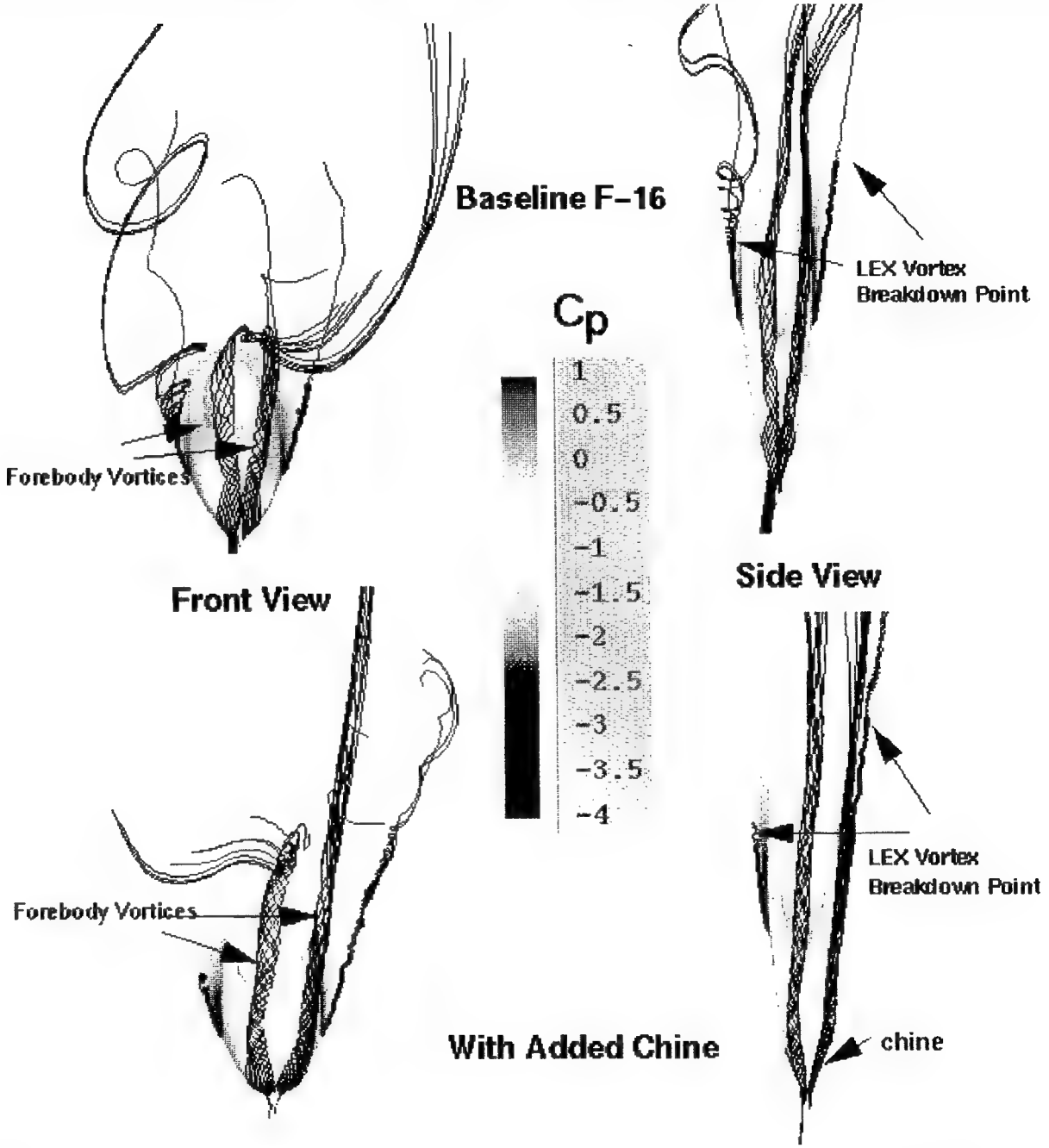

Figure 3.16 Effect of Added Chines on Lateral Directional Stability of an F-16 Forebody; α=40° and β=8°

differently from the ones for the baseline F-16 in that upwind side vortex swirls into the LEX vortex on the same side, and downwind side vortex has no interference with LEX vortex.

As revealed from the surface pressure coefficients, the fact of downwind LEX vortex moving upward and outward implies that suction level in upwind side is greater for chined forebody. This in turn promotes side force toward the upwind side, and hence higher directional stability. Figure 3.17 illustrates the development of cross-sectional streamlines under non-zero sideslip.

The improvement due to added chine to the directional stability can be seen from Figure 3.18. Again, experimental data are also shown for comparison. For standard F-16 body, a positive sideslip generates a negative yawing moment, meaning instability. With added chine, a positive sideslip generates a positive yawing moment, for F-16 forebody from computation and a less negative moment for F-16 full body from the experiment.

3.5 Use of Added Chine and Cutback LEX

Figure 3.19 shows the flow field around the F-16 forebody with both added chine and cutback LEX at angles of attack of 27.5°, 30°, 35°, and 45°. The vortex system above the Leading Edge Extension (LEX) is represented by the vortex core, vortex breakdown point, and particle traces from the vortex breakdown point. At $\alpha = 27.5°$, the vortex breakdown point is located at the rear end of the forebody. It is seen that the breakdown is of spiral type. The aircraft surface is rendered by pressure coefficient. As seen, associated LEX vortices is local high suction pressure, which dissipates rapidly downstream from the vortex breakdown point. The forebody vortices are represented by particle traces released form the nose. The view of the 3D flow field illustrates that the forebody vortices propagate over the canopy region, and then interact with the LEX flow field. At $\alpha = 30°$, the LEX vortex breakdown points move to the tail of the canopy. It is due to this movement that the high suction pressure zone on the LEX is reduced. With further increase in α, the LEX vortex burst points shift toward the apex of LEX. At $\alpha = 40°$, they reach the tip and vortex system associated with LEX has fully broken down. Also, the forebody

vortices lift further away from the body of the model.

In comparison to Figure 3.4, the vortex breakdown is expedited for 5° relative to the standard F-16 body. Cutting LEX can reduce the pitching moment at high angles of attack by controlling vortex breakdown.

The directional stability for chine and cutback LEX is given in Figure 3.20. Again, very favorable comparison is obtained. Due to nearly full breakdown of LEX vortices at $\alpha = 40°$, the forebody vortices dominate the yawing moment and one sees a higher slope of C_n with respect to β.

3.6 Jet Blowing

The purpose of using jet blowing is to improve the static lateral-directional characteristics at high angles of attack by forcing symmetric separation of forebody vortices. Figure 3.21 shows the configuration of jet slot location. The jet is located near the top of the forebody and just above the chine. The air was blown laterally over the forebody chines. The blowing ratio is at $C_\mu = 0.002 \sim 0.004$. The focus is on the blowing from the right slot at static conditions.

LeMay et al[60] carried out experimental study of pneumatic control of the forebody vortices of the F-16. They used 1/15 scale model, and M = 0.24, Re = 2.5×10^6. Two different longitudinal nozzle positions were investigated. It was shown that the direction for the yawing moment is opposite to the side where the blowing occurred. Progressively higher blowing rates produced larger yawing moments.

Given in Figure 3.22 is the front view of the flow field at $\alpha = 40°$ with $C_\mu = 0.0$ and $C_\mu = 0.004$. It is seen that the blowing from the jet slots lifts the forebody vortex on that side, and hence reduces the suction pressure associated with it. The net result is a force to the left (seeing from the pilot's view). The flows in several cross-sections are given in Figure 3.23 which clearly show the offset of forebody vortices due to the blowing.

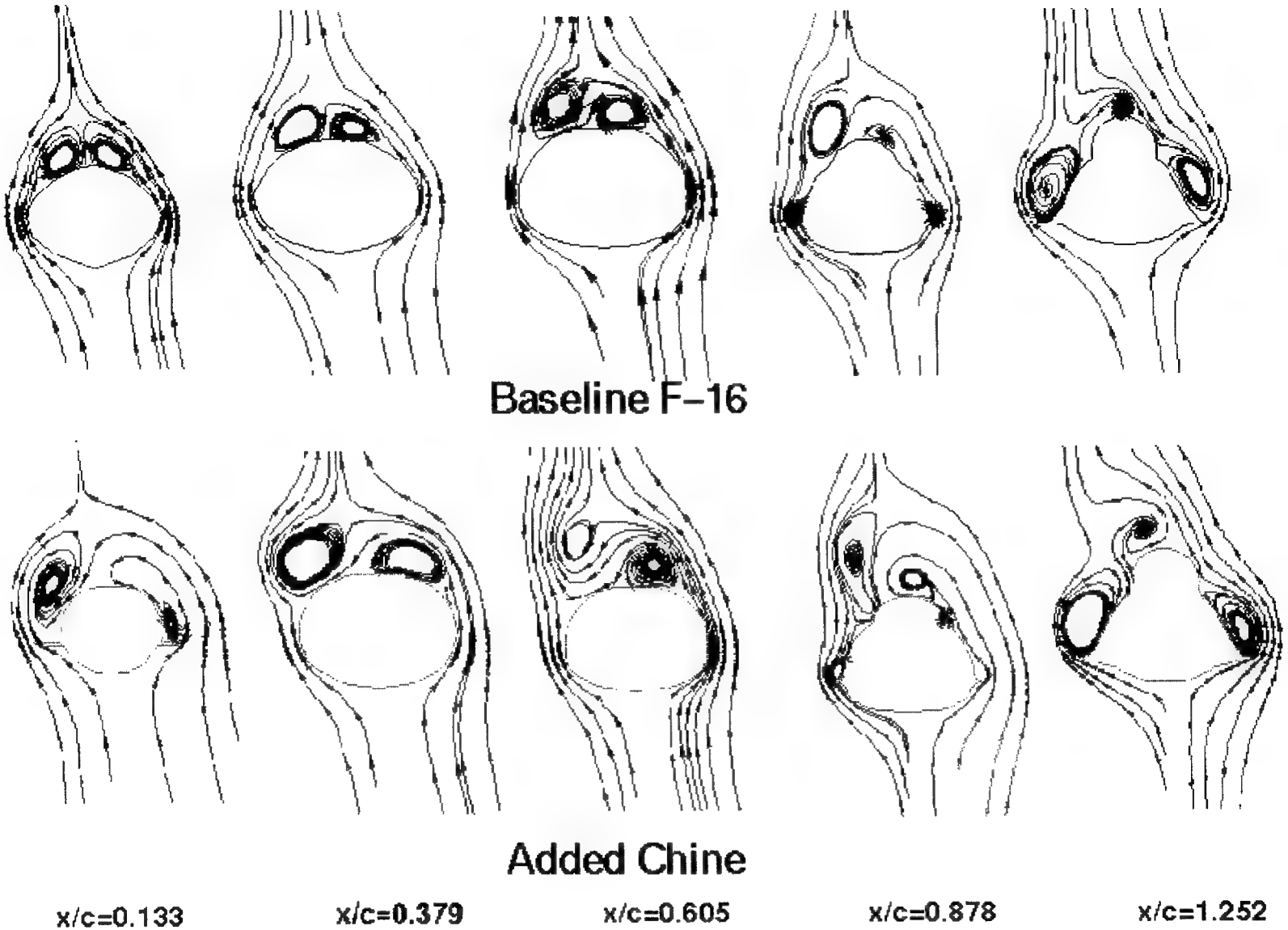

Figure 3.17 Cross-Sectional Streamlines for an F-16 Forebody with and Without Chines; $\alpha=40^{o}$, $\beta=8^{o}$

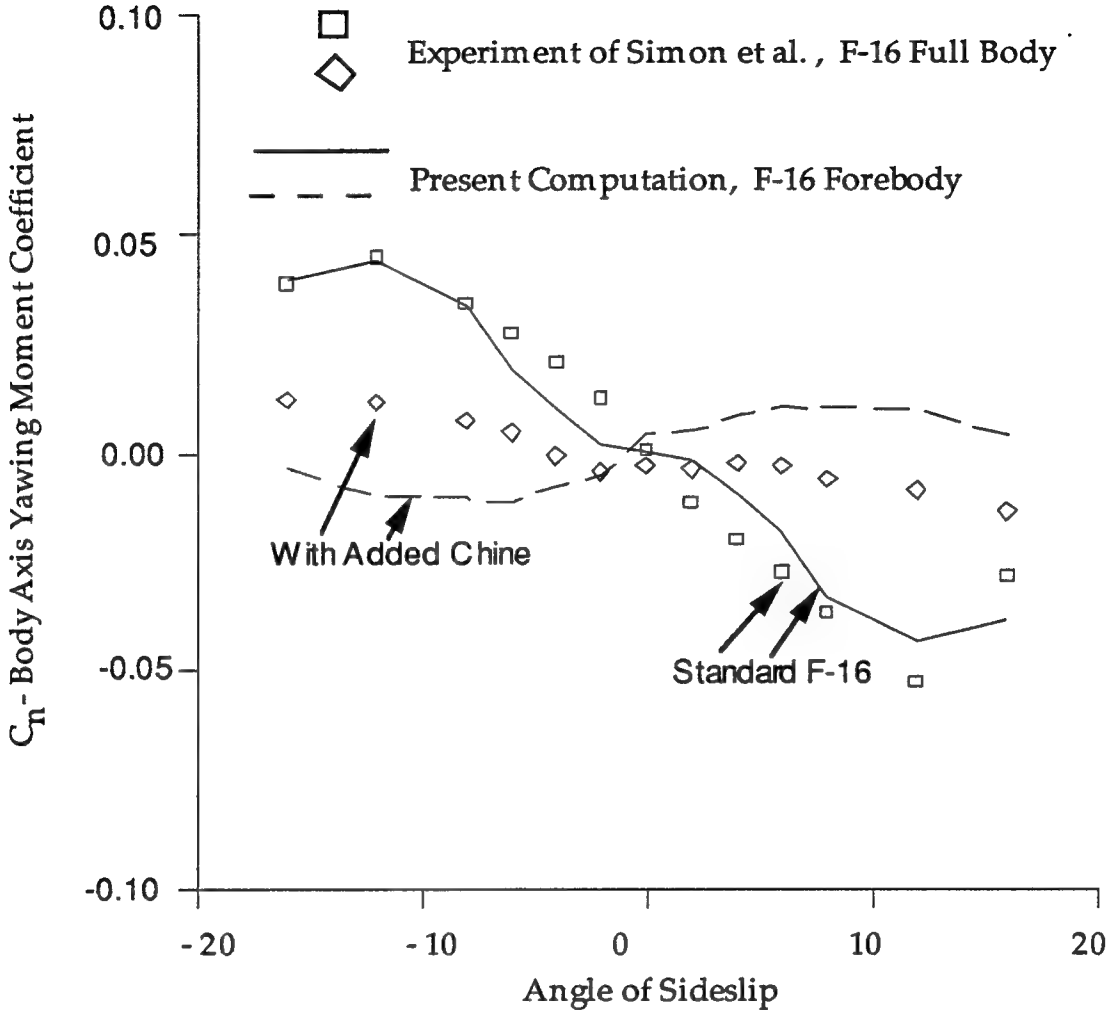

Figure 3.18. Yawing Moment Coefficients as a Function of Angle of Sideslip at α = 40° for Standard F-16 and F-16 with Chine

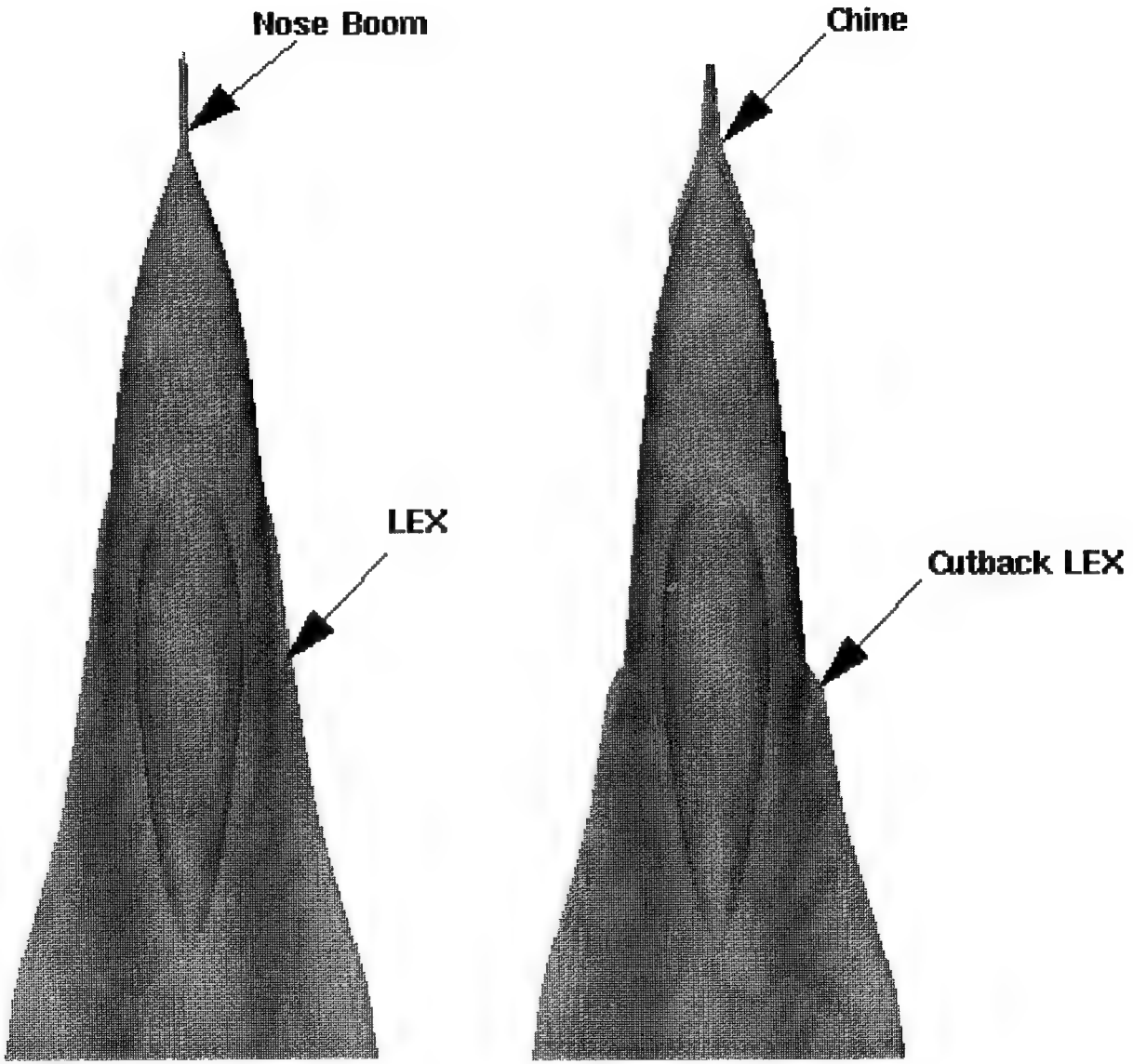

Figure 3.19 Configurations of Standard F-16 Forebody and F-16 Forebody with Chine and Cutback LEX

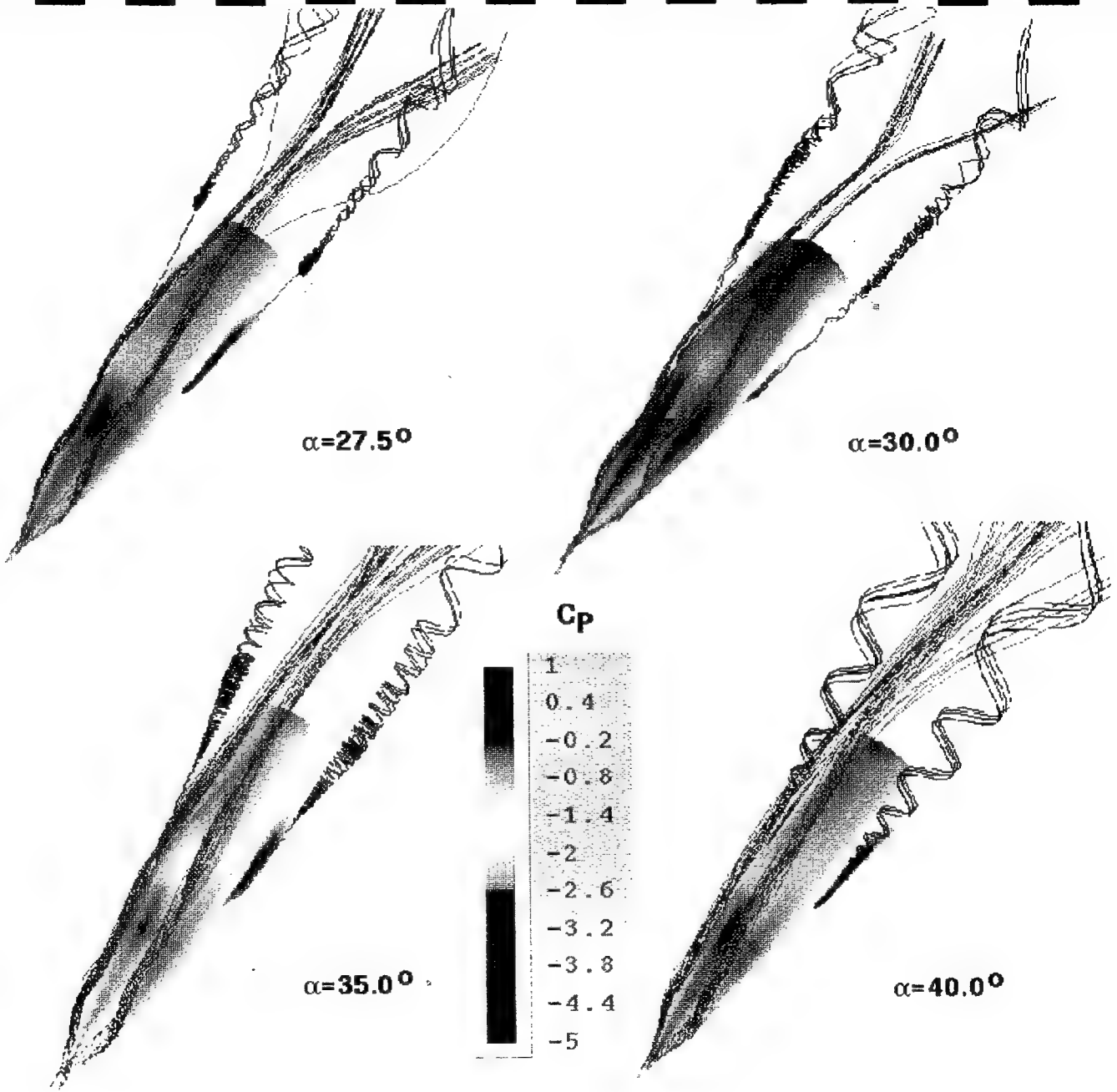

Figure 3.20 Vortical Flows Over an F–16 Forebody with Chine and Cutback LEX at Different Angles of Attack

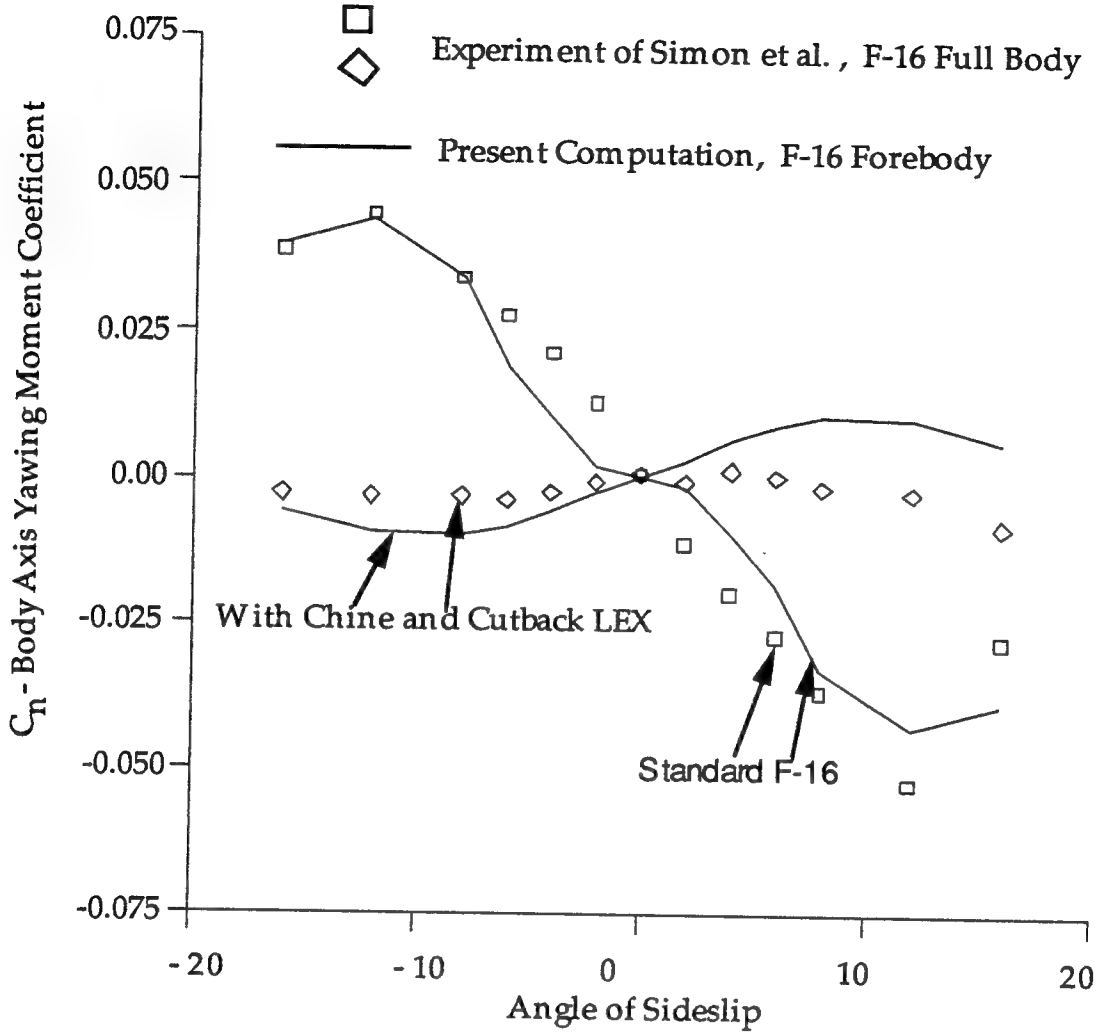

Figure 3.21. Effect of Chine and Cutback LEX on Yawing Moment Coefficients at α = 40°

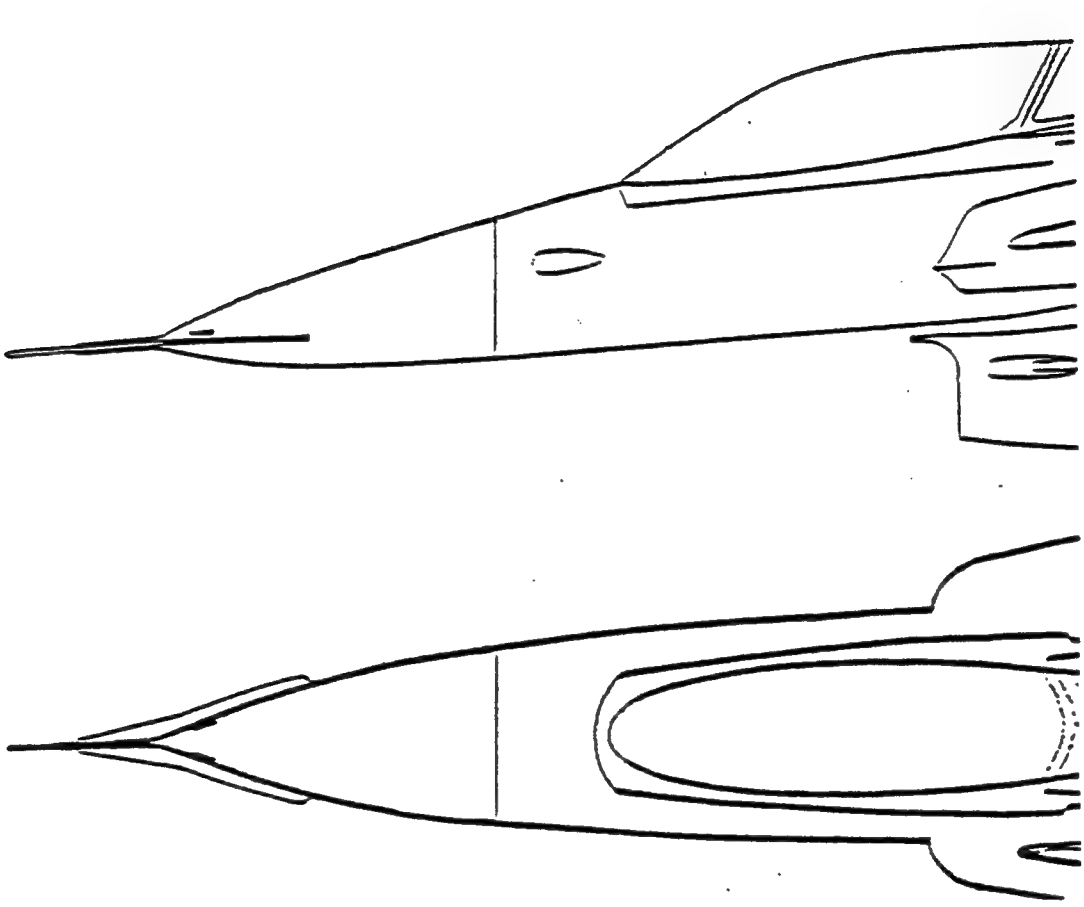

Figure 3.22. Forebody Blowing Slots

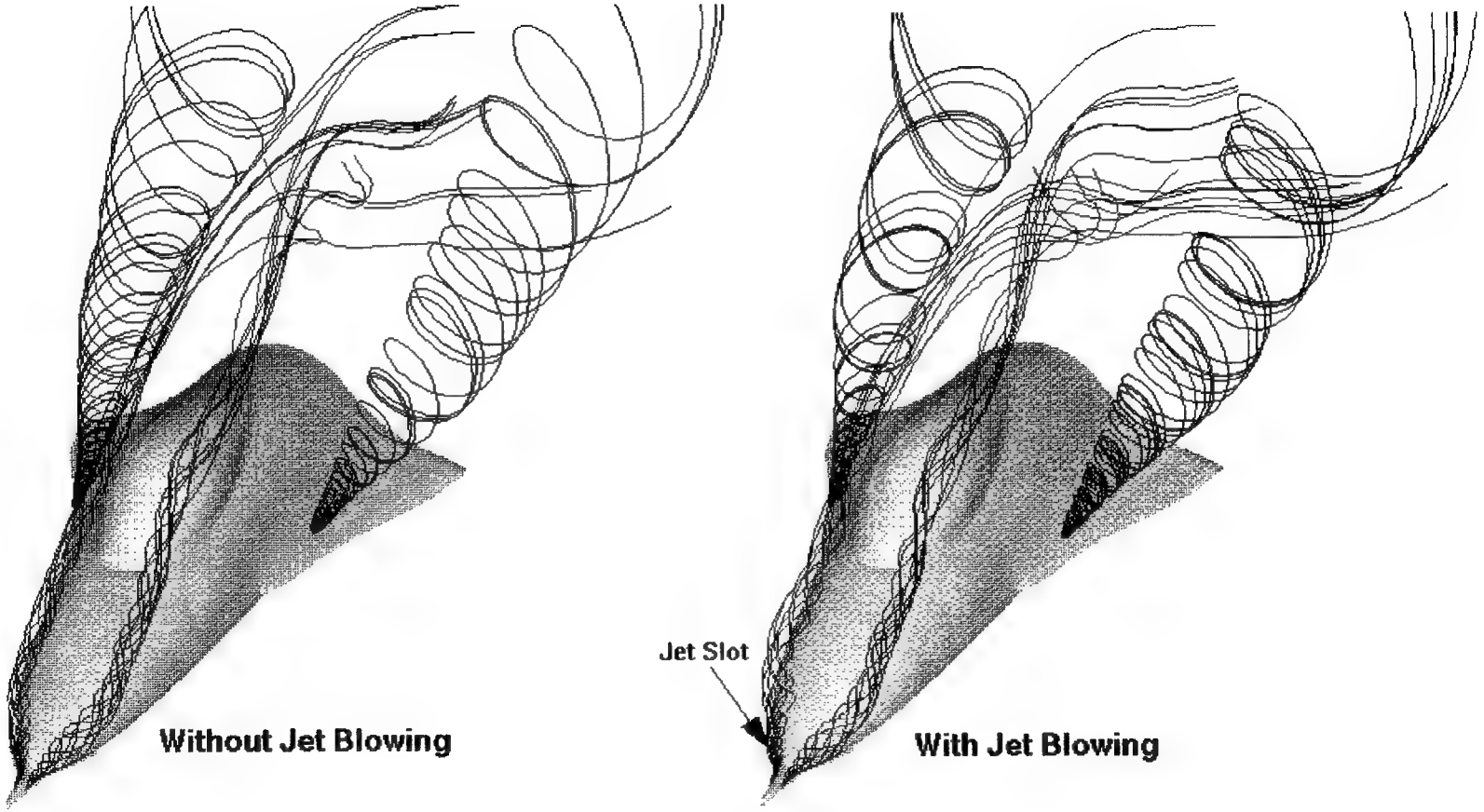

Figure 3.23 Effect of Jet Blowing at Right Side on Vortical Flow Fields Over an F-16 Forebody With Chine and Cutback LEX, α=40^{o}

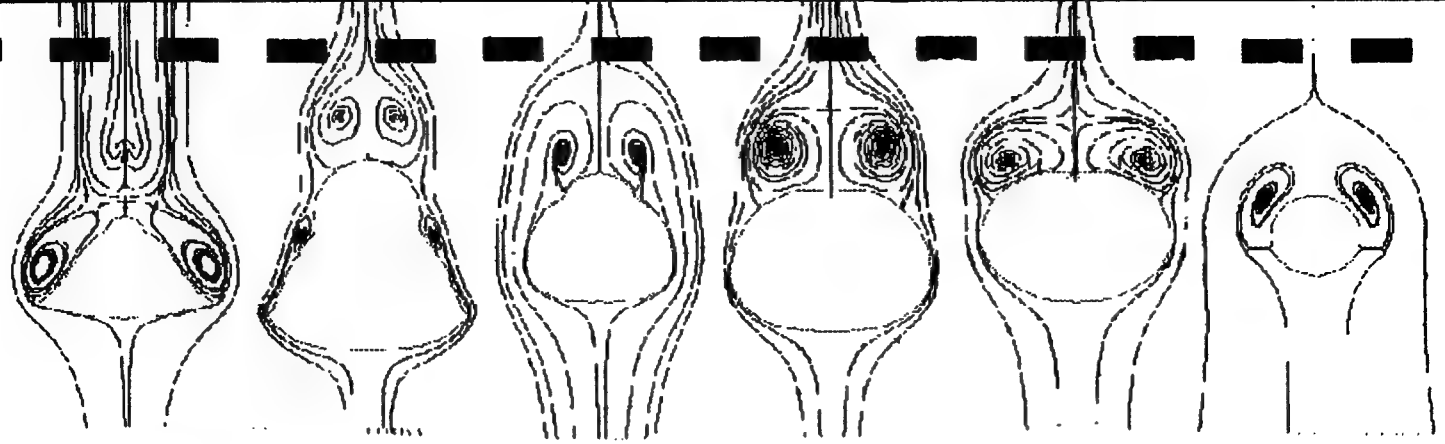

(a) without jet blowing

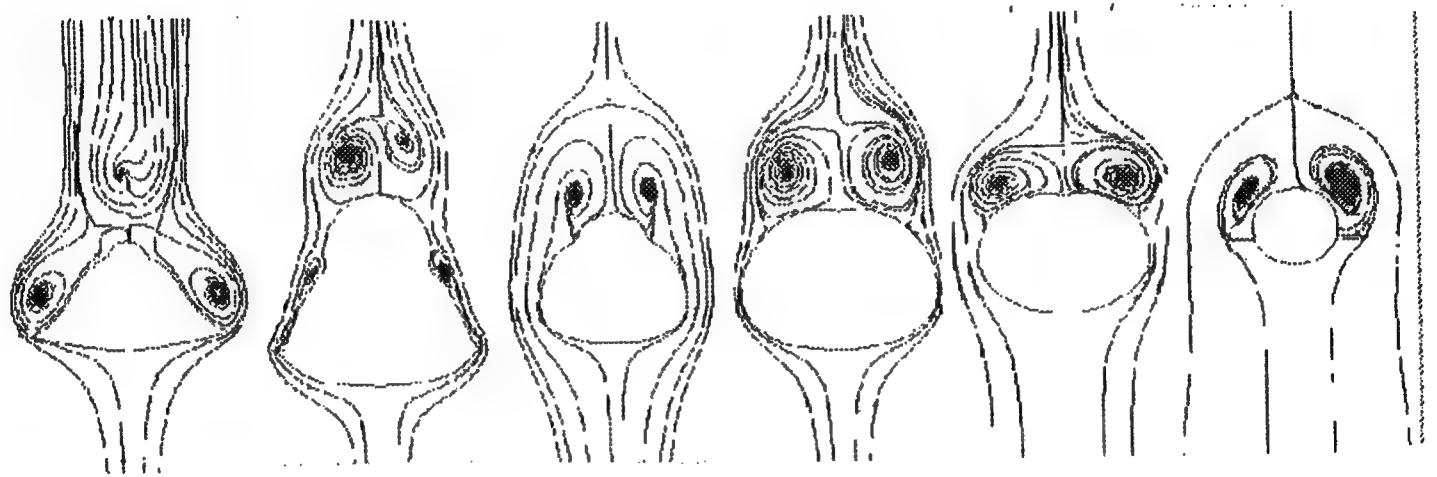

(b) with jet blowing

x/c = 1.252 x/c = 1.00 x/c = 0.878 x/c = 0.605 x/c = 0.379 x/c = 0.133

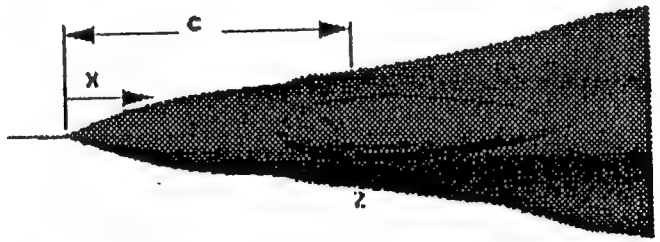

Figure 3.24. Cross-Section Streamlines for an F-16 Forebody with and without Jet Blowing; α - 45°, β = 0.0°

3.7 Summary of Observations for F-16 Forebody Control

This section reported the investigation of vortical flow management over a F-16 forebody. The effort was focused on understanding the physics of directional instability of F-16 forebody at high angles of attack. Topological analysis was applied to identify the LEX vortex core, breakdown location and breakdown type, and to shed light on the interaction of LEX vortex system and forebody vortex system. Comparisons were made on pitching moment coefficient, lift coefficient and yawing coefficient from the present computation using different forebodies and the experimental measurements with the corresponding full forebody. The following conclusions can be made.

1. For the baseline F-16 forebody at zero sideslip, the LEX vortex breaks down at the rear end of the canopy at $\alpha = 30°$, the breakdown point moves upstream with the increase in angle of attack. By $\alpha = 50°$, the LEX vortex is almost fully burst. The forebody vortex pair flows over the canopy region and then interacts with the swirling LEX flow field.

2. For standard F-16 forebody, when the sideslip is non-zero, both LEX and forebody vortices shift laterally, with downwind side LEX vortex moves outward and upward. The sideslip promotes LEX vortex breakdown in the upwind (near) side and suppresses it in the downwind (far) side. The net result is a side force to the downwind side, and an unstable moment. Near the F-16 nose, the sideslip shifts the forebody vertices to the downwind side, hence promoting the directional instability. At a further downstream station in the longitudinal direction, the bursting of forebody vortex on the downside produces a stable force.

3. The directional stability of F-16 forebody is mainly controlled by LEX vortex and forebody vortex system. At small angles of sideslip, for $\alpha > 30°$, asymmetrical bursting of LEX vortices dominates and the forebody is under directional instability. With increase in angle of sideslip, the forebody vortices become important and bursting and shifting of downwind side vortex improves the directional stability.

4. When the LEX of standard F-16 is cutback 48 inches full scale, the LEX breakdown is expedited. The result is a nose-down pitching moment at high angles of attack.

5. When a chine is added at the nose of a standard F-16 forebody, it has little effect on LEX vortex system. At non-zero sideslip, the forebody vortex on the downwind side further lifts off the surface, and reduces the suction pressure associated with it. As a result, it produces a net side force to the upwind side.

6. Comparisons of pitching moment coefficient, lift coefficient, and body axis yawing moment coefficient from the present computation with various forebodies and experimental measurements were made whenever possible. Favorable comparisons were obtained.

7. The present study showed that the use of cutback LEX and chine can provide a nose-down pitching moment and can increase directional stability at $\alpha > 30°$.

8. When jet blowing is applied from the slot above the chine, the forebody vortices are offset with the vortex on the blowing side lifting off the surface. A side force to the non-blowing side can be produced.

4. POTENTIAL APPLICATIONS

All of the objectives of the Phase II effort have been met and the work planned has been successfully completed. During the Phase II funded effort, CFDRC has been actively pursuing commercial applications opportunities taking advantage of the advanced computational technology developed during this effort. This section describes the successful commercialization of the developed software and planned future activities.

4.1. Examples of Successful Commercialization

The numerical methodology developed and validated in the project has been implemented into CFDRC's advanced general-purpose CFD code, CFD-ACE and visualization software, CFD-VIEW. The commercialization efforts of CFD-ACE and CFD-VIEW has begun. A sample CFD-ACE and CFD-VIEW advertisement is shown in Figures 4.1. and 4.2. In addition, the two codes are in use for the following commercial applications:

1. BDM International Inc.: Analysis of hypersonic flows to study aero-optical and aero-thermal characteristics of new designs and endo-leap interceptors.

2. Aerojet Corporation: Analysis of current and future rocket combustion chambers.

3. Martin Marietta Corporation: Investigation of "pressure slump" problem in LOX tank of space shuttle.

4. Solar Turbines, Inc.: Optimization of industrial gas turbine combustors.

5. Caterpillar, Inc.: Under-hood cooling problem analyses, catalytic converter design assessments, and engine fuel injector design modifications.

6. Chrysler Corporation: Windshield ice-melting and climate control in passenger compartment, and analysis of novel designs for two-stroke engines.

7. Textron Defense Systems: (Anticipated Application) Flow over missile, shroud separation problem.

In addition to the above commercial organizations, both of the CFD codes are also in use for several projects from U.S. Government agencies including:

1. NASA (MSFC and LeRC)
2. U.S. Army (BRL and ARTC)
3. U.S. Air Force (AFOSR and AF/WL)
4. U.S. Navy (NAWC/ADT and NAWC/AD)

This following sections describe the plan for future activities aimed at commercialization of software, industrial applications and potential use by the Federal Government.

4.2 Commercialization of Codes

This activity will consist of the following steps:

a. Packaging software (i.e. enhanced user documentation, tutorial problems, interfacing with solid/geometry modeling and grid generation software;
b. Marketing the code(s), and issuing trial (low cost) licenses;
c. Providing seminars, courses, and technical support to users; and
d. Marketing and technical support for the conversion of trial licenses to regular licenses.

Three of the CFDRC staff members have over twenty man-years experience in commercialization of another CFD code. At present there are about 600 licensed users of commercial CFD codes (PHOENICS, FLUENT, and FIDAP). These and all other CFD codes in use in industry are neither accurate nor robust for 3-D unsteady

flows as applicable to dynamic stall type conditions. The presently developed code is considerably superior in terms of: accuracy, robustness, computational efficiency, and graphical user interface. Therefore, it will have good commercial potential for this difficult class of flows.

4.3 Industrial Applications

Static and dynamic stall flows occur in several practical applications when flow transverses a moving body. Flow through rotating devices such as turbomachinery, compressors, fans, propellers, etc. are representative examples of flows where stall conditions occur. In most of the cases the best operating performance of the rotating machinery is close to the stall (or surge) conditions in the high angle of attack incidence flow regime. Figure 4.3 illustrates stall flow configurations for axial turbomachinery, stall flow and stall suppression for an automotive fan flow behind a radiator and a rotating stall flow on a rotating blade passage.

The developed CFD methodology can be directly applied to analyze the stall flow conditions for axial and radial rotomachinery. The code could be coupled with blade vibration and an acoustic model to predict undesired blade oscillations and noise generation during stall flow conditions.

Separation control, directly related to stall flows, is also of great importance for air, land and sea vehicles. One such application of the proposed methodology is the unsteady aerodynamics of automotive vehicles in varying wind approach angle. Flow over submarine sterns, flow through diffusers, spoilers and flow deflectors could also be analyzed with the proposed methodology.

4.4 Aircraft Related Applications

Dynamic stall flows occur on several components of airplanes and helicopters. Rapidly moving conventional aircraft wings or aircraft or missile control surfaces or helicopter rotor blades can be analyzed with the proposed methodology. The major part of this project is devoted to development of the wing or blade design methodology for dynamic stall flow conditions. The method would also be applicable to analyze the stall flows over aircraft turbomachinery components.

CFDRC, being the developer of the methodology, has a very good potential for obtaining contracts for such applications of the software.

4.5 Potential Use by Federal Government

The developed methodology and computer software will be significant interest to the U.S. Government for the following:

a. independent assessment of various designs and control concepts for advanced aircraft proposed by prime contractors for military and/or civil applications;
b. further development of selected concepts; and
c. research and development work at various national research centers.

CFDRC will support all such needs by providing the software and the technical support needed for its effective utilization.

CFD-ACE

Update
June 1994

Advanced General Purpose CFD Code

ADVANCED FEATURES :

- Multi-block grids with local refinement
- Multi-media Conjugate Heat Transfer
- Rotating, moving, sliding grids
- Multi-component diffusion
- Lagrangian droplet tracking with collision, coalescence and evaporation
- Two-phase spray and particulate combustion
- Multi-step homogenous and catalytic chemical kinetics
- Advanced fan model

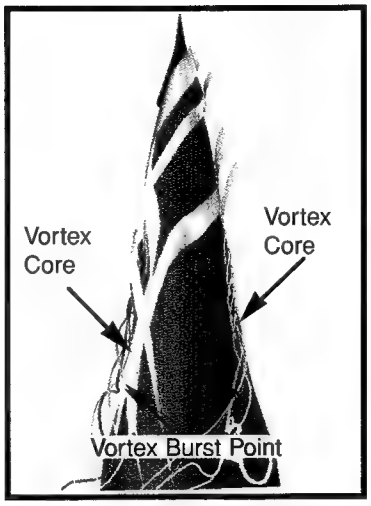

Flow Around F-16 Forebody with Chine, α=30° β=30°

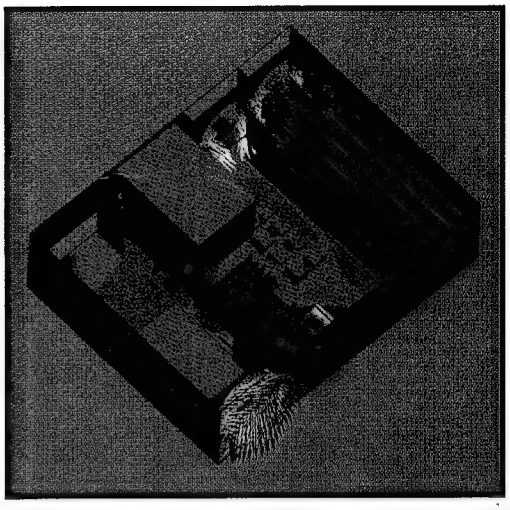

Fan Induced Cooling Flow with Conjugate Heat Transfer in a Computer Box

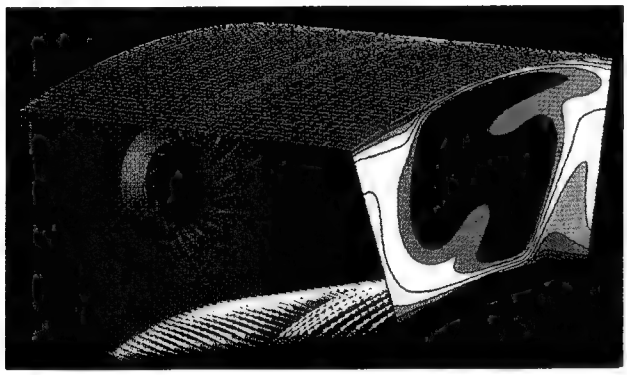

Effusion-Cooled, High Temperature Rise Combustor

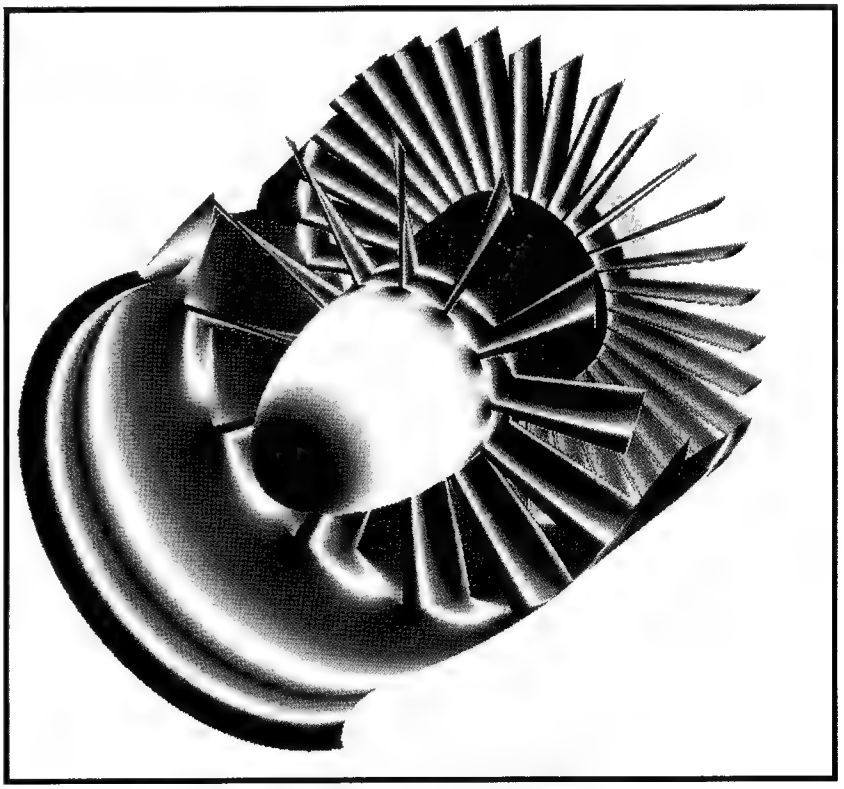

Pressure Field in a NASA 1.15 Pressure Ratio Fan

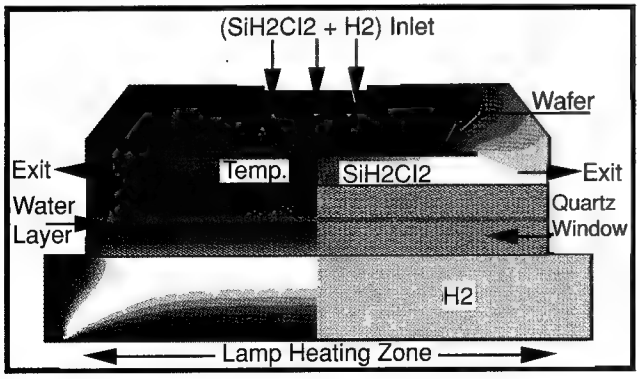

Radiant Heating of Wafer in a Silicon CVD Reactor, with Multi-Media Conjugate Heat Transfer

On the Leading Edge Of CFD Technology

CFD Research Corporation

Figure 4.1.

CFD-VIEW

Update

Interactive 3D Graphics, Animation And Flow Visualization Software

Advanced Features

- Structured/Unstructured/ Hybrid Data Sets
- Flow Ribbons
- Optical Images – Schlieren, Shadowgraph, Interferogram
- Built-in Function Calculator
- Point and Line Data Probes
- Transient Display of Liquid Spray Data
- Interactive Animation

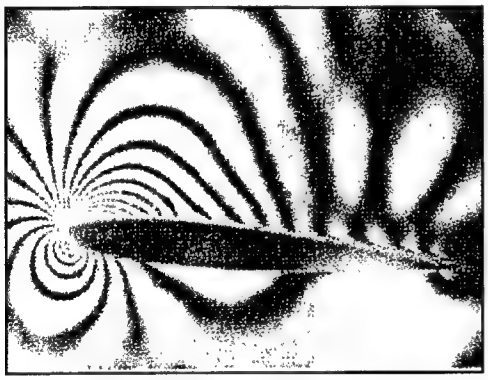

Experimental

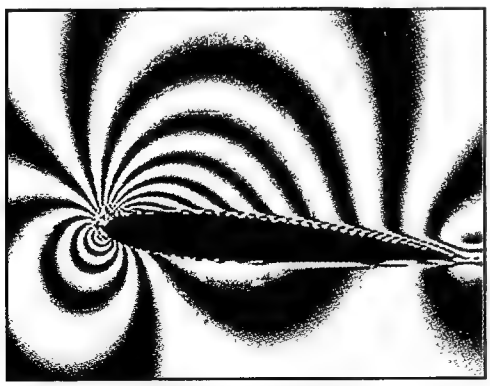

Numerical

Interferograms of Dynamic Stall Flow Development over an airfoil. Mach Number = 0.45, Angle of attack = 5°. (Numerical Solution from CFD-ACE, CFDRC's Advanced General Purpose CFD Code).

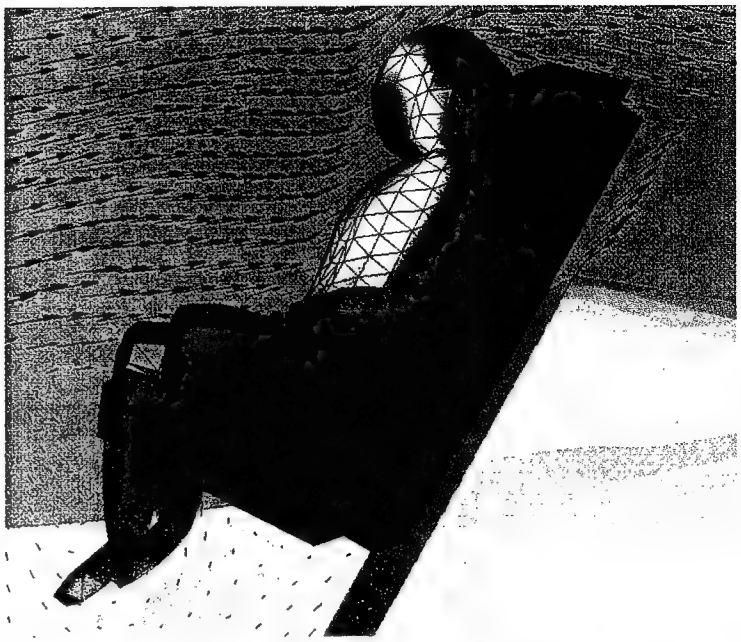

Unstructured (above), Hybrid Unstructured/Structured (below) Grid Model of Pilot Ejection from an F16 (Simulation using CFD-FASTRAN, CFDRC's High Accuracy Compressible Flow Solver).

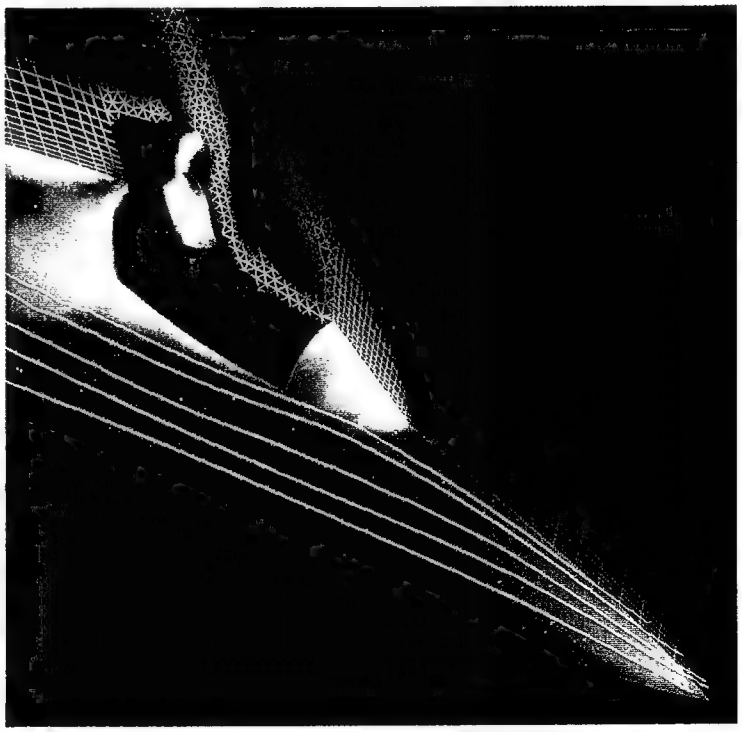

CFDRC

Your View Matters to Us **CFD Research Corporation**

Figure 4.2.

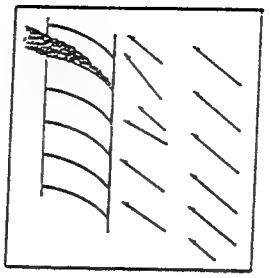

(a)

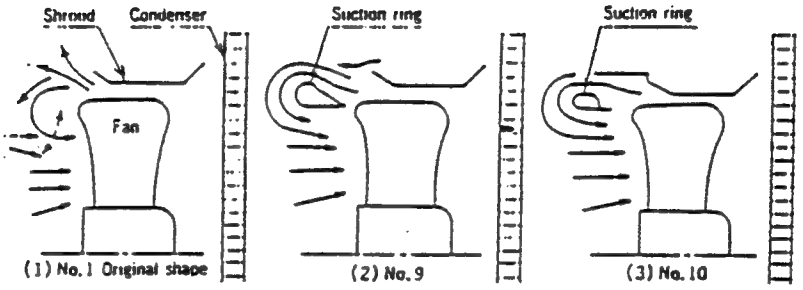

(b)

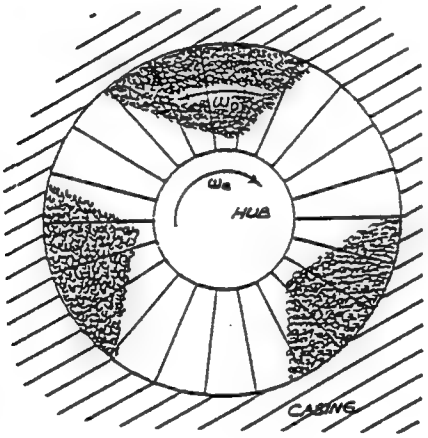

(c)

Figure 4.3. Sample Stall Flows through Rotating Machines: (a) effect of stalled vane on inlet flow; (b) stall suppression for a flow through an automotive fan; (c) three-cell stall flow pattern on a rotating blade passage (ωB = velocity of blades relative to cases, ωD = velocity of stall cells relative to blades)

5. REFERENCES

1. W.J. McCroskey, "The Phenomenon of Dynamic Stall," NASA TM- , 1981.
2. W.J. McCroskey, "Unsteady Airfoils," *Ann. Rev. Fluid Mech.*, vol. 14, pp. 285-331, 1982.
3. L.W. Carr, "Progress in Analysis and Prediction of Dynamic Stall," *J. Aircraft*, vol. 25, no. 1, pp. 6-17, 1988.
4. M. Gad-el-Hak and D.M. Bushnell, "Separation Control: Review," *Journal of Fluid Engineering*, vol. 113, pp. 5-30, 1991.
5. K.E. Hoffle, M.R. Dhanvada and M.C. Frassinelli, "Basic Studies on Delta Wing Flow Modifications by Means of Apex Fences," *Vortex Flow Aerodynamics Conference Proceedings*, NSA CP-2416, Hampton, VA, October 8-10, 1985.
6. R.M. Dhanvada, C. Moskovitz and D.G. Murri, "Forebody Vortex Management for Yaw Control at High Angles of Attack," *Journal fo Aircraft*, vol. 24, no. 4, pp. 248-254, 1987.
7. R.E. Boalby, W.L. Ely, and D.E. Hahne, "High Angle of Attack Stability and Control Concepts for Supercruise Fighters," NASA High Angle of Attack Technology Conference, Oct. 1990.
8. Z.Z. Celik, L. Roberts, and N.J. Wood, "An Investigation of Asymmetric Vortical Flows Over Delta Wings with Tangential Leading Edge Blowing at High Angles of Attack," AIAA-90-103, Jan. 1990.
9. K. Iwanski, T. Ng, and R. Nelson, "An Experimental Investigation of Delta Wing Vortex Flow With and Without External Jet Blowing," AIAA-89-0084, Jan. 1989.
10. T. Karagounis, T. Maxworthy, and G.R. Spedding, "Generation and Control of Separated Vortices Over a Delta Wing by Means of Leading Edge Flaps," AIAA-89-0997, March 1989.
11. S. LeMay, and L. Rogers, "Pneumatic Vortex Flow Control on a 55 Degree Cropped Delta Wing with Chined Forebody," AIAA-90-1430, June 1990.
12. T.T. Ng, "On Leading Edge Vortex and Its Control," AIAA-89-3346, 1989.
13. D.A. Tavella, L.B. Schiff, and R.M. Cummings, "Pneumatic Vortical Flow Control at High Angles of Attack," AIAA-90-0098, Jan. 1990.
14. K. Visser, R. Nelson, and T. Ng, "A Flow Visualization and Aerodynamic Force Data Evaluation of Spanwise Blowing on Full and Half Span Delta

Wings," AIAA-89-0192, Jan. 1989.

15. J.L. Thomas, S.L. Taylor, and W.K. Anderson, "Navier-Stokes Computations of Vortical Flows Over Low Aspect Ratio Wings," AIAA-87-0207, Jan. 1987.
16. N.J. Wood, L. Roberts, and K.T. Lee, "The Control of Vortical Flow on Delta Wings at High Angles of Attack," AIAA-87-2278, Jan. 1987.
17. F.W. Roose and J.T. Kegelman, "An Experimental Investigation of Sweep-Angle Influence on Delta-Wing Flows," AIAA Paper 90-0383, 1990.
18. W.H. Wentz and D.L. Kohlman, "Vortex Breakdown on Slender Sharp-Edged Delta Wings," *J. Aircraft*, vol. 8, no. 3, kpp. 156-161, March 1971.
19. D. Hummel, and P.S. Srinivasan, "Vortex Breakdown Effects on the Low-Speed Aerodynamic Characteristics of Slender Delta Wings in Symmetrical Flow," *J. Royal Aero. Soc.*, vol. 71, pp. 319-322, 1967.
20. P.B. Earnshaw and J.A. Lawford, "Low-Speed Wind-Tunnel Experiments on a Series of Sharp-Edged Delta Wings," ARC R&M no 3424, 1964.
21. J.A. Lawford and A.R. Beauchamp, "Low-Speed Wind-Tunnel Measurements on a Thin Sharp-Edged Delta Wing with 70° Leading-Edge Sweep, with Particular Reference to the Position of Leading-Edge Vortex Breakdown," ARC R&M, no. 3338, 1961.
22. F.M. Payne, T.T. Ng, and R.C. Nelson, "Experimental Study of the Velocity Field on a Delta Wing," AIAA Paper 87-1231, 1987.
23. G.E. Erickson, "Flow Studies of Slender Wing Vortices," AIAA-80-1423, 1980.
24. D.O. Rockwell, R. Atta, C.H., Kuo, C. Hefele, C. Magness, and T. Utsch, "On Unsteady Flow Structure from Swept Edges Subjected to Controlled Motion," *Proc. of the Second Workshop on Unsteady Separated Flow*, U.S. Air Force Systems Command, Frank J. Seiler Research Lab Report FJSRL-TR-88-0004, pp. 299-312, 1988.
25. R. Atta and D. Rockwell, "Leading-Edge Vortices Due to Low Reynolds Number Flow Past a Pitching Delta Wing," *AIAA Journal*, vol. 28, pp. 995-1004, 1990.
26. G.A. Reynolds and A.A. Abtahi, "Instabilities in Leading-Edge Vortex Development," AIAA Paper 87-2424, 1987.
27. C. Magness, O. Robinson, and D. Rockwell, "Control of Leading-Edge Vortices on a Delta Wing," AIAA Paper 89-0999, 1989.
28. M. Gad-el-Hak and C.M. Ho,"The Pitching Delta Wing," *AIAA Journal*, vol. 23, pp. 1660-1665, 1985.

29. C. Magness, O. Robinson, and D. Rockwell, "Unsteady Crossflow on a Delta Wing Using Particle Image Velocimetry," *AIAA J. of Aircraft*, vol. 29, pp. 707-709, 1992.
30. C. Magness, O. Robinson, and D. Rockwell, "Instantaneous Topology of the Unsteady Leading-Edge Vortex at High Angles of Attack, *AIAA Journal* 1993.
31. C. Magness, O. Robinson, and D. Rockwell, "Laser-Scanning Particle Image Velocimetry Applied to a Delta Wing in Transient Maneuver, " *Experiments in Fluid*, 1993.
32. M.R. Visbal, "Structure of Vortex Breakdown on a Pitching Delta Wing," AIAA Paper 93-0434, 1993.
33. Gu, W., O. Robinson, and D. Rockwell, "Control of Leading-Edge Vortices on a Delta Wing by Unsteady Injection at the Leading Edge," *AIAA Journal*, to appear.
34. Z. Shi, J. M. Wu and A. D. Vakill, "An Investigation of Leading-Edge Vortices on Delta Wings with Jet Blowing", AIAA-87-0330, 1987.
35. McKernan, J.F., and Nelson, R.C., "An Investigation of the Breakdown of the Leading Edge Vortices on a Delta Wing at High Angles of Attack," AIAA-83-2114, 1983.
36. K. D. Visser, K. P. Iwanski, R. C. Nelson and T. T. Ng, "Control of Leading Edge Vortex Breakdown by Blowing", AIAA-88-0504, 1988.
37. D. Findlay, S. Kern and O. Kwon, "Numerical Investigation of the Effects of Blowing on High Angle of Attack Flow Over Delta Wing", AIAA -91-1809, 1991.
38. M.R. Visbal and R.E. Gordnier, "On the Crossflow Topology of Vortical Flow," *AIAA Journal*, to appear.
39. D. Rockwell, "Three-Dimensional Flow Structure on Delta Wings at High Angles-of-Attack: Experimental Concepts and Issues," AIAA-93-0550, 1993.
40. D.M. Rao, J.F. Campbell, "Vortical Flow Management Techniques," *Progress in Aerospace Science*, vol. 24, pp. 1730224, 1987.
41. Kluter, S.M., Martin, R.A., Redinotis, O.K., Tellionis, D.P., "Flow Control Over Delta Wings at High Angles of Attack," AIAA Paper 93-3494, 1993.
42. Helin, H.E. and Watry, C.W., "Effects of Trailing-Edge Jet Entrainment on Delta Wing Vertices," *AIAA Journal*, Vol. 32, pp. 802-804, 1994.
43. Shih, C., Lourenco, L., Ding, Z., and Krothapalli, A., "Thrust-Induced Effects on a Pitching-Up Delta Wing Flow Field," AIAA-94-1856, 1994.

44. Hall, R.M., Erickson, G.E., Straka, W.A., Peters, S.E., Maines, B.H., Fox, M.C., Hames, J.E., and LeMay, S.P., "Impact of Nose-Probe Chines on the Vortex Flows about the F-16C," AIAA Paper 90-0386, 1990.
45. Stahl, W., "Suppression of Asymmetry of the Vortex Flow Behind a Circular Cone at High Incidence," AIAA Paper 89-3372-CP, 1989,
46. Murri, D.G. and Rao, D.M., "Exploratory Studies of Actuated Forebody Strakes for Yaw Control at High Angles of Attack," AIAA Paper 87-2557-CP, 1987.
47. Malcolm, G.N., Ng, T.T., Lewis, L.C., and Murri, D.G., "Development of Non-Conventional Control Methods for High Angle of Attack Flight Using Vortex Manipulation," AIAA Paper 89-2192, 1989.
48. Moskovitz, C., Hall,R., and DeJarnette, F.,"Effects of Surface Perturbations on the Asymmetric Vortex Flow Over a Slender Body," AIAA Paper 88-0483, 1988.
49. Moskovitz, C., Hall, R., and DeJarnette, F., "Experimental Investigation of a New Device to Control the Asymmetric Flowfield on Forebodies at Large Angles of Attack," AIAA Paper 90-0068, 1990.
50. Ng, T.T., and Malcolm, G.N., "Aerodynamic Control Using Forebody Strakes," AIAA Paper 91-0618, 1991.
51. Skow, A.M., Moore, W.A., and Lorincz, D.J., "Forebody Vortex Blowing - A Novel Concept to Enhance the Departure/Spin Recovery Characteristics of Fighter Aircraft," AGARD CP-262, Conference on Aerodynamics of Controls, Naples, Italy, May 1979.
52. Moore, W.A., Skow, A.M., and Lorincz, D.J., "Control of Forebody Vortex Orientation by Asymmetric Air Injection - Application to Enhance Departure/Spin Recovery," AIAA paper 80-0173, 1980.
53. Malcolm, G.N., and Skow, A.M., "Enhanced Controllability Through Vortex Manipulation on Fighter Aircraft at High Angles of Attack," AIAA Paper 86-2277-CP, 1986.
54. Rosen, B. and Davis, W., "Numerical Study of Asymmetric Air Injection to Control High Angle of Attack Forebody Vortices on the X-29 Aircraft," AIAA Paper 90-3004, 1990.
55. Tavella, D.A., Schiff, L.B., and Cummings, R.M., "Pneumatic Vortical Flow Control at High Angles of Attack," AIAA Paper 90-0098, 1990.
56. Ng, T.T., and Malcolm, G.N., "Aerodynami Control Using Forebody Blowing and Suction," AIAA Paper 91-0619, 1991.

57. Erickson, G.E. and Brandon, J.M., "Low-Speed Experimental Study of the Vortex Flow Effects of a Fighter Forebody Having Unconventional Cross-Section," AIAA Paper 85-1798, 1985.

58. Cornelius, K.C., Pandit, N. , Osborn, R.F., and Guyton, R.W., "An Experimental Study of Pneumatic Vortex Flow Control on High Angle of Attack Forebody Model," AIAA Paper 92-0018, 1992.

59. Simon, J.M., LeMay, C.S., and Brandon, J.M., "Results of Exploratory Wind Tunnel Tests of F-16/VISTA Forebody Vortex Control Devices," WL-TR-93-3013, Flight Dynamics Laboratory, Wright Lab., WPAFB, OH, 1993.

60. LeMay, S.P., Sewall, W.G. and Henderson, J.F., "Forebody Vortex Flow Control Using Tangential Slot and Jet Blowing," AIAA-92-0019, 1992.

REPORT DOCUMENTATION PAGE

Form Approved
OMB No. 0704-0188

1. AGENCY USE ONLY (Leave blank)	2. REPORT DATE	3. REPORT TYPE AND DATES COVERED
	November 1994	Final Rpt. 9/30/92-9/29/94

4. TITLE AND SUBTITLE
Pressure-Based High-Order TVD Methodology for Dynamic Stall Control - SIBR Phase II Final Technical Report

5. FUNDING NUMBERS

6. AUTHOR(S)
H.Q. Yang, Z.J. Wang, V.J. Harrand, A.J. Przekwas

7. PERFORMING ORGANIZATION NAME(S) AND ADDRESS(ES)
CFD Research Corporation
3325 Triana Blvd.
Huntsville, AL 35805

8. PERFORMING ORGANIZATION REPORT NUMBER
4171/4

9. SPONSORING/MONITORING AGENCY NAME(S) AND ADDRESS(ES)
U.S. Air Force Office of Scientific Research
Bolling Air Force Based, DC 20332

10. SPONSORING/MONITORING AGENCY REPORT NUMBER

11. SUPPLEMENTARY NOTES

12a. DISTRIBUTION/AVAILABILITY STATEMENT

12b. DISTRIBUTION CODE

13. ABSTRACT *(Maximum 200 words)*

The design of future generation combat aircraft for post-stall manuevering requires detailed knowledge, exploitation, and control of the highly unsteady vortical flow field in the vicinity of the vehicle. The objective of the present SBIR study is to develop and validated an advanced Navier-Stokes solver for the simulation of unsteady separated flows and to investigate flow separation control concepts. During this project, close collaboration with government laboratories, NASA and Universitites have been established to accomplish the above objectives.

This Final Report summarizes the second year effort in the areas of flow control concepts for wing body and forebodies, especially in: steady suction and blowing along the leading edge of a delta wing; alternate suction and blowing on the delta wing; vortex breakdown control on a delta wing using apex flap; vortical flow control of delta wing configuration with a vectored trailing edge jet; development of directional instability on F-16 forebody; mechanical control of directional instability on F-16 forebody with chine and cutback LEX; and jet blowing control of F-16 forebody.

The potential applications of the developed methodology to rotating machinery, automotive, and aircraft design are discussed and commercialization activities are planned.

14. SUBJECT TERMS	15. NUMBER OF PAGES
pressure-based, dynamic stall, TVD	94
	16. PRICE CODE

17. SECURITY CLASSIFICATION OF REPORT	18. SECURITY CLASSIFICATION OF THIS PAGE	19. SECURITY CLASSIFICATION OF ABSTRACT	20. LIMITATION OF ABSTRACT
Unclassified	Unclassified	Unclassified	

NSN 7540-01-280-5500

Standard Form 298 (Rev. 2-89)
Prescribed by ANSI Std. Z39-18
298-102